DEVELOPMENT OF AN ADVANCED COMPOSITE EXTERNAL FUEL TANK FOR AIR PLATFORMS

A THESIS SUBMITTED TO
THE GRADUATE SCHOOL OF NATURAL AND APPLIED SCIENCES
OF
MIDDLE EAST TECHNICAL UNIVERSITY

BY

UĞURCAN KARAHAN

IN PARTIAL FULFILLMENT OF THE REQUIREMENTS
FOR
THE DEGREE OF MASTER OF SCIENCE
IN
MECHANICAL ENGINEERING

FEBRUARY 2014

Approval of the thesis:

DEVELOPMENT OF AN ADVANCED COMPOSITE EXTERNAL FUEL TANK FOR AIR PLATFORMS

submitted by **UĞURCAN KARAHAN** in partial fulfillment of the requirements for the degree of **Master of Science in Mechanical Engineering Department, Middle East Technical University** by,

Prof. Dr. Canan Özgen _____
Dean, Graduate School of **Natural and Applied Sciences**

Prof. Dr. Süha Oral _____
Head of Department, **Mechanical Engineering**

Prof. Dr. Levend Parnas _____
Supervisor, **Mechanical Engineering Dept., METU**

Examining Committee Members:

Prof. Dr. Bülent Doyum _____
Mechanical Engineering Dept., METU

Prof. Dr. Levend Parnas _____
Mechanical Engineering Dept., METU

Asst. Prof. Dr. Merve Erdal _____
Mechanical Engineering Dept., METU

Asst. Prof. Dr. Ergin Tönük _____
Mechanical Engineering Dept., METU

Fikret Şenel, M.Sc. _____
R&D Manager, Barış Electrical Ind. Inc.

Date: 07.02.2014

I hereby declare that all information in this document has been obtained and presented in accordance with academic rules and ethical conduct. I also declare that, as required by these rules and conduct, I have fully cited and referenced all material and results that are not original to this work.

Name, Last name : Uğurcan Karahan

Signature :

ABSTRACT

DEVELOPMENT OF AN ADVANCED COMPOSITE EXTERNAL FUEL TANK FOR AIR PLATFORMS

Karahan, Uğurcan
M.Sc., Department of Mechanical Engineering
Supervisor: Prof. Dr. Levend Parnas

February 2014, 145 pages

This thesis provides a design approach for an external fuel tank, which permits external mounting to the air platforms including rotorcrafts and aircrafts. The development stages include both a computational and an experimental study. In this thesis, unique combination of advanced composite material solutions is investigated in the structural design process. Filament-wound tank structure is modeled as multi-layered orthotropic structure. Various worst-case loading scenarios defined by internationally recognized design standards and regulations are performed by utilizing a software platform based on Finite Element Method (FEM). Results obtained by means of FEM are examined in order to determine a proper winding angle and to verify the performance of the structure exposed to combined static and transient loadings in the operating environment of the structure. The insight gained by means of such analyses allows examining every structural aspect of the tank structure. The failure prediction is performed according to the Reserve Factor index calculated for Tsai-Wu Failure Theory. The dynamic response of the structure

during a crash is determined with a full-scaled prototype of the External Fuel Tank. The most severe conditions that the tank would experience when deployed within the entire operational envelope are simulated at the first non-destructive sled test facility of Turkey which is the Vehicle Safety Facility of METU-BILTIR. The result of the simulation indicates that the survival of the tank structure is ensured during severe crash impact conditions. Finally, this study has resulted in obtaining an External Fuel Tank, which maintains its structural integrity for all loading conditions, while meeting the weight target.

Keywords: Composite Materials, Filament Winding Method, Structural Design, Finite Element Analysis, Experimental Simulations

ÖZ

HAVA PLATFORMLARI İÇİN İLERİ KOMPOZİT HARİCİ YAKIT TANKI GELİŞTİRİLMESİ

Karahan, Uğurcan
Yüksek Lisans, Makina Mühendisliği Bölümü
Tez Yöneticisi: Prof. Dr. Levend Parnas

Şubat 2014, 145 sayfa

Bu çalışmada, helikopter ve uçak gibi hava platformlarına harici olarak entegre edilebilecek bir harici yakıt tankı için hesaplamalı ve deneysel yöntemler kullanılarak geliştirilen bir tasarım yaklaşımı sunulmaktadır. Yapısal tasarım aşamasında özgün kompozit malzeme kombinasyonları incelenmiştir. Filaman sargı tekniği ile üretilmesi planlanan yakıt tankı gövdesi çok tabakalı ortotrop yapıda modellenerek, yapının kullanım esnasında maruz kalabileceği farklı yükleme senaryoları, Sonlu Elemanlar Metodu (SEM) temelinde çalışan bir yazılım platformu yardımıyla ile incelenmiştir. Uluslararası geçerliliği bulunan standart ve yönetmeliklere uygun olarak oluşturulan yükleme koşullarına ait analiz sonuçları detaylı olarak incelenerek, harici yakıt tankının operasyon şartlarında maruz kalabileceği statik ve süreksiz yükleme koşulları altındaki performans doğrulaması ile uygun sarım açısının tayini gerçekleştirilmiştir. Bu tür analizler yapıyı her yönüyle detaylı bir şekilde incelemeye olanak sağlamaktadır. Yapısal performans değerlendirmesi, Tsai-Wu kriterine göre hesaplanan emniyet katsayısına göre

yapılmaktadır. Yapının düşme esnasında göstereceği dinamik davranışlar, ağırlık kriterini sağlayan tam ölçekli bir prototip ile incelenmektedir. Yakıt tankının ömür döngüsü içerisinde deneyimleyeceği en sert koşullar, Türkiye'nin ilk hasarsız çarpışma test tesisi olma özelliğini taşıyan ODTÜ-BİLTİR Taşıt Güvenliği birimi altyapısında bulunan test sisteminde simüle edilmiştir. Ortaya çıkan sonuçlar neticesinde, yakıt tankının, zorlu çarpma koşullarında bütünlüğünü koruyabileceği gösterilmektedir. Sonuç olarak bu çalışma kapsamında, her yükleme koşulunu altında bütünlüğünü sağlayan ve ağırlık limitleri içerisinde kalan bir harici yakıt tankının tasarımı gerçekleştirilmiştir.

Anahtar Kelimeler: Kompozit Malzemeler, Filaman Sargı Metodu, Yapısal Tasarım, Sonlu Elemanlar Analizi, Deneysel Simülasyon

To My Family

ACKNOWLEDGEMENTS

I would like to express my thanks and deepest gratitude to my thesis supervisor Prof. Dr. Levend Parnas for his guidance, advice, criticism and motivation throughout the study.

My sincere thanks goes to all of the Barış Electrical Industry Inc. staff, especially to Emel Billur, Fikret Şenel, Gökhan Güven and Bora Balya for their help and support.

Last but not the least; I am deeply grateful to my loving parents for their endless love, patience, encouragement and faith in me. Without their persistent support, this thesis would not have been possible. Words are not enough to express my appreciation and love to my sister, İpek, who has been and always be my preciousss. The unconditional love and support of my future wife, Reyhan, is gratefully acknowledged. This thesis is dedicated to them.

TABLE OF CONTENTS

LIST OF FIGURES

FIGURES

LIST OF TABLES

TABLES

CHAPTER 1

INTRODUCTION

An air platform, by definition, is any vehicle, which has the capability of sustained atmospheric flight [1,2]. Air platforms vary uniquely with respect to propulsion, lifting method, intended usage etc. Hence, there are diverse ways to classify them. In general, any air platform could be considered to fall into one of the groups given in Figure 1 [3].

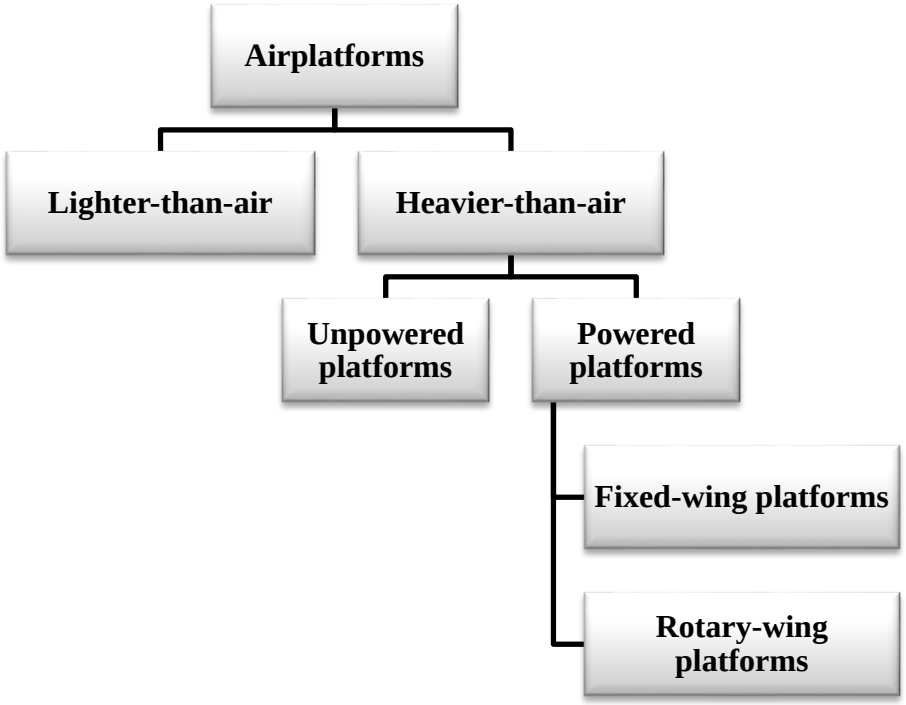

Figure 1: Air platform Classifications [3]

The primary differentiation to classify the air platforms in terms of type depends on identifying whether the platform itself is lighter or heavier than air.

Lighter-than-air platforms, such as balloons and zeppelins, are also referred as aerostats. Such air platforms use their own buoyancy to obtain lift without a requirement of power source. In addition, they are designed in such a way that they contain an envelope that to be filled with a sufficient volume of buoyant, less dense than air gases such as hot air, hydrogen and helium. As the relatively lighter gas displaces the surrounding air, the platform tends to float in the ambient [4].

Heavier-than-air platforms, on the other hand, require a proper source of power in order to become airborne and balance the corresponding flight forces: lift, the upward-acting force that hold the platform aloft; drag, the retarding force acting opposite to the direction of motion; thrust, the forward acting force generated by the propulsion system and weight, the force generated by the gravity. Both weight and drag are the quantities that any object in nature has in common, whereas lift and thrust are the elements created artificially to make heavier-than-air flight possible [4,5].

Heavier-than-air platforms could be grouped basing upon the propulsion system. Unpowered platforms refer to the vehicles having flight capability without onboard propulsion. Examples of such platforms are gliders. U.S. Federal Aviation Administration (FAA) defines a glider as a heavier-than-air aircraft that is supported in flight by the dynamic reaction of the air against its lifting surfaces, and whose free flight does not depend on an engine [6]. Modern gliders are towed to a proper soaring altitude by a powered platform. Once gliders are launched, since there is no source of thrust, they cannot maintain a flight for long periods of time. Therefore, they designed specifically to create least drag by means of aerodynamically shaped narrow fuselage and to maximize lift with wings having high aspect ratio. In addition, they are equipped with thermal scans to make use of

thermal currents with the aim of gaining height and remaining airborne for remarkably long distances [4,7]. On the contrary side, unlike unpowered platforms, powered ones utilize onboard propulsion to create flow over their wings, which result in aerodynamic lift. Powered air platforms could be examined in two categories; fixed-wing air platforms and rotary-wing air platforms. U.S. Federal Aviation Administration (FAA) defines a rotary-wing air platform as an aircraft that is lifted and propelled by one or more horizontal rotors and each rotor consists of two or more wings [8]. Rotary-wing air platforms could be best exemplified by helicopters in which the source of lift is wings called rotor blades revolving around a mast. In order to distinguish from rotary-wing air platforms, fixed-wing air platforms could be defined as any heavier-than-air vehicle, which gain support, by the dynamic reaction of air over the wings. Powered fixed-wing air platforms are commonly called airplane, aeroplane or plane [4,9].

All of these identified air platforms have been deployed extensively for both civil and military applications. It is a very well known fact that air platforms are regarded as the key elements of military power including fighters, bombers, ground-support platforms, helicopters, transport/cargo platforms and unmanned aerial platforms. Besides, platforms being used other than military applications are entitled as civil platforms. Civil applications include private or business air platforms and commercial airliners.

Humankind has always been a keen observer due to the nature and temper. Therefore, it could be said that the very first idea of flying dated back to the ancient times. Leonardo da Vinci is known to be the one who made the first scientific attempts to design an aerial mechanism. After him, the Wright Brothers are recognized as the first to put into practice the sustained and controlled flight of a heavier-than-air manned flying vehicle on Dec. 17, 1903 [5,10]. Starting from a clean sheet of paper, air platforms have been evolved progressively. Over the years, the potential of them has been broaden by experience and advances in technology.

Besides, technological breakthroughs have been the key element leading new design paths to open. As new platforms have been introduced together with modern software, electronic systems and equipment, higher and higher levels of effectiveness have been reached. It is obvious that the platforms utilized today are admitted to be better performing, when they are compared to the original versions. In terms of hardware and fundamental performance standards such as speed, altitude and range, most of the platforms were reached the peak of efficiency. In such cases, it might appear that further development would be possible only through the initiation of a brand new design. However, since the combination of hard facts such as cost-effectiveness and budget is the driving factor, changing the operational characteristics of existing platforms or the modification of the current design has become preferable over the introduction of a new platform to match the required service [11]. Regardless of development level, air platforms have a certain limit in remaining airborne. For powered platforms, the range could be defined as the distance the aircraft could fly from a given speed and altitude until it runs out of fuel; whereas the endurance is the time it takes to run out of fuel [12]. Therefore, both range and endurance of a platform are directly proportional to fuel load and consumption rate. Determining the range and endurance is complex in nature because of the variables involved. Fuel load, consumption rate and airspeed are changing continuously during a flight. It must be emphasized that a flight is not performed at a constant speed; rather it changes from zero at take-off, reaches up to cruise speed and goes back again to zero at landing. Hence, as it is expected the fuel consumption rate tends to increase during climbing and maneuvering. Moreover, the weight varies as fuel is burned, so does the lift and drag [13].

In the light of the aforementioned information, in order to meet the operational requirements, large quantities of fuel are supposed to be stored onboard. Main tanks are the primary source of fuel, which provides a certain range for a given load. Operational requirements may give rise to the need of increased operation duration and/or radius of action. Since the main tanks are permanent by nature, further

increase in fuel capacity, without refueling, would come only with the introduction of external systems. Consequently, modern air platforms have been designed to be able to adapt External Stores Support System (ESSS). The elements of the system involve a wing, a vertical support and removable store pylons, which are constructed of carbon-epoxy to provide required strength with minimum the weight [15].

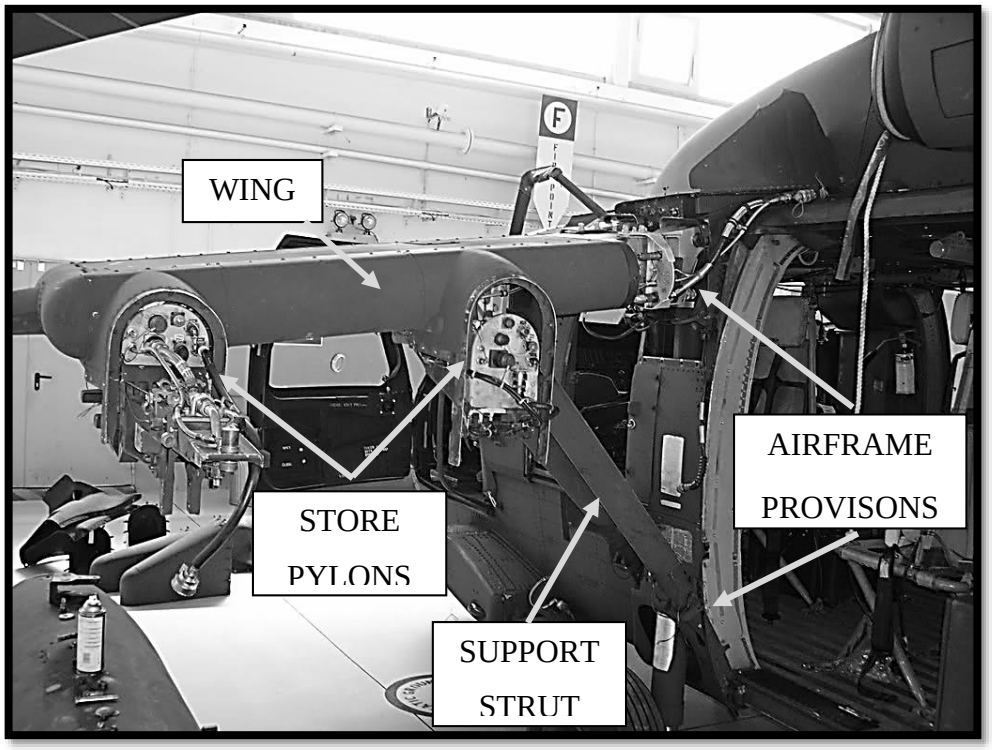

Figure 2: External Stores Support System [14]

Generally, External Stores Support System is located both sides of the body and it generally involves two pylons each providing hard points for various items like munitions and add-ons to be integrated to the platform [14]. The airframe provisions

are fixed structural components that enable the support system to be installed to the fuselage of the air platform. There are two vertical store pylons located on the wing, which are supported by two support struts. Under the wing, there are two ejector racks attached to the wings at a nose up angle of 4 degrees measured from the ground level as reference. Ejector racks, also known as bomb rack, are the components used to suspend the stores onboard. In addition, through an internal release mechanism, racks provide a secure separation of the stores when intended in a flight. The design of the racks could differ by the weight and the size of the stores. Therefore, design criteria are established and specifically defined in the Military Standard for the General Design Criteria of Bomb Rack Unit (BRU), MIL-STD-2088. According to MIL-STD-2088, two types of rack unit are introduced and the classification of these racks basically depends on the weight of the stores to be carried onboard as shown in Table 1.

Table 1: Design Characteristics of Ejector Racks [15]

Type	Vertical Support Spacing	Maximum Carriage Mass
I	14 in (355,6 mm)	1450 lbs (657,7 kg)
II	30 in (762 mm)	5000 lbs (2267,9)

It should be noted that the system is designed to carry 2500 kilograms on each side. What relates external stores support system to range and fuel capacity is a unique mission equipment called External Auxiliary Fuel Tank. As the name implies, External Fuel Tanks (EFT) refer to auxiliary fuel tanks carried externally by an air platform. External Fuel Tanks, simply being considered as fuel tight component, are connected to the main tanks to supply contained fuel, which provides an extra range.

EFT structures are rarely found on platforms utilized for civil operations; besides, they have military dominant utilization especially on rotary-wing air platforms. [16]. For instance, Lockheed Martin F-16 Fighting Falcon is regarded as a multirole aircraft. The platform is equipped with seven store pylons and the equipment that to be selected might vary depending on the intended operation, as shown in Figure 3.

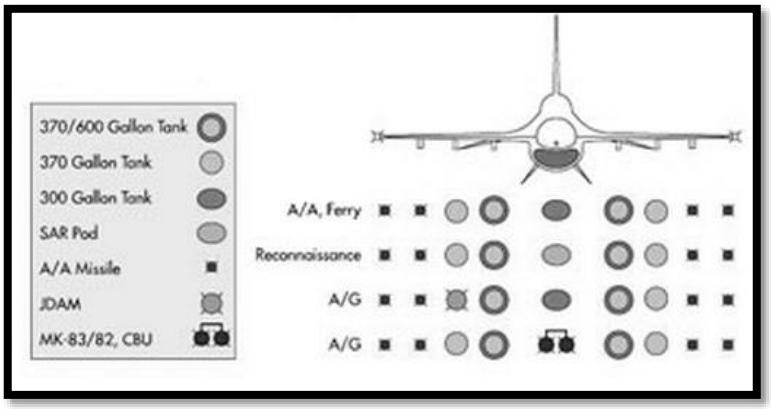

Figure 3: F-16 Fighting Falcon Typical Carrying Configuration [17]

F-16 has the capability to carry External Fuel Tanks, Synthetic Aperture Radar Pod, Air to Air, Air to Ground Missiles and Joint Direct Attack Munitions. A total of five external fuel tanks could be integrated to the platform which results in 40% extended range, 25% increased mission radius and doubled endurance [17]**.**

Table 2: Fuel Capacity of Fighting Falcon F-16 [17]

Fuel Location & Quantities	**F-16 Single-Seater Total Fuel Qty. [kg]**	**F-16 Two-Seater Total Fuel Qty. [kg]**
Internal	3175,1	2585,5
External	2267,9	2267,9
Total Usable Fuel	5543	4853,4
Increase in Fuel Quantity	***71,4%***	***87,7%***

Figure 4: Fighting Falcon with EFT [Turkish Air Force]

Sikorsky UH-60 Black Hawk has been offering a wide range of operational versatility including tactical transport and aeromedical evacuation since the day it entered the service in 1979 [11]. Sikorsky UH-60 Black Hawk is one of the platforms that utilize External Support System frequently. Two pylons on each wing enable the platform to carry up to four external fuel tanks as shown in Figure 5.

Figure 5: Sikorsky UH-60 Black Hawk [18]

With the fuel inside the main fuel tanks, UH-60 has a standardized range of 350 nautical miles (648.2 km); whereas two external tanks containing 757 liters of fuel permit UH-60 fly almost 600 nautical miles (1111,2 km). This additionally supplied fuel does not only extends the range by 71.4%, but also increases the endurance by one hour for the maximum endurance to reach beyond 5.5 hours [18].

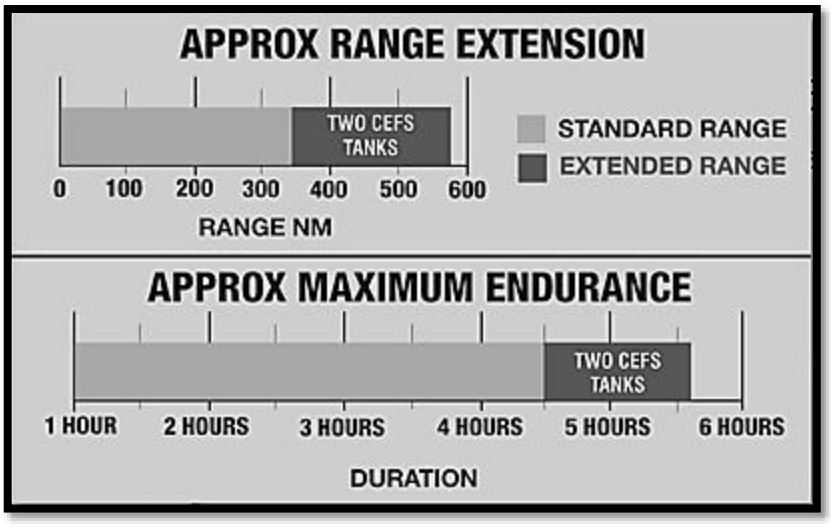

Figure 6: Range Chart of UH-60 [18]

On the contrary to the advantages of External Fuel Tanks, there are valid concerns associated with the use of EFT. It is a fact that weight is one of the key factors for a safe and efficient flight. Each unit of weight added to the platform would result in a loss of operational of the platform in terms of altitude, maneuverability, speed and range [19]. Keeping in mind that platforms have a certain allowable onboard weight to be able to operate, the EFT itself together with the contained fuel might impose a weight penalty. Moreover, Integration of External Stores Support System that accommodates External Fuel Tanks results in an increase of the flat plate area of the platform by 14,2 square-feet (1,32 m^2) [20]. As a result, a platform having ESSS installed suffer some inevitable drag during flight. However, as one of the most essential operational characteristics of air platforms is to transfer power and superiority to distant points, it is obvious that the future operations would have been performing farther from the aptitude areas. Thus, External Fuel Tanks would be not only choice but necessity to increase the capability of tactical mobility.

1.1. LITERATURE REVIEW

In 1940s, various methods and materials were being used to produce external fuel tanks, which were expected to provide specific requirements during World War II. When the U.S. Air Force first intended to develop external fuel tanks for fighter aircraft in the 1960's, strategic material of the era such as steel and aluminum were the common in production. McDonnell Douglas F-4 Phantom was known to be the first platform to utilize metal EFT having a capacity of 2271 liters.

In June 1967, an unfortunate incident happened on the flight deck of aircraft carrier, USS Forrestral. A missile was launched from a fighter by accident. While the incident could be considered as a disaster on its own, things got even worse when the missile hit a parking A-4 jet. There were external fuel tanks installed on the

platform and the missile ruptured them all. Due to the fuel spread, flames engulfed the platforms parked on the deck immediately. Sheer number of casualties, more than 100 seamen, revealed gravity of the situation. Hard facts came to light after the investigation. Studies showed that all-metal tanks performance in terms of ballistic piercing and rupture upon impact were below the expectations. Therefore, the Navy brought a specialized set of design and performance requirements including the ability to maintain the structural integrity in case of a release onto a hard surface etc. When General Dynamics and McDonnell Douglas collaborated to design an external fuel tank to meet the established standards in 1970s, that was the first time advanced composites became the material of choice in manufacturing [21].

Producing external fuel tanks requires appreciable know-how and experience, which makes them quite expensive to build and use. Besides, they require highly trained personnel for maintenance. Taking the aforementioned factor in consideration, external fuel tanks have military dominant utilization as strategic equipment. As a matter of the fact that the literature is quite limited, the literature could only be reviewed basing on patents related to the field of applications.

- **Collapsible Fuel Tank by Christian Kurrle (1944) [22]**

The first patent on the subject dates back to 1944. The aim of this study is to develop a collapsible fuel tank of the same capacity with the available metal tanks. The unique feature of collapsibility creates the difference. By nature, collapsible tanks require relatively less shipping volume so that a large number of tanks could be shipped abroad to field of World War II. During the war, fighters were sent on missions beyond their radius of action. To be able to perform such duties, platforms utilized steel or aluminum fuel tanks located under the wings. Such tanks are

discarded when empty. Hence, each flight corresponds to one or more expensive tanks loss. The second purpose of this study is to protect strategic material.

In this study, the body of the tank is made of cotton duck, canvas or cotton cloth instead of expensive metals, so that; they could be cut and sewed together to obtain the body. Eight cotton duck or canvas gores are sewed together along longitudinal edge to form the outer shell shown in Figure 7 . Each stitch has cotton stripes at the free edges. These cotton stripes provide both stiffness and reinforcement. In order to ensure the integrity, two or more bulkheads are placed inside the tank. The shell, bulkheads and seams are assumed to offer the required strength of the tank during its service.

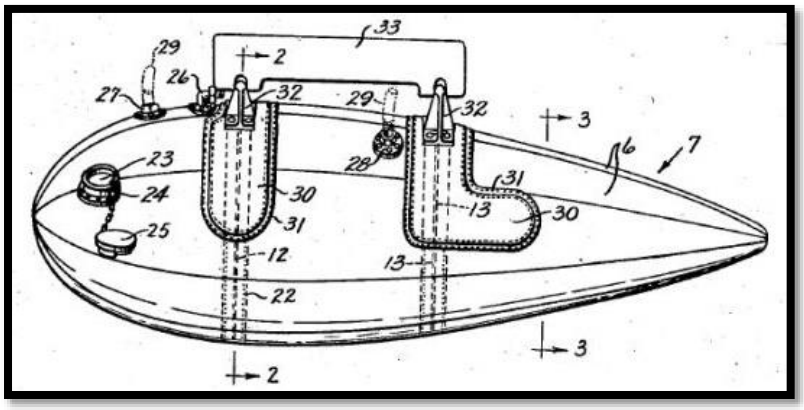

Figure 7: Collapsible Tank Body [22]

This invention claims that the tank described is lighter and much cheaper than aluminum fuel tank. The tank's capacity is about 283 liter and in terms of shipping space, one collapsible fuel tank is equivalent to fifteen of aluminum version.

- **Compartmented, Filament Wound, One-Piece Fuel Tanks by Edward Morrisey (1984) [23]**

The subject of the patent is a study related to an improved external fuel tank consisting of a cylindrical fuel cell with aerodynamically shaped ends. The effectiveness of an external fuel tank could be investigated through some operational factors. Weight is the driving factor that should be kept at minimum during development phase. External Fuel Tanks are intended to be operated at a temperature in range of -53^{o}C to +93^{o}C and a pressure in the range of -0,35 bar to 7 bar. Therefore, the aim of the invention is to provide an improved tank that satisfies all the identified factors.

The outer shell of the body consists of an elongated cylinder fuel cell with dome shaped ends. Multi layers are structured onto the assembled shell with resin-impregnated filament winding. This study provides the design and the method for manufacturing the claimed fuel tanks.

The fuel cell consists of a fuel-tight liner having dome shaped end portions. The liner is reinforced by laminations of resin-impregnated filament windings. The liner may be any kind of material, which is light in weight, fuel resistive, inert and insoluble in aviation fuel. Suitable materials for the liner, includes thermoplastic materials such as cross-linked polyethylene, polyester, elastomers, acetals and polyamides. To form the fuel cell, suitable filament having high modulus and high strength should be selected such as glass fiber or yarn, carbon yarn or fiber, aromatic polyamide fiber or yarn. The thickness and shape of the filaments may differ depending on the desired structural characteristics. Thermosetting adhesive resin should be selected according to the bonding and structural properties in impregnating the filaments. A proper selection could be made among polyester and epoxy. Upon the completion of the winding process, the body is cured as a final

step of the manufacturing. The curing process conventionally takes place in a temperature/time controlled oven.

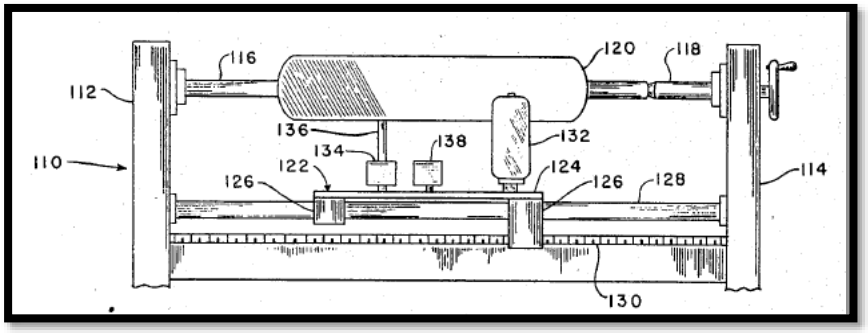

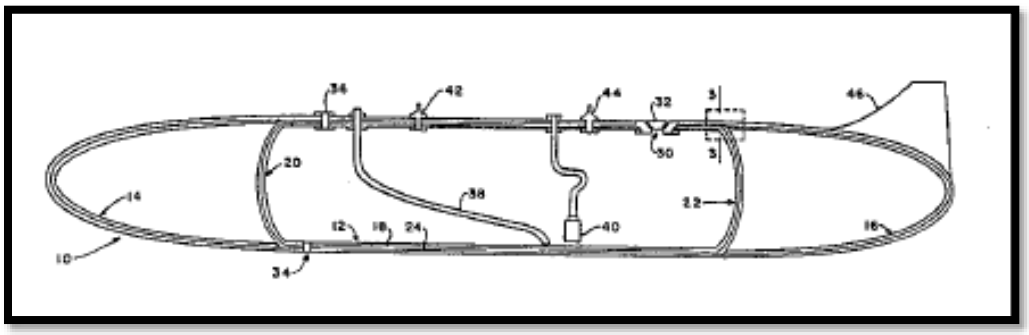

Figure 8: (a) Filament Winding Process (b) Overall View of the EFT [23]

- **Inflatable External Fuel Tank by Richard Lyman (1990) [24]**

Nestable fuel tanks are metal tanks that may be disassembled for the easiness of shipping and storage. As the name implies, the component of a nestable tank could be nested within each other, which provides a packaging density of 4:1 to 10:1. When these ratios are compared to the conventional fuel tanks, the volume

necessary to pack the components of 4 to 10 nestable tanks appears to be equivalent to the volume that is needed for a fully assembled external fuel tank. Nestable fuel tanks could be disassembled into three parts: nose and tail dome-shaped sections and cylindrical center section. Besides the advantages of the nestable tanks, they have some serious disadvantages need to be taken into account. For nestable tanks, there is no impact resistance. They break away easily which poses fire hazard. Nestable tanks being constructed of metal often explode when exposed to electrical short circuit, static electricity discharge, lightning strike, ballistic impact. Standard small-arms fires from thirty caliber rounds lead to catastrophic failures.

In contrast, external fuel tanks made of high strength composite materials using filament winding are not nestable in nature, but they offer an intense resistance to crash impact, fuel vapor ignition, ballistic impact and fire. These types of fuel tanks generally consist of filament wound inner/outer layers and structural rigid plastic foam or honeycomb structure located between them. Such high strength composite materials are often applied on a thin sealed metal or plastic liner. Thermosetting plastic resin is used frequently to impregnate the fiberglass. The aim of the invention is to provide a safe and survivable external tank, which also has high packing density. In this context, a tank whose outer shell is constructed by filament winding is developed. Instead of an internal frame, outer shell carries an I-beam shaped planar central support member. When the tank is empty, the shell of the tank collapses towards the support, which reduces the density. Otherwise, when the tank is filled, the original shape having extremum dimensions could be achieved easily. The outer shell around the support structure around is manufactured with filament winding technique. Thermoplastic or thermosetting resin is used to provide desired flexibility. In order to pre-stress the shell, a liner is kept inflated during the manufacturing process. For the central support member inside the tank, any suitable method of manufacturing may be used. The common technique is that the structure may be constructed in the form of two halves along the longitudinal axis center. Derived half structures are joined later. Perspective view of the central support

structure of the product developed in this study is given in Figure 9 where the numbers 37 and 38 are designated to show baffles consisting of semi-circular elements hinged to the central support. In case of nesting, baffles are closed towards the support shown with the number 37. As a matter of the fact that a sudden change in center of gravity cause flight dynamics problems and put the flight safety at risk. Baffles made of composite materials, prevents sloshing of the fuel in the extended position denoted by 38.

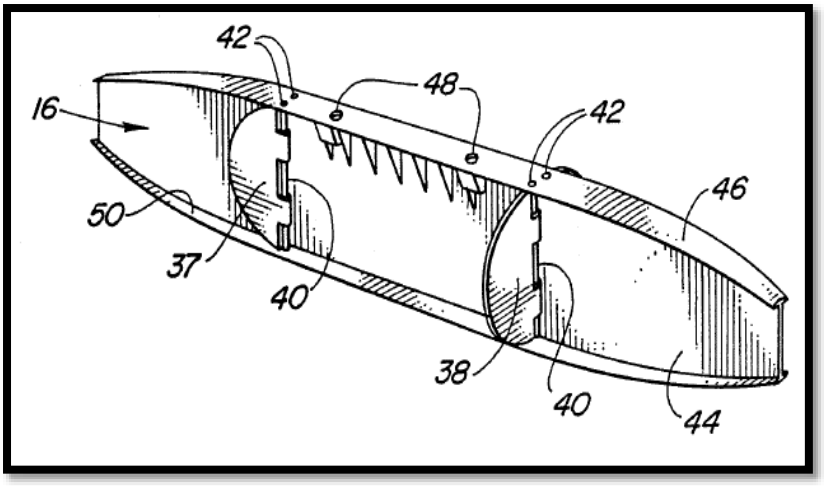

Figure 9: Perspective View - Central Support Member of Inflatable EFT [24]

- **Crashworthy External Auxiliary Fuel Tank by Jeff Bracken (2002) [25]**

The objective of the invention is to provide a new and improved external fuel tank. The novelty of the claimed tanks is that they offer crashworthiness. The term crashworthiness stands for the ability to assure structural integrity in the situation of crash. Depending on the platform involved, external fuel tanks could be

jettisoned. However, there may be limited time for the tanks to be ejected properly. Therefore, crashworthiness becomes a vital factor in increasing the survivability of the platforms. Furthermore, in the situation of combat, external fuel tanks are vulnerable to small-arm fires. It is therefore could be considered as an objective to self-sealing ability to the developed tanks so that they withstand small-arm fires without any leakage or rapture. The developed external fuel tanks consist of a forward and a rearward aerodynamically shaped shell being joined by a center structure as most of the conventional fuel tanks do. The outer shell is constructed of composite materials with a honeycomb configuration. There is a polymeric liner within the outer shell, which provides crashworthiness. All of the openings in the bladder are sealed for fuel tightness and high-pressure resistance. In this particular embodiment, the total weight of the tank with the fuel is carried by the center structure. Therefore, it is constructed of lightweight but very strong glass-fiber.

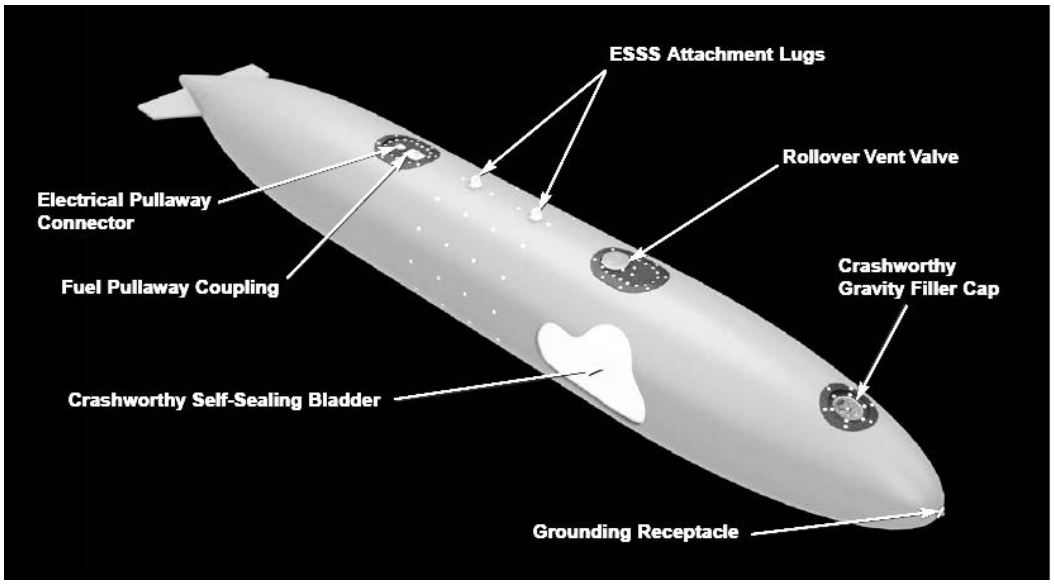

Figure 10: Perspective View of the Crashworthy External Fuel Tank [18]

1.1.1 Current Trends in Material and Manufacturing Technology

In chronological order, the reviewed patents reveal the current trends for material and manufacturing technologies. Since the first external fuel tank employed over 70 years ago, various development paths have been opened by time and technology. The materials and techniques used to manufacture EFT have progressed continually. While the traditional materials have been replaced by advanced composite materials, new manufacturing methods have been developed concordantly.

Composite materials could be described as a unique combination of two or more materials resulting in superior properties that cannot be obtained with the individual components employed alone. These components being the reinforcement and matrix are not dissolved in the combination, and they retain their own chemical, physical properties. Fibers or particulates are usually preferred as the reinforcement, which are the major load-carrying member, whereas the matrix as a load transferring medium, keeps the reinforcing elements in the desired orientation, protects them from environmental damages and supports the reinforcing elements in the transverse direction. The matrix might be a polymer, a metal or a ceramic [27,28].

The most common form of the composite materials in structural use is Fiber-Reinforced Polymers (FRP). FRP features polymer matrix such as epoxy, polyester and vinyl ester, and commercially available glass, aramid and carbon fibers as the reinforcing elements.

1.1.1.1. Reinforcing Fibers

As mentioned before, fibers are essential constituents of FRP. Selection of the fiber has a direct influence on the density, cost and the mechanical properties of the composite material. Therefore, a proper selection of the fibers requires the consideration of the type of loading, operational environment and manufacturing process. There are four frequently used and commercially available fibers in the market, namely E-Glass, S-Glass, Aramid and Carbon.

Glass fibers are the most commonly used reinforcing fibers in industry. The main reasons for preferring glass extensively as the reinforcement are low cost, high tensile strength, good chemical resistance and high impact resistance. However, they have low tensile modulus and high density [27,28].

E-Glass has the lowest cost among the reinforcing fibers. Although E-Glass does not provide superior impact resistance, it has high strength and stiffness. S-Glass which was developed especially for aerospace and defense industries has relatively high tensile strength when compared to E-Glass, whereas it is much more expensive than E-Glass [27,28,29].

Aramid fibers are organic and aromatic polyamide fibers. Due to the highly crystalline structure of the aramid fibers, they provide thermal stability and lowest density together with highest tensile strength-to-weight ratio among the aforementioned fibers. A unique advantage of the aramid fibers is their impact resistance. Combining the impact resistance with high tensile strength and modulus, aramid fibers are the most prevalent form used for the applications including ballistic impact. On the other hand, aramid fibers are weak in compression, and cutting or machining the aramid fibers are extremely difficult with ordinary tools,

since the fibers tends to fuzz easily. Therefore, special tools are needed for machining operations [27,28].

With high tensile and compressive strength, high modulus and good fatigue characteristics, carbon fibers are frequently used for structural components. Carbon fibers provide a wide range for mechanical properties. Therefore, for applications requiring different mechanical properties, different types of carbon fibers could be preferred. The major disadvantages of the carbons fibers are low strain-to-failure characteristics, weak impact resistance and high cost. Tensile stress-strain graph shown in Figure 11 is obtained from single filament tests of the commercially available reinforcing fibers.

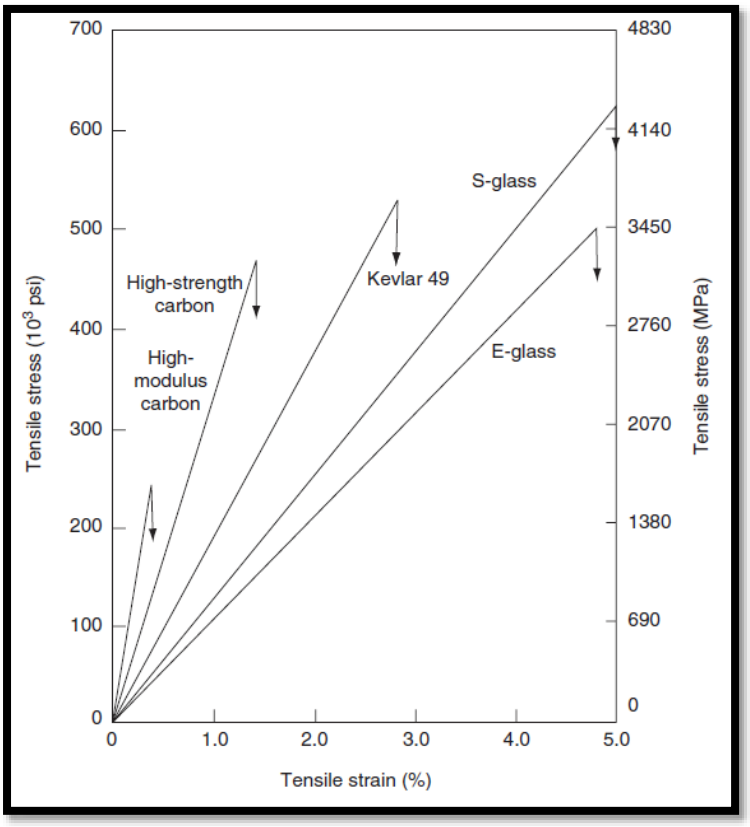

Figure 11: Stress-Strain Graph of Reinforcing Fibers [28]

1.1.1.2. Matrix Systems

The matrix materials play a critical role in keeping the reinforcing fibers in desired orientation, transferring the loads to fibers and protecting the fibers from the adverse environment including chemicals and moisture. In addition to the major roles, the selection of the matrix determines the in-plane shear properties, damage tolerance and the maximum operating temperature of the composite material such that the glass transition temperature should be higher than the use temperature [27,28].

Polymeric matrices (Resins) could be divided into two sub-categories: thermoplastics and thermosets. Thermoset polymers have low molecular weight, and they are chemically combined by three-dimensional cross-links during polymerization reaction. Once the thermoset polymers are fully cured, they cannot be remelted. In contrast, thermoplastic polymers are not chemically cross-linked, but rather they are joined by weak secondary bonds. Due to the fact that they are not cross-linked, the weak bonds of the thermoplastic polymers could be broken upon the heat application. After the bonds are broken temporarily, thermoplastic polymers could be consolidated in a new configuration, and the bonds are restored on cooling [27,28,29].

For high-performance composite applications, thermoset polymers are preferred. Thermoset polymers provide thermal stability, chemical resistance and better fiber-matrix interaction over thermoplastic polymers. The most commonly used thermoset polymers could be listed as: polyester, vinyl ester and epoxy [27].

Polyester polymers are used in wide variety of commercial applications. Although, polyester offers versatility in processing with fast curing time and low cost, they have low mechanical properties, poor adhesive characteristics and high shrinkage

Vinyl esters are very similar to polyesters in nature. However, vinyl ester matrices are tougher and exhibit better adhesive strength when they are compared to polyesters [27,28].

Epoxy matrices have proven their value in high performance composite applications. Epoxy matrix has many advantages over the other thermoset polymeric matrices such as they offer low shrinkage, excellent chemical resistance and superior adhesive characteristics. The polymerization reaction transforms the liquid form of epoxy to the solid state. The mechanical properties, curing time and curing temperature directly depends on the curing agent and cross-link density. Higher the curing temperature and longer the curing time, higher the mechanical properties could be achieved [27,28].

1.1.2. Filament Winding Process

The prominent manufacturing method in the presented patents is a process having a high production rate called Filament Winding. Filament Winding is regarded as one of the oldest and basic composite manufacturing method in which the continuous resin-impregnated fibers are wound on a rotating mandrel in a controlled manner. This method could be used to manufacture cylindrical composite structures such as drive shafts, pressure vessels, motor cases, pipelines and missile launchers [30]. A schematic of a basic filament winding process is shown in Figure 12.

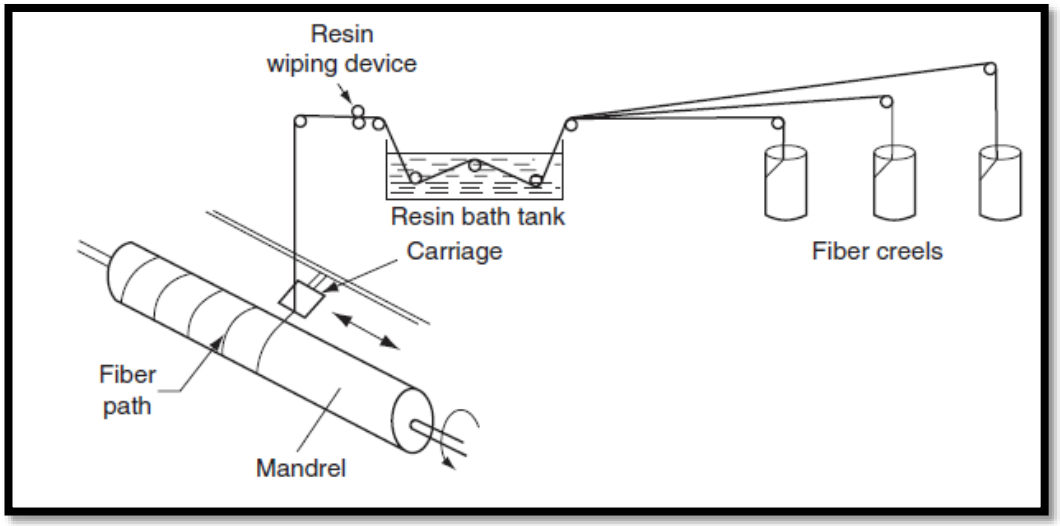

Figure 12: Schematic View of a Filament Winding Process [28]

The fundamental manufacturing process includes pulling the dry fiber rovings from the creels. The dry fibers go through a liquid matrix bath. At the exit of the bath, wet fibers are directed through a wiping mechanism to remove excessive matrix from the rovings. Properly wiped resin-impregnated fiber rovings are gathered together in the form of a band and applied on the mandrel [28,30].

By adjusting feed rate of the carriage unit and the rotational speed of the mandrel, three basic winding patterns could be obtained as shown in Figure 13. In polar winding, the mandrel remains stationary, while the carriage rotates about the longitudinal axis. Hoop winding is the relatively simple process. In this winding process, mandrel is rotating at a higher speed than in the case of helical and polar winding and one full rotation of the mandrel advances the carriage forward for one bandwidth. Thereby, the bands are wound adjacent to each other. In helical winding, the mandrel rotates, while the carriage is fed back and forth. The motion of the carriage enables the fiber band to create a weaving with plus and minus winding angle [27,30].

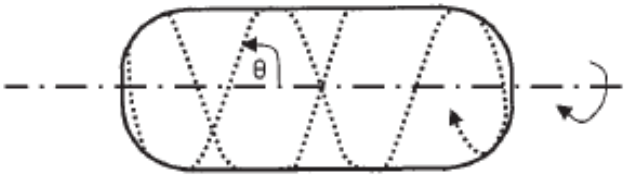

(a) Helical Winding

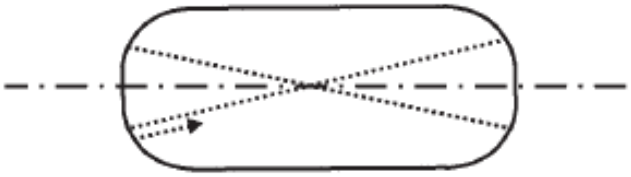

(b) Polar Winding

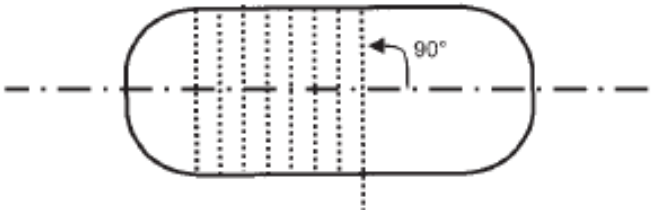

(c) Hoop Winding

Figure 13: Winding Patterns [27]

It should be emphasized that the hoop winding could only be applied to the cylindrical portion mandrel, yet the helical and polar windings could be applied to both the cylindrical and domed portions [27].

After the winding is attained to the desired thickness, the filament-wound should be cured on the mandrel. Therefore, mandrels should be extractable from the filament-wound shell after the curing is complete [30]. The choice of the mandrel depends on the size and the structural requirements of the part to be wound. For the parts having a closed geometry, a steel extractable mandrel, which has a taper along

its length, might be used. But in this case, the filament-wound body should be produced by first manufacturing and integrating two symmetrical shells. However, in order to facilitate a one-time manufacturing and eliminate the necessity of bonding operation, dissolvable mandrels could be used. Especially for the parts having small openings, water-soluble mandrels could be used without damaging the filament-wound structure. The mandrel is dissolved out with water after the curing process so that a seamless one-part composite shell is achieved. One last alternative for the mandrel used for one-time manufacturing is inflatable mandrels, which might be left inside as a permanent component of the composite body or extracted from an opening [27,30].

In the research article written by Cohen [31], the design and manufacturing variables that play a critical role in the quality of composite vessels were examined. In order to assess the hoops strength, stiffness, fiber and void volume fraction, residual stress and inter-laminar shear strength, an experimental approach was used. Material and process variables were identified prior to the experiments. The results presented statistically showed that the composite vessel strength was a function of manufacturing and design variables. Specifically, stacking sequence, winding tension and winding time had a major influence on the quality. The samples having high fiber volume in the hoop layers posed high strength according to the conducted experiments. Since high winding tension resulted in high fiber volume, the key variable effecting the composite strength became winding tension.

Analysis of multi-layered filament-wound composite pipes under internal pressure could be investigated from the research article written by Xia, Takayanagi and Kemmochi [32]. An exact elastic solution for the stress and deformation of the multi-layered composite pipes was examined by means of three-dimensional anisotropic elasticity. In the analysis, three different stacking sequence with a winding angle ranging from 30 to 55-degrees was employed. For a pipe having an inner radius of 50 mm was subjected to an internal pressure of 10 MPa. The results

showed that the resultant stresses and deformations depended directly on the stacking sequence. The assigned wall thicknesses were found to have the major effect on the stress distribution.

Another aspect of filament-wound composite structures was investigated in the research article written by Mertiny, Ellyin and Hothan [33]. The performance of multi-angle filament wound against an internal pressure and an axial force was evaluated. In this present study a filament-wound structure with a $[\pm 60_3]_T$ lay-up was selected as a baseline, and it was compared to $[\pm 45, \pm 60_2]_T$ and $[\pm 30, \pm 60_2]_T$ configurations basing on the experimental data. The results revealed that the $[\pm 45, \pm 60_2]_T$ and $[\pm 30, \pm 60_2]_T$ configurations reduced the axial strain, and increased the structural strength.

The influence of winding patterns on the damage behavior of the filament-wound pipes was studied in the article written by Rousseau, Perreux and Verdiere [34]. The objective was set to identify the influence of the winding pattern on the mechanical performance of filament-wound structured under various loadings. For this purpose, tubes with $[\pm 55_6]$ lay-up made of glass-epoxy was manufactured and put through mechanical testing. Damage growth was shown to be increased by the degree of interweaving of the tubes. The authors claimed that the crossovers of the helical windings represented defects where cracks could appear.

A unique study investigating the grid-stiffener was presented in the article written by Buragohain and Velmurugan [35]. In this experimental study, three different types of circular cylindrical structures were taken into consideration: unstiffened shell, lattice cylinder (with ribs only) and grid-stiffened shell (with skin and ribs). Axial compression tests were carried out and the results were compared with finite element analysis. Although processing and testing imperfections existed, the positive effect of the stiffeners demonstrated under compressive loading.

Mertiny et al. [36] investigated the influence of the stacking sequence on the strength of the multi-angle filament wound tubular composite structures. In the experiments, two batches of specimens with the $[\pm 45, \pm 60_2]_T$ and $[\pm 60_2, \pm 45]_T$ layup were used. By applying axial force and internal pressure, failure characteristics, stresses and strains at failure and the failure modes of the specimens were compared. The winding angle of 60-degress was chosen to provide good characteristics for a pressurized structure. The winding angle of 45-degrees was chosen to provide hoop as well as axial reinforcement. The results showed that positioning of axial reinforcement on the outside provided higher strength under stress ratios with a high axial component, whereas an axial reinforcement on the inside of the tubes resulted in higher strength under strongly hoop-dominated loading scenarios.

The influence of the winding pattern on the mechanical behavior of filament wound cylinders was examined by Hernandez-Moreno and his research group [37]. In order to obtain mechanical response of filament-wound tubes, cylindrical specimens that were 350 mm long, 125 mm internal diameter, 4.4 mm thickness were used. Winding angle in the central section was ±55-degrees. Two pattern architectures were selected as one or five unit cells. The experimental results revealed that the winding patterns had not strong influence on the buckling behavior of the filament-wound composite tubes. Therefore, it was shown that the winding pattern did not play a significant role in the buckling behavior of the tubes.

An experimental study with ±55° filament-wound composite tubes was performed by Tarakçıoğlu et al [38]. In this study, the fatigue behavior of filament-wound composite pipes under alternating internal pressure was examined. The manufactured specimens had a winding angle of 55-degrees. These specimens were put through a fatigue test conducted according to ASTM-D2292. During the tests three major damage mechanism were observed, whitening, leakage and final failure. The results of the experiments were presented as S-N curves.

Will, Franz and Nurick presented their work, which focused on the effect of the stacking sequence of the filament-wound tubes subjected to projectile impact. [39] The specimens used in the study were two filament-wound tubes having a lay-up [-35º/+35º/90º$_3$/-35º/+35º/90º$_3$/-35º/+35º] (A) and [90º$_6$/(-35º/+35º)$_3$] (B) respectively. These two tubes were subjected to impacts up and above the ballistic limits. According to the results, specimen having the stacking sequence of (B) was found to be better performing. The ballistic limit for (A) was about 70 m/s, while the limit for (B) was determined to be 95 m/s. The major energy dissipating mechanism due to material failure was found to be delamination followed by shear fracture. Matrix cracking posed a small proportion of the energy dissipated by material failure.

In a research article written by Martin, Fernando and Hale [40], the usage of embedded fiber sensor for impact damage detection was introduced. The goal of the study was to detect threshold levels of impact damage in filament-wound tubes. Two types of sensor were used, (i) a simple crack detection system where the fracture of the optical fibers was correlated to the level of impact damage and (ii) a novel intensity-based optical fiber sensor, which was used to measure the stiffness, change in the filament-wound tube as a function of impact damage. The first sensor was on-line which provided information during service, whereas the second sensor was designed for off-line analysis to provide more detailed information about the impact damage. The crack damage detection system was tested on ±75° glass-reinforced epoxy filament-wound tubes upon a low-velocity impact. An impact level of 8J was determined as the critical case for thin-walled tubes. Embedded optical fiber crack interceptors, which fractured when they experienced a direct impact, were succeeded in capturing the impact damage. The primary damage characteristics was matrix crack beneath the impact point

CHAPTER 2

STRUCTURAL DESIGN PROCESS

Although the importance of the fuel systems is not generally recognized, the utilization and the functional features of them are regarded as essential in terms of the design and operational characteristics of the platform. In order to provide a full comprehension on the subject of external fuel system, the correlation of the external fuel system with the air platform should be investigated carefully.

The system design is the most vital phase on the product development process. During this phase, all of the interfaces and the subsystems of which the fuel tank should be composed should be well defined. The design drivers of the external fuel tanks as a complex system are directly related to fundamental performance and operational requirements. Therefore, it is critical that all the factors involved should be examined carefully. These important factors, which should be taken into account, could be listed as follows [26]:

- The intended air platform operation
- External fuel tank boundaries and location
- Measurement and management system
- Electrical power system

Each design drivers is identified and discussed under the following headlines.

2.1. INTERFACE DESIGN

External fuel tanks establish dynamic relationships with both ambient and the platform on which they are installed. Figure 14 is a diagram illustrating the interfaces between air platform and external fuel tanks. Platform provides accommodation and electrical power to EFT. As a jettisonable equipment, EFTs are installed on the store pylons, which are designed to allow jettison of loads when necessary. Furthermore, electrical power required by the tank for the fuel transfer pump and level switch to operate properly is supplied by the platform through mating connectors. In return, EFT provides the information for the cockpit indications including the status and the amount of fuel remaining in each of the tanks installed.

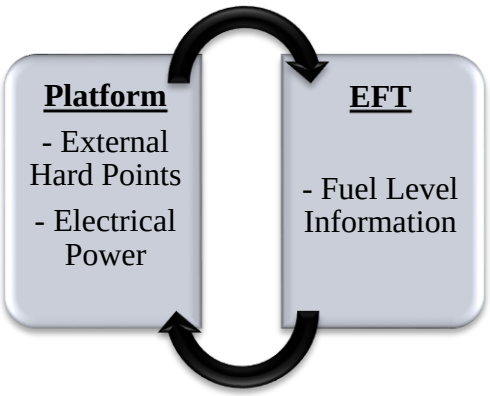

Figure 14: Interface between Platform and EFT

Besides the platform, EFT is in interaction with the external ambient. EFTs are supposed to have a capability allowing any water and foreign objects that settles to

be drained to the outside environment. Moreover, EFT breathes in order to prevent build-up of pressure reaching critical level during refueling process. For installation, maintenance and inspection purposes, all sub-systems of the tank should be designed to permit full access from the outside.

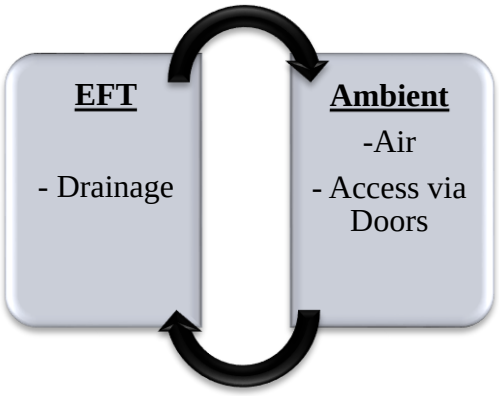

Figure 15: Interface between EFT and Ambient

2.1.1. User Interface

A system having a complexity as such in external fuel system requires a quite sophisticated management system. For this purpose, a cockpit control panel capable of monitoring and managing the fuel transfer is located on the central panel shown in Figure 16. Fuel management control panel monitors the amount of fuel in both internal and externally installed tanks by means of fuel probes. The system is operated in one of the two transfer modes through the series of switches on the panel; automatic or manual transfer mode.

Figure 16: Central Cockpit Panel [14] & Fuel Management Control Panel [41]

In order to minimize the workload, automatic transfer mode could be selected by placing the XFER MODE switch to AUTO. In the case of AUTO mode, fuel transfer starts when the fuel in main tank falls below a critical level. Fuel transfer continues until the fuel in main tanks reached up to certain level. Finally, the AUTO MODE could be deactivated by placing the XFER MODE switch to OFF or MAN, or when the external tanks are empty. However, the common practice is to use the manual mode rather than the automatic mode. Similarly, Manual transfer mode could be selected by placing the XFER MODE switch to MAN. The pilot gains absolute control with manual mode. Fuel transfer will continue as long as MAN is selected. When the internal tanks are full, management system warns the pilot with NO FLOW light appearing on the control panel. To avoid pumping air into the main tanks, fuel transfer should be directed to a relatively empty external tank to maintain the balance on the platform [14,41].

First versions of the external fuel tanks being developed and used during World War II were intended to be discarded when the fuel inside the external tanks was consumed. Formerly admitted practice is quite contrary to the modern external fuel

tanks. Since the modern external tanks are superior on the structural and performance aspects, the need of discarding in order not to suffer from drag and additional weight is eliminated. In other words, modern external fuel tanks do not pose vulnerability in normal flight as well as in combat. However, in an emergency, external fuel tanks should be designed to be jettisoned during flight. Furthermore, in a combat situation, external fuel tanks may be jettisoned for the sake of gaining maneuvering and speed advantage. In such situations, while pilot is forced to choose between jettisoning the installed tanks or retaining them; there are some factors must be considered such as environmental aspects, performance limits of the platform, structural capability of platform and the tank itself. Similar to fuel management system, store jettison could be controlled by rotary selector switch located on the top of the lower panel as shown in Figure 17. This panel enables pilot to jettison all external stores in a selective manner or symmetrical jettison of the fuel tanks in order not to disrupt the balance of the platform.

Figure 17: Jettison Panel [14]

2.2. SUBSYSTEM DESIGN

A wide range of fuel system designs are implemented on today's air platforms. In contrast to the increasingly difficult operating requirements, the capabilities of the external fuel tanks are improved by time and technological developments. Although similar in appearance, modern external fuel tank incorporates latest fuel system equipment to meet the requirements throughout the operational envelope. Under this headline, detailed description of the subsystems associated with a reliable external fuel system is given. A modern external fuel tank consists of three subsystems as shown in the Figure 18.

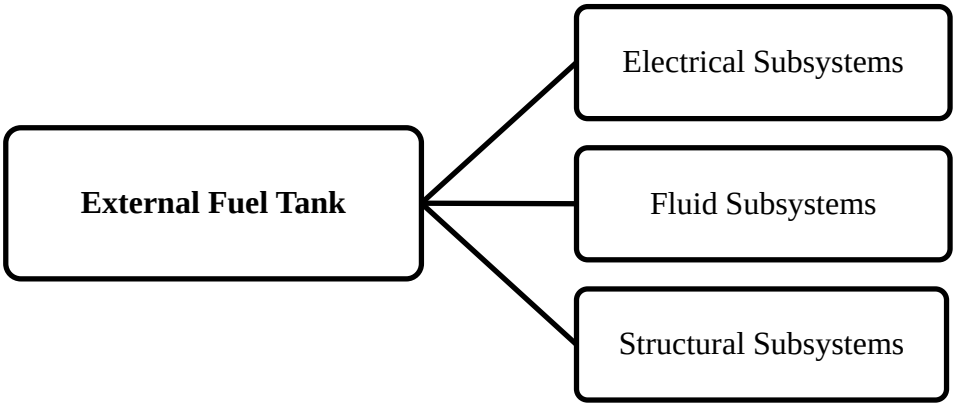

Figure 18: Subsystems of an External Fuel Tank

2.2.1. Electrical Subsystem

The primary purpose of the electrical system is to provide electrical power required to operate fuel transfer pump and level switch. All components of the electrical subsystem are designed in accordance with MIL-DTL-38999. The electrical subsystem of the EFT consists of the following components:

- Electrical Connector
- Electrical Line

2.2.2. Fluid Subsystem

For any fuel system including external fuel tanks, it is necessary to provide clean fuel flow to the engine. Regardless of the flight conditions, engine power, altitude and maneuvers, it would be desirable to ensure an uninterrupted supply of the stored fuel for flight safety. Therefore, the design and the selection of the fluid system become a major operational issue. A typical fluid subsystem of a modern external fuel tank consists of the components listed below:

- Refueling Cap
- Transfer Pump
- Level Sensor
- Drain Valve
- Vent Line
- Breakaway Valve
- Fuel Transfer Lines & Fittings

The intent of this study is to develop an advanced external fuel tank structure. No effort was made on the choice of electrical and fluid subsystems. Due to the fact that the tanks being developed within the scope of the study would be interchangeable with the existing tanks, the currently used electrical and fluid subsystems are integrated to the tank structure that is being developed.

2.2.3. Structural Subsystem

Structural subsystems consist of the tank body and the interfaces required to integrate the subsystems. The design and construction of the aforementioned structural subsystems are investigated in this particular study. The main structure of an external fuel tank is designed to carry and transfer fuel to the main tanks of the platform. The subsystem is intended for the storage of aviation fuels such as jet propellant-4, -5 and -8 (JP-4, JP-5 and JP-8). External fuel tank as a slim cylinder joined to the aerodynamically designed torpedo-shaped nose and tail cone, acts as a leak-proof housing to all the parts required for a reliable fuel system and supports external mounting on air platforms [42,43]. Since appreciable amount of fuel is supposed to be carried on the tanks, external fuel tanks should have a sufficiently strong body.

External fuel tanks vary in geometry and capacity being directly linked to the operating envelope of the platform. During structural design process, the objectives and design criteria are established by the manufacturer of the air platform and the military as the end-user. Once the design characteristics and the physical interfaces are identified, 3D modeling process has been initiated. The design process relies on the core elements of Computer-Aided Engineering (CAE) software. 3D Computer-Aided Design (CAD) is created by means of one of the world's leading commercial software in aviation industry, Computer Graphics-Aided Three-Dimensional

Interactive Applications (CATIA™) Version 5 that is developed by Dassault Systemes. Part design, assembly design and generative shape design workbenches are used in different stages of the modeling process. In order to secure the removal and jettison operations, the outer diameter and the length of the external fuel tank should stay within the limits of the port zones.

Structural design process was carried out in two stages; the construction of the main body consisting cylindrical shell joined to nose and tail cones and the sump. The reason why the sump is handled separately from the main body is that the sump has its own unique design characteristics.

Fuel contamination poses a serious threat for fuel system safety. If left unwary, contamination results in corrosion of the system components, clogging of the filters of the transfer pump and even blocking the fuel transfer to the main fuel tanks. Once the fuel transfer is interrupted, the engine becomes destitute of fuel, which causes the air platform to experience power loss. Although, there could be various types of fuel contaminants in aviation fuel, the most common ones are given below.

- Water: Water in the aviation fuel is either suspended or present as a liquid. During high altitude operations, both external fuel tanks and the contained fuel get cold. As a result, fuel accumulates at the bottom of the structure and eventually freezes. The resulting ice particles might clog the filter of the fuel transfer pump. Moreover, as the platform descents to the altitudes having warmer temperatures, absorption of the moisture from the environment might take place. If measures are not taken and the water remains in the fuel, it will promote corrosion and microbial growth [26,44].

- Microbial Growth: As the name implies, microbiological growth is the presence of living organisms that grow wherever water exists in the fuel tank. For microbiological organism to grow, water should be present in the

fuel. Unless the fuel system is cleaned entirely, the organisms continue to develop increasingly. The presence of microorganisms causes fuel filters to plug and it promotes the corrosion of the components of the fuel system [44].

- Sediment: Sediment consists of dust, powder, fiber and strains which could enter the system through the opening of the tank. Maximum allowed sediment contamination is in the order of 2 milligrams per liter. Exceeding the contamination limit is an indication of inadequate cleaning which results in clogging of the filters [26,44].

Preventing the fuel contamination reaching critical levels requires a proper construction of the sump. Fuel systems should have a sump allowing drainage of contaminants to the external environment. In addition, running the fuel transfer pump dry for extended periods of time over the specifications stated by the manufacturer might lead to the failure of the fuel transfer. Although the transfer pumps are designed to maintain the functionality for at least 100 hours of dry operation, the sump being the housing for the fuel transfer pump ensures the pump would be submerged into the fuel at times during flight. As a result, the pump together with the components would not prone to any failure caused by the fuel starvation.

The fuel stored at the sump is regarded as unusable. As a matter of the fact that the unusable fuel forms an inevitable weight penalty since the portion of fuel cannot be used and delivered to the platform, minimizing the requirement for unusable fuel is crucial. The amount of unusable fuel is directly related to the tank geometry and the selection of the fuel transfer pump. Therefore, it is preferable that the sump is located at the low point of the external fuel tank, permit any contaminant that settles from the fuel to be drained under gravity and provide the required amount of fuel to the transfer pump so that it does not cavitate during fuel transfer [26,42].

The last factor in determining the internal capacity of the external fuel tank is the expansion space. Expansion space as necessary in all fuel systems is the volume required to prevent overfilling during refueling process, and to compensate the thermal expansion of the fuel. According to Federal Aviation Regulations, each external fuel tank must have an expansion space, which corresponds at least two percent of the overall tank capacity [26]. In the light of the given information, the design criteria defined for the design of the external auxiliary fuel tank, which is being developed in this particular study, are given in Table 3.

Table 3: Design Characteristics of the Main Body

Design Characteristics	**Specification**
Length	3100 mm
Outer Diameter	430 mm
Usable Fuel Capacity	350 lt. at the attitude of 0°
Unusable Fuel Capacity	8 lt. at the attitude of 0°
Expansion Space	2 percent of the total fuel capacity (usable plus unusable fuel)
Depth of the Sump	80 mm
Target Weight	25 kg (maximum)

The structure, which is being developed in accordance with this study, consists of a cylindrical shell joined to dome shaped nose and tail shells. The sump with the identified features is aligned to the center at the bottom of the cylindrical shell as shown in Figure 19.

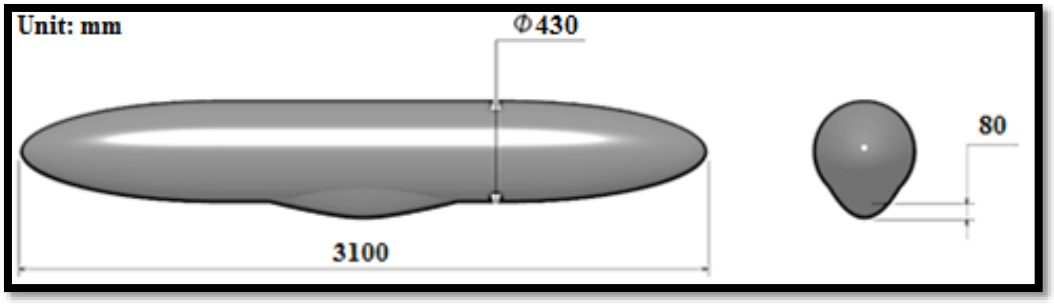

Figure 19: Overall Dimensions of the External Fuel Tank

Following the identification of the design criteria, studies are conducted in order to provide an optimum system layout. Components, which ensure the functionality of the fuel system, are positioned on the predefined installation points of the filament wound shell. The installation of each individual component is achieved through the interfaces providing a secured and sealed connection. For that purpose, mounting interfaces meeting the specific installation requirements are designed. General assembly layout is given in Figure 20 to provide full comprehension on how refueling and transfer functions are accomplished.

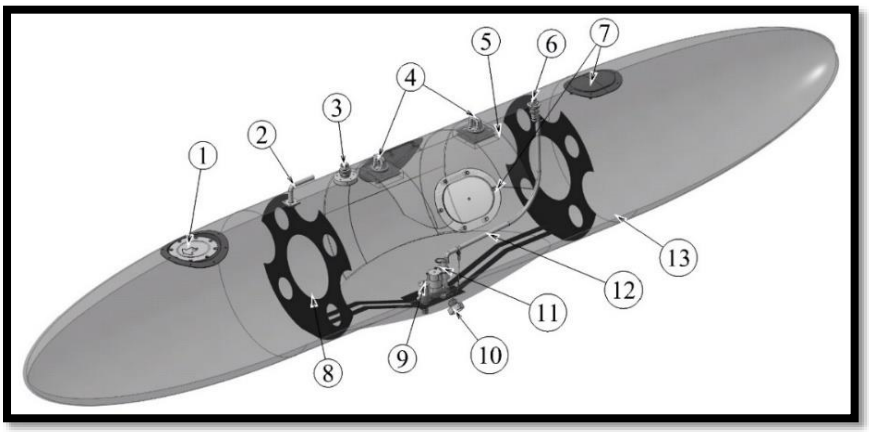

Figure 20: External Fuel Tank Assembly

Figure 20 shows the external fuel tank assembly in which the fuel system hardware is indicated by reference numbers. The following table gives the list of the parts indicated in Figure 20.

Table 4: Part List of the EFT Assembly

Part No.	Description	Quantity per Each Tank Assembly
1	Refueling Port	1
2	Vent Line	1
3	Electrical Connector	1
4	Suspension Lugs	2
5	Inner Frame	1
6	Breakaway Coupling	1
7	Access Doors	3
8	Slosh Baffles	2
9	Fuel Level Switch	1
10	Drain Valve	1
11	Fuel Transfer Pump	1
12	Fuel Transfer Line	1
13	Filament Wound Outer Shell	1

Returning to Figure 20, external fuel tank should carry a total of three access doors, one on the upper surface and two symmetric ones on the central section. The access doors permit access to the interior of the tank for inspection, maintenance and installation of the fuel system components. In order to prevent leakages, each door

is required to be sealed into the place with a gasket. Bolts are used to secure each door as shown in Figure 21.

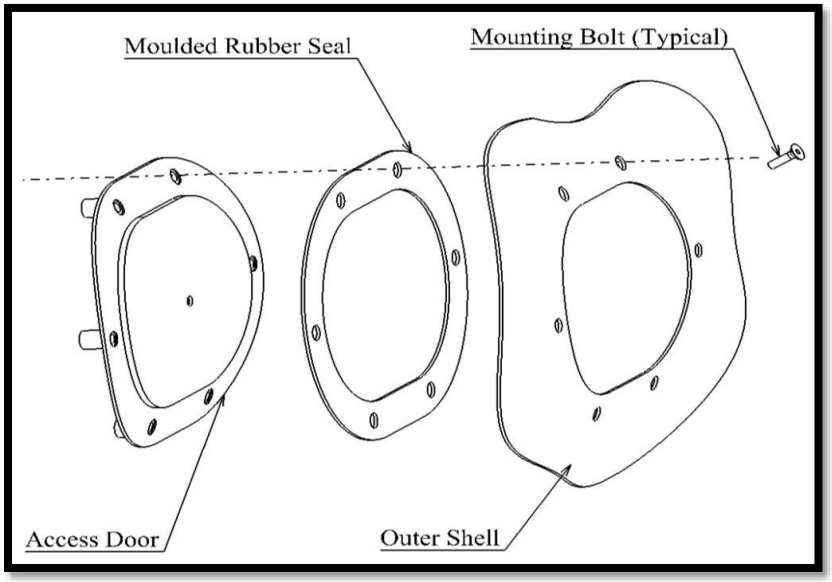

Figure 21: Access Door Location

In the center of the tank, a structural component called the frame is located inside the filament wound shell. The frame is designed to have an outer radius that is compatible with the interior of the shell. As a load-carrying component, frame is utilized to provide internal support and the mounting assembly. Storage weight is the major driving factor in determining the design characteristics of the mounting assembly.

The key property of the fuel is the density concerning the operational range requirements. Since the measure of the energy stored in the external fuel tanks is a function of mass, the available fuel load required to meet the operational

requirements is directly proportional to the fuel density. According to the detailed specification of the kerosene type aviation turbine fuel, MIL-DTL-83133H where the chemical and physical properties of the jet propellant-8 (JP8) are specified, the average density of JP8 is 0.81 kg/L [45]. Therefore, basing on the design characteristics given in Table 3, the external fuel tank, when filled to full capacity, reaches a maximum weight of 315 kilograms.

Referring to Table 1, it could be seen that the selection of the ejector racks denoted as Type I would be sufficient for the system being developed (see Figure 22).

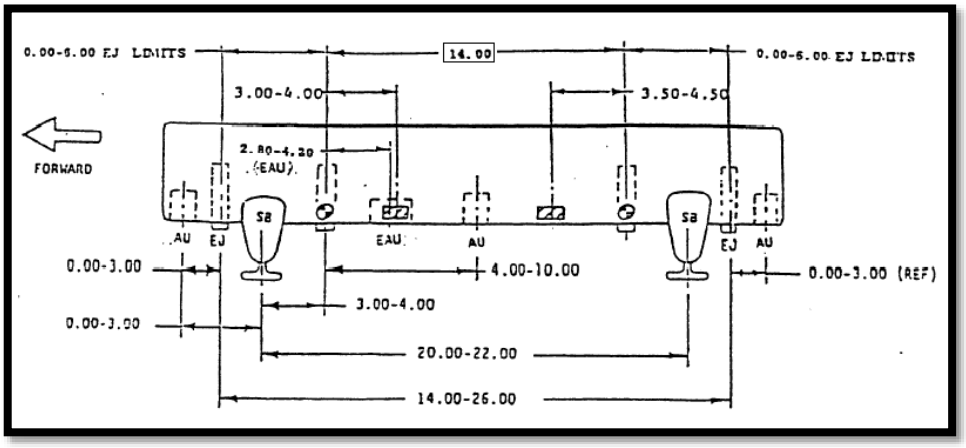

Figure 22: Geometric Relations of the Type I Rack Unit [15]

Type I rack unit is symmetrical about the midpoint and it provides two store suspension hooks, which are 14-inch away from each other. The interface between the external fuel tanks and the rack unit of the platform is provided by the suspension lugs, which could be considered as the primary attachment points enable the tank to be hung to the ejector rack unit. The required number and the spacing of the suspension lugs are specified in the Military Standard for Airborne Stores and

Suspension Equipment, MIL-STD-8591. Table 5 gives the detailed lug configuration by weight class.

Table 5: Weight Class and Lug Configuration [46]

Weight Class [kg]	Weight Range [kg]	Number of Suspension Lugs	Spacing [in]
45,36 (100 lbs)	9,07 to 45,36	2	14
453,59 (1000 lbs)	45,81 to 657,71	2	14 or 30

The specification for two-store suspension hook with a spacing of 14-inch configuration suggests two weight class of which the selection is based upon the store weight. The maximum weight that the external fuel tank would reach lays between the ranges defined for the 1000 lbs weight class. The suspension lugs for 1000-lb weight class conforms the specifications given in Figure 23.

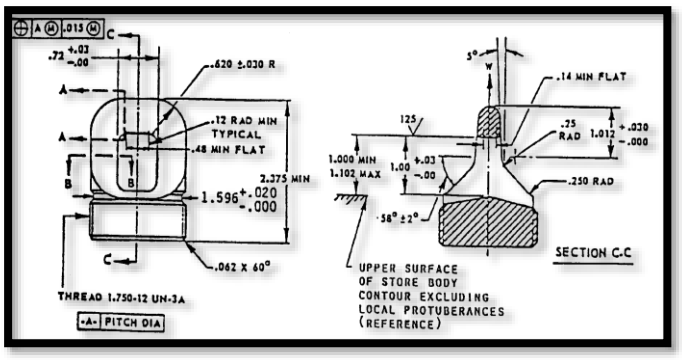

Figure 23: Suspension Lugs for 1000-lb Weight Class [46]

The suspension lugs are steel which provide a strength of 18143,69-kilograms (40000 lbs). A threaded steel mounting interface is designed to provide a safe junction for suspension lugs. Suspension lug mounting interfaces are anchored to the filament wound outer shell of the tank and they are not replaceable by nature (see Figure 24).

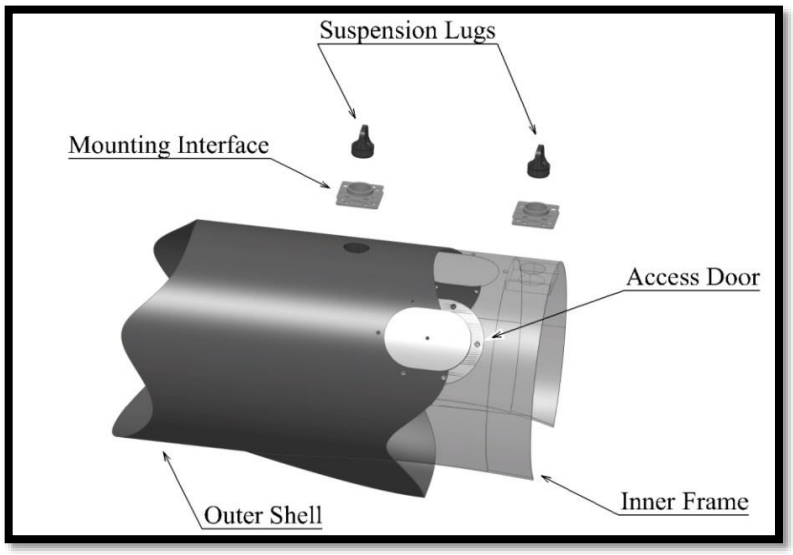

Figure 24: Exploded Perspective View of the Center Structure

As mentioned earlier, outer shell of the external fuel tank carries the fuel system components. The upper surface of the tank receives a gravity refueling port, ventilation valve, electrical connector, breakaway coupling and a rearward access door. Hereinafter design and installation details are included in considerable detail.

Aviation fuel nozzles have a unique design having a static bonding wire that must be attached to the platform before refueling. The refueling cap should be designed accordingly to provide a safe connection with the refueling adapter through the

hose. Gravity refueling is the simplest system for fuel delivery. Nose cone carries the gravity filler port as shown in Figure 25 in such a configuration that the remaining volume above the lower limit of the port corresponds to the minimum required volume for the expansion space. In other words, excessive filling into the expansion space is prohibited by the location of the gravity filler port itself. The common refueling practice starts with unlocking the cap lifting and rotating the tab in counterclockwise direction as defined in MIL-C-38373. Fuelling nozzle is compatible with the filler adapter; so it could easily be inserted inside the tank. Once the tank is properly filled to a desired level, the refueling cap locks and seals the filler port [26,47].

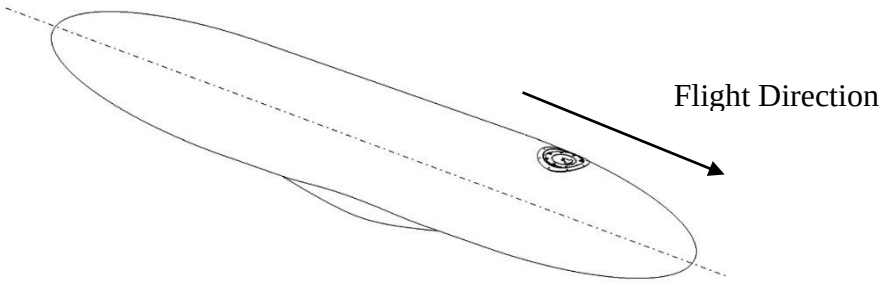

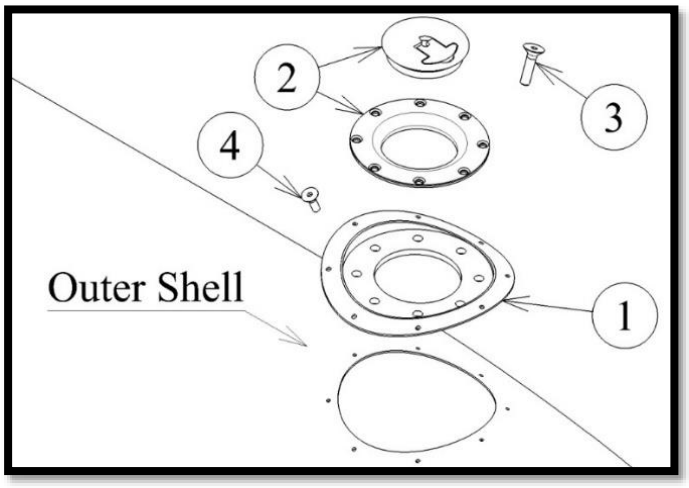

Figure 25: Locator View of the Gravity Filler Cap

Table 6: Part List of Filler Cap Assembly

Part No.	Description	Quantity per Each Tank Assembly
1	Filler Cap Mounting Interface	1
2	Filler Cap	1
3	Self-Tapping Hexagon Socket Countersunk Head Screw (M7)	8
4	Self-Tapping Hexagon Socket Countersunk Head Screw (M4)	8

As a component of the external fuel tank that is being developed, filler cap interface ensures a reliable integration for the filler cap as specified in MIL-C-38373. A surface preparation is required prior to the installation of the filler cap mounting interface. The bonding area, the tank wall and the bottom surface of the particular interface, should be wiped with a solvent moistened cheesecloth. The epoxy adhesive should be prepared first; and it should be applied on the surfaces intended for bonding. The self-tapping screws should be inserted to the pre-drilled holes to verify the alignment of the filler cap mounting interface. After the screws are tightened, the epoxy adhesive should be left to cure for further operations. A proper sealant should be selected and applied in the form of a fillet at the edges of the interface. Once the sealant is fully cured, the filler cap interface could be considered integrated to the filament-wound outer shell. The installation of which the details are introduced could also be applied for the installation of filler cap to the interface itself.

Within the operational envelope of an air platform, quite high pressure differences occur as the platform ascends and descends. That much of a pressure difference might lead to a catastrophe for the external tank. In order to avoid resultant

excessive pressure difference, external fuel tank is connected to the atmosphere through vent line. Vent line located in front and on the upper face of the tank as shown in Figure 26 performs the breathing function during flight and gravity refueling [26,48].

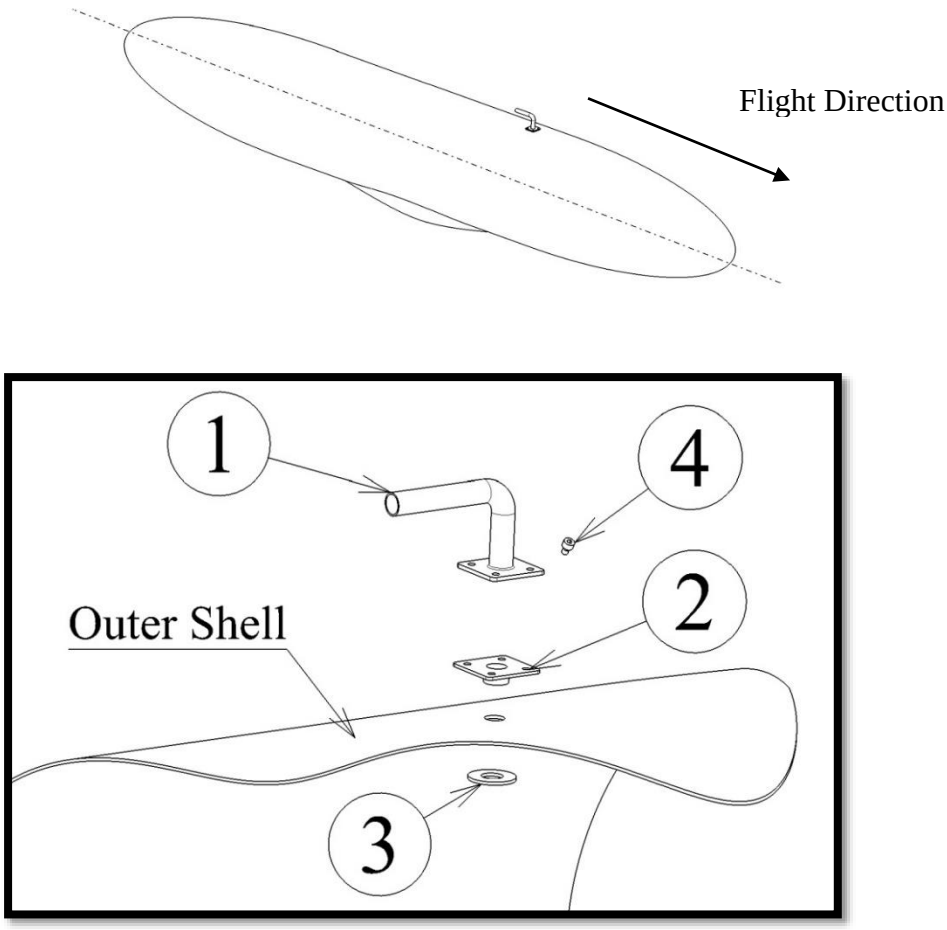

Figure 26: Locator View of the Vent Line

Below is a list of components that enable the vent line to be installed on the predefined zone of the outer shell.

Table 7: Part List of Vent Line Assembly

Part No.	Description	Quantity per Each Tank Assembly
1	Vent Line	1
2	Vent Line Mounting Interface	1
3	Vent Line Housing	1
4	Hexagon Socket Head Cap Screw (M5)	4

Installation process is carried out as described previously in detail. After cleaning of the surface, an epoxy adhesive is prepared and applied to the tank wall and underside of the mounting interface. In order to obtain maximum bonding performance, the interface is inserted, aligned and allowed to cure. A sufficient period of time should be given for curing; then, the vent line is placed into place and its assembly is accomplished by means of the screws. After making sure that the venting line is in position, the installation is completed by tightening the threaded housing down securely. Finally, sealant is applied to the component liberally.

The electrical connector should be located on the upper surface of the outer shell, and in the case when the pilot decides to jettison the external fuel tanks; it should ensure a safe disconnection of the connectors between platform and the tank. Figure 27 provides the locator view of the electrical connector.

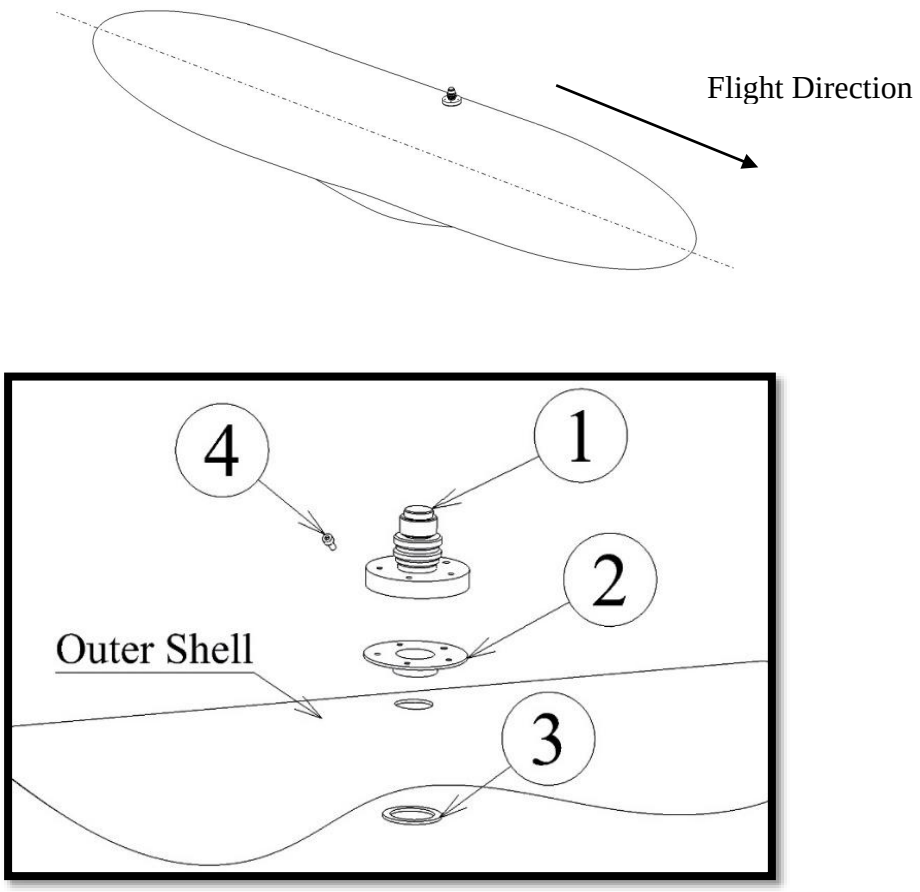

Figure 27: Locator View of the Electrical Connector

The list of the components in the exploded view is given in Table 8.

Table 8: Part List of Electrical Component

Part No.	Description	Quantity per Each Tank Assembly
1	Electrical Connector	1

Table 8 (continued)

2	Electrical Connector Mounting Interface	1
3	Connector Housing	1
4	Hexagon Socket Head Cap Screw (M4)	5

For installation, the procedure defined for vent line and gravity refueling cap should be referred and followed.

As mentioned in the previous sections, external fuel tanks are designed to be jettisoned in an emergency situation. During jettisoning operation, breakaway connections establish the interface with the platform's systems such as avionic, electrical and weapon. It is the responsibility of the breakaway coupling to prevent fuel spillage that might adversely affect the systems on the platform [26]. Therefore, breakaway coupling gives the external fuel tank the ability to be disconnected from the platform easily during jettison or disengagement. The breakaway coupling should be installed on the upper surface of the filament-wound outer shell as shown in Figure 28.

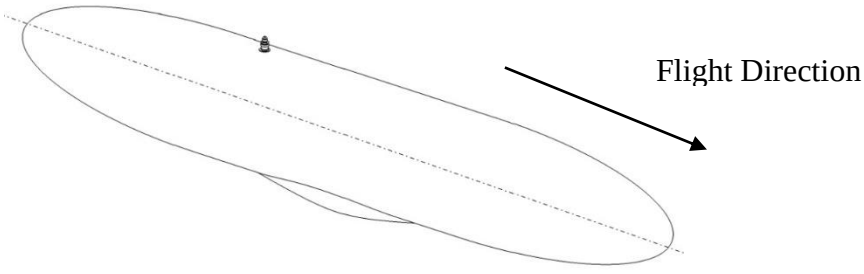

Figure 28: Locator View of the Breakaway Coupling

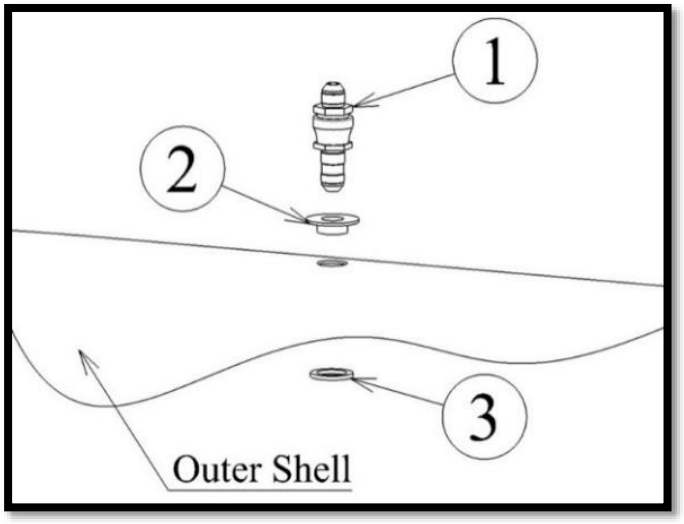

Figure 28 (continued)

Table 9 gives the list of components required for breakaway coupling to be integrated to the outer shell.

Table 9: Part List of the Breakaway Coupling Assembly

Part No.	Description	Quantity per Each Tank Assembly
1	Breakaway Coupling	1
2	Breakaway Coupling Mounting Interface	1
3	Breakaway Coupling Housing	1

For the integration of the breakaway coupling, the installation steps defined previously should be referred. After applying the bonding procedure, the breakaway

coupling is threaded into the mounting interface. The tightening could be performed with the help of a spanner wrench. Tightening the threaded housing down and applying the sealant are the last steps of the installation process.

Providing at least one drain valve of suitable size to an air platform fuel system is a standard design implementation. When the plane is on the ground, drain valve allows drainage of the entire fuel including water and foreign objects that settle down at the sump. In the case of utilizing multiple valves, each should be located properly so that both usable and unusable fuel could be drained safely. Hence, the locating of the valve should be in the bottom centerline of the external fuel tank. Another feature of a reliable drain valve is that, it must be readily accessible from outside and it should ensure a safe locking mechanism [26,42].

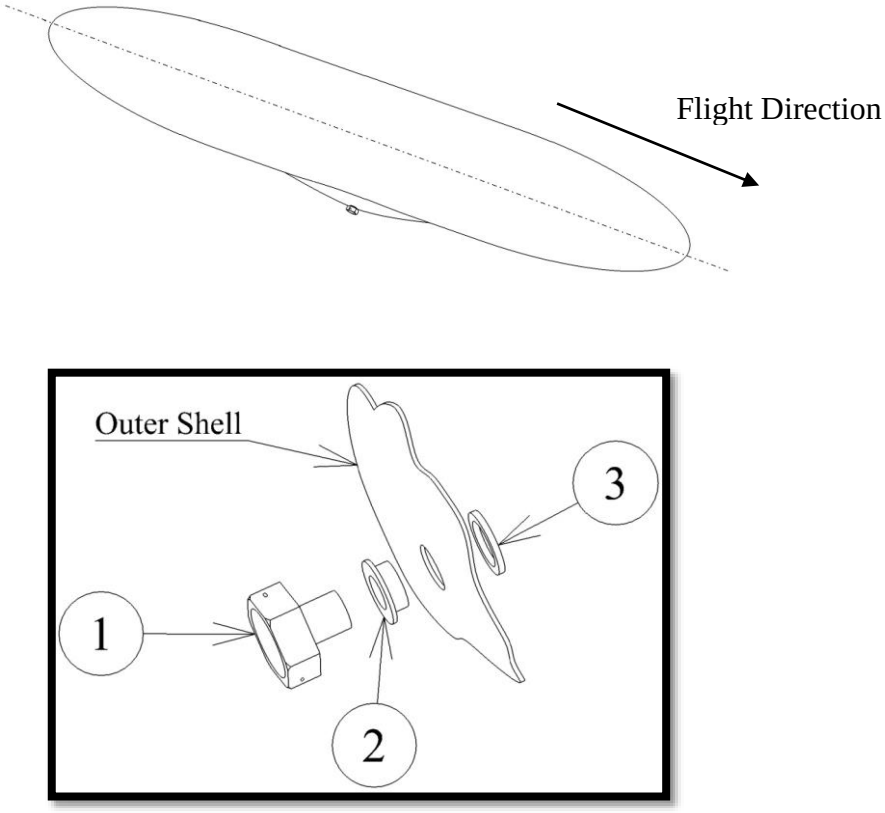

Figure 29: Locator View of the Drain Valve

Table 10 gives the list of components shown in the locator view of the drain valve.

Table 10: Part List of the Drain Valve Assembly

Part No.	Description	Quantity per Each Tank Assembly
1	Drain Valve	1
2	Drain Valve Mounting Interface	1
3	Drain Valve Housing	1

In order to install the drain valve in place, the mounting interface is inserted through the installation hole located in the tank wall. Then, the drain valve is directly threaded into the mounting interface. After making sure that the drain valve is in correct position, the mounting interface is secured in position by tightening the threaded housing down securely.

In external fuel tanks, free surface motion is a common problem. Sloshing being induced by the maneuvers of the platform imposes additional forces and moments, which may affect the stability and the control of the platform adversely. Rapid motion and sloshing, therefore, should be damped and prevented. Rigid slosh baffles are designed and employed inside the external fuel tank to suppress excessive weight variation caused by free fuel motion 143[49]. Prior to the winding process, slosh baffles are positioned on the mold and they would be left inside filament wound outer shell. Consequently, baffles shown in Figure 30 are bonded to the shell to increase the hoop stiffness of the structure, and they are not replaceable and repairable.

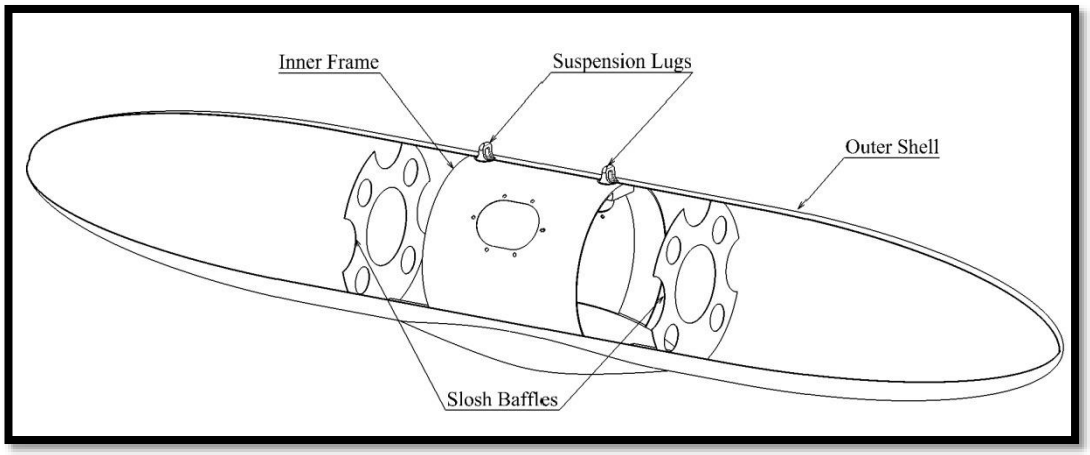

Figure 30: Locator View of the Slosh Baffles

The task of delivering fuel from the external tank to main fuel tanks is carried out by fuel transfer pumps. Although, the fuel transfer could be performed by fuel pressurization, electrically driven centrifugal transfer pumps offers a simple system with low weight, high reliability and easy installation. They could be adapted to perform over a variety of operation conditions. Military standard established for transfer pumps is MIL-F-8615. According to the standard, the transfer pump should be located on the bottom end of the tank body since it should be submerged in fuel at all times during a flight in order to prevent cavitation. Furthermore, transfer pumps are expected to be operated at elevated temperatures together with high vapor pressure. Therefore, for a reliable fuel transfer, pumps should incorporate necessary hardware not to affect engine operation by overheating [50].

In addition, modern external fuel tanks utilize level sensors, which measure the fuel level inside the tank. In order to maintain the flight safety, pilots should be provided with an accurate reading of the fuel inside the external tank so that they plan the flight accordingly. Therefore, level sensors are the key elements of the fuel management system; since they ensure that, the fuel level does not drop under a critical level. There are a number of different sensor types: float type, optical etc.

Float level sensors offers a simple and effective way of determining the fuel level. As the float rises or lowers to the actuation level, the sensor measures the fuel level and provides cockpit indications through fuel management system. Together with the fuel transfer pump, level sensor should be located at a predefined level on the bottom end of the tank body [26,48].

The space envelope required for installation and operation of the fuel transfer pump and level sensor is provided by a structural component, which is designed as an extension of the slosh baffles. Together with the baffles, the mounting base shown in Figure 31 would be left inside filament wound outer shell, which makes them irreplaceable and irreparable.

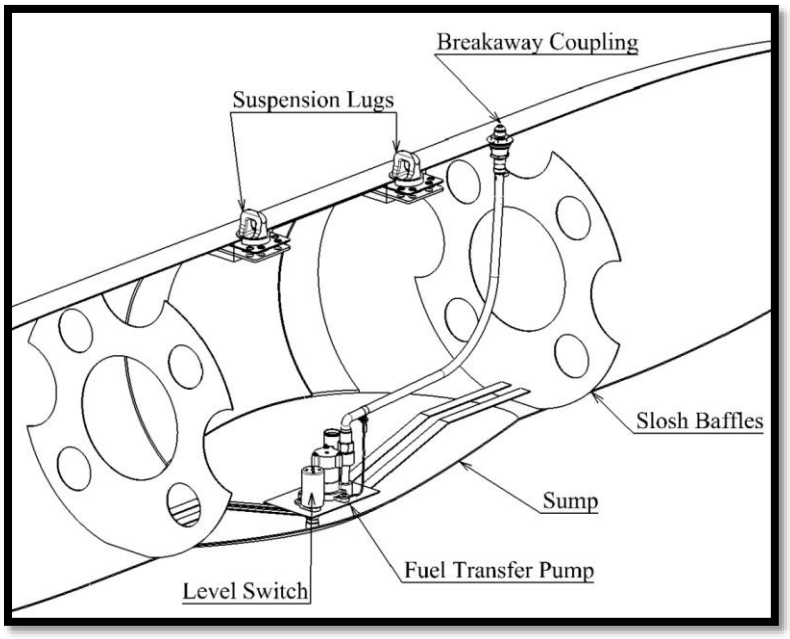

Figure 31: Perspective View of the Sump Area

The fuel level float located on the same level with the transfer pump flange opens the circuit as the fuel descends to the predefined level, which corresponds to the minimum volume of fuel required to preserve the transfer pump from cavitation.

Fuel transfer lines are used to deliver the fuel supplied by the fuel transfer pump to the breakaway coupling, which is also, knows as fuel connection port. Both installation and implementation of the fuel lines and fittings have strict standards to ensure the reliability of the external fuel tank. Selection of all the fitting and lines depend on the location, application and requirements of the fuel flow of the fuel system. Fuel transfer lines could be either flexible or rigid in nature. It is expected from the fuel lines to withstand to fuel pressure and flight loads. Therefore, in a fuel system like external tanks where vibration exists, flexible hoses are preferred over the rigid ones. In addition, fuel lines should be installed so that there is no strain left on the fittings. A small bend might be necessary to absorb vibration or expansion/contraction caused by temperature changes. In order to be able to match these requirements, some flexible fuel lines have a synthetic rubber interior with a reinforcing fiber braid wrapped on it, whereas some may have a braided stainless steel casing [42].

CHAPTER 3

VERIFICATION PROCESS

As with all fuel systems, modern external fuel tanks are as both unique and complex. As is known external fuel tanks are utilized in intolerable conditions. In case of a possible failure, the effects associated with it could cause serious structural damage to the platform and could put the flight safety at risk. In order to ensure safe functionality of the fuel system, structural integrity becomes one of the most vital consideration. Therefore, these specialized tasks bring a number of strict requirements associated with the design of the external fuel tanks.

According to the Military Specification identified for the design, test and installation of external aircraft fuel tanks, MIL-T-18847, external fuel tanks should be designed to carry fuel satisfactorily, without any leakage, under the conditions of installation, vibration, temperature, pressure, and loadings [51]. Given the external fuel system as a whole, fuel load comprises the majority of the weight of the system. Therefore, within the entire mission and operational spectrum, inertia load induced by the fuel, varying fuel loads and shifts in weight should not adversely affect the outer shell of the external tank. In order to be able to reach a sufficient level of performance, the external fuel tank structure must be designed strong enough to maintain structural integrity and ensure fuel transfer to the main tanks under various loads.

Before the external fuel tanks could be manufactured and introduced to market, the success of the proposed design solutions needs to be verified and the functional

performance of the product is required to be examined in every structural aspect. Traditionally, the anticipated verification methods consists of basic engineering calculations; however, as the level of complexities involved in the structure gets higher, traditional methods become inadequate. In addition to the complexities associated with the geometry, a number of hard challenges are introduced by the very nature of the composite materials. Composite materials features unique modelling challenges including multiple layers, various fiber orientations and thicknesses [52]. Unlike conventional isotropic materials, composite materials extend the limits of structural design since the unique properties of advanced composites enable to tailor the structure according to the requirements in question [53]. In order to meet the conformance with the desired task, variables like fiber orientations, thicknesses and the number of layers should be taken into consideration.

Traditionally, in order to verify the structural performance of the structure, a sufficient number of product should be manufactured. Then, the prototypes are put through several test cycles. The primary objective of conducting physical testing is to examine the behavior the structure being exposed to wide range of forces encountered in the real-world environment. It is obvious that the cost of the design and installation of the test setup is quite a lot. When manufacturing costs are added to this, the resulting costs reach a level that becomes challenging to compensate within the project budgets. Considering the fact that the design and development is an iterative process, the resulting cost is likely to increase as the process progresses.

At this point, a special approach, which is more comprehensive when it is compared to the trial-and-error methods, is needed. With the advancements in the computer technology, the demanded approach comes with CAE tools. As a CAE tool, computerized simulations are adopted at different stages within the design and development phase. The ability of highly developed simulation tools enable to reflect the real-world into a virtual environment where complex model could be

created and various operational conditions could be tried within a short period of time. Hence, rather than putting the products into actual experimentation cycles, simulation tools help to reduce physical prototyping and expensive testing [54]. Another benefit of using simulation tools is that they provide an accurate and deep understanding about the actual performance of the structure.

There is a wide variety of commercially available simulation tools specifically dedicated to structural simulations by taking the continuous system and idealizing it as an assemblage of small but finite sized elements [52,55]. This method is referred as Finite Element Method (FEM) that is the approach used as the basis of the numerical analysis. Each of the commercial software platforms, which are being used effectively for structural analysis, offers their own advantages. On the other hand, due to the capability of modelling layer composite materials, one of the most preferred and reliable simulation software, ANSYS™, is employed throughout the verification process. The Finite Element Analysis (FEA) is performed in ANSYS Mechanical interface by employing ANSYS Workbench based workflow given in Figure 32.

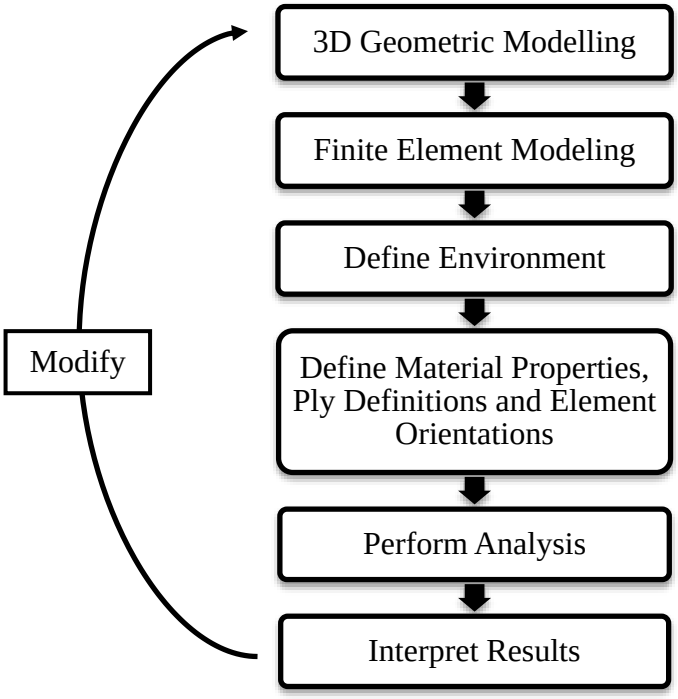

Figure 32: FEA Workflow [55]

In this workflow, ANSYS Composite PrepPost (ACP), which is a recently developed add-on module, is introduced to the workflow for modelling and tailoring layered composite structure. In order to define the intended simulation properly, interaction of the systems is required. The project schematic shown in Figure 33 illustrates how the workflow of the project is identified. The links between the columns represents data sharing. The link with a square indicator implies that the systems share the common geometry, whereas the link with spherical indicator implies that the solution is transferred to the following cells [56].

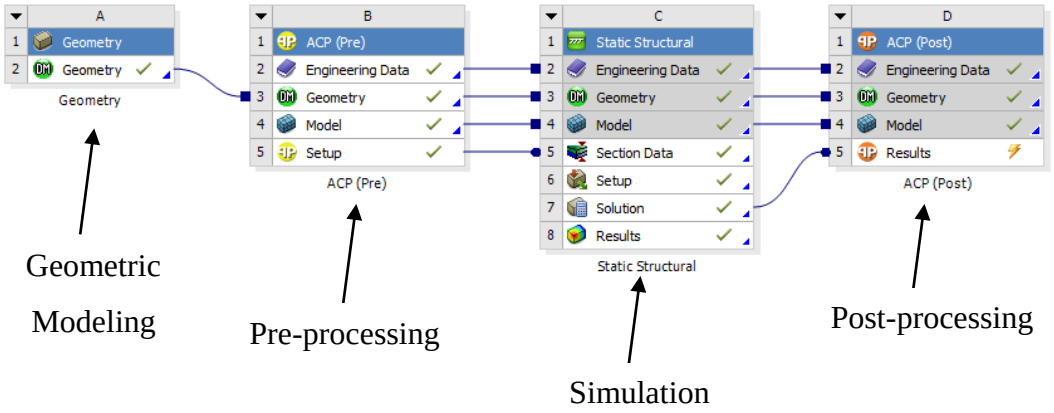

Figure 33: Project Schematic

3.1. 3D GEOMETRIC MODELING

Because of fact that all of the simulations are based on the geometry representing the actual design of structure, generation of the 3D CAD model is the initial task of the entire development process. Although, ANSYS provides a feature-based application called Design Modeler to execute 3D models, existing CAD geometries could easily be imported to ANSYS Mechanical platforms. Since ANSYS provides enhanced capabilities and supports, CATIA V5, without the need to change the format, readily available geometry is introduced to workflow.

3.2. FINITE ELEMENT MODELING

An approach called top-down is used to create FE Model. Top-down approach refers to creation of 3D CAD model first and representing it as a complex system of elements and points called nodes [57]. As most of the commercial simulation

software, ANSYS provides an automated mesh generation. The quality of the mesh associated with the given geometry plays an essential role in achieving an accurate and reliable solution.

While, a mesh containing a high amount of elements provides a closer approximation in defining geometric details, as the number of elements increases, computation time increases accordingly; and in some cases employing excessive number of elements could lead to convergence errors [58]. Therefore, the mesh density could vary throughout the domain. The regions at which high stress and strain gradients are expected to be observed require an intense mesh. However, coarser mesh could be enough at relatively simple regions. In general, a good quality mesh is considered to have a proper density and a reasonable mesh distribution. Unfortunately, the discrimination of the mesh quality whether good or bad, depends very much on the modeler's meshing strategies [56]. By means of Finite Element Modeler capabilities, ANSYS provides assistance to the user for investigating the quality of the mesh with respect to various quality metrics shown in Figure 34.

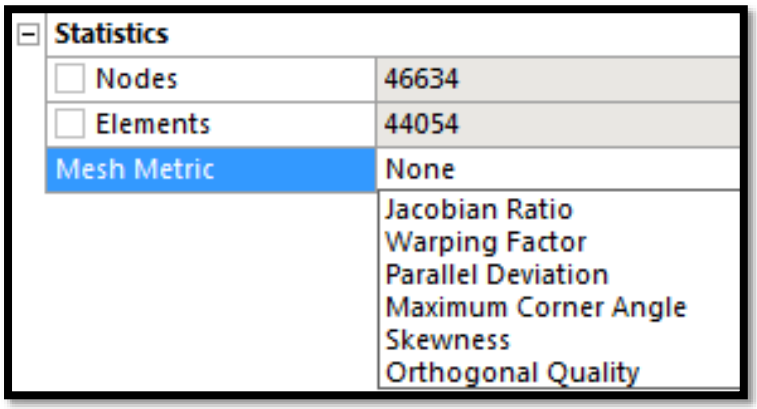

Figure 34: Mesh Metrics in ANSYS

To give the statistics, FE Model is constructed by a total of 46634 nodes and 44054 elements. SHELL181 element is generally preferred in the applications including thin to relatively thick-layered composite shells. SHELL181 is a four-node element with six degrees of freedom: translation along x, y and z direction and rotations about x, y, and z axes [56].

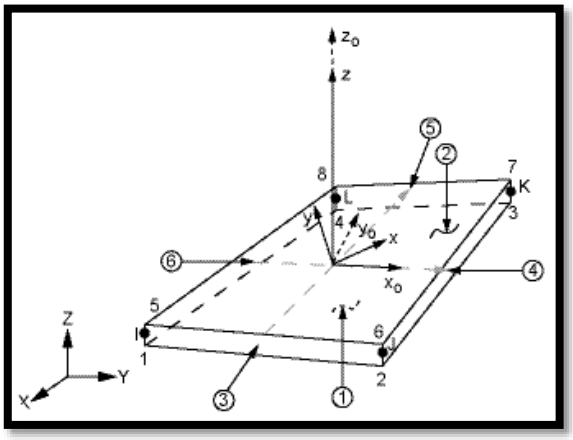

Figure 35: SHELL181 Structural Shell Element [56]

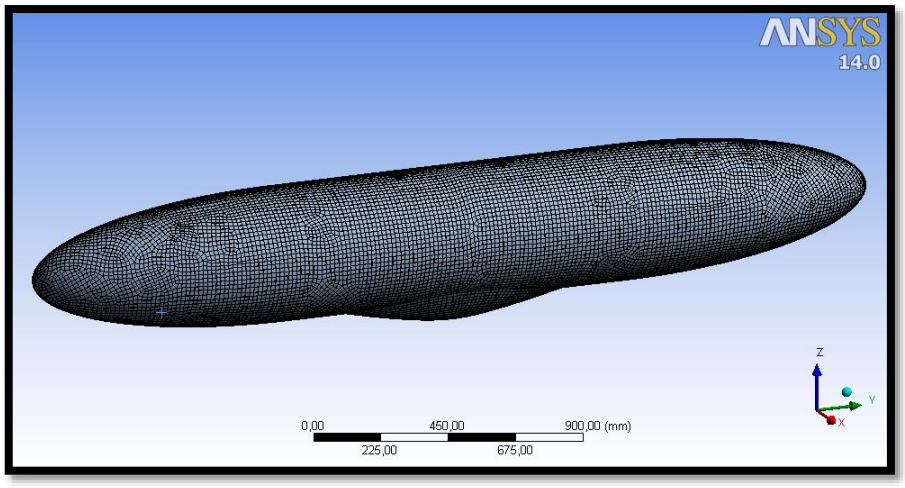

Figure 36: Finite Element Model

Mesh metric options provided in order to examine the Finite Element Model established by SHELL181 elements include:

- **Element Quality:** Element quality is defined for every single element of the FEM. Ranging from zero to one, element quality metric provides a global indicator basing on the ratio of the volume to the edge length. Element quality of unity defines a perfect element, while zero value indicates that the element does not have a volume [56]. As seen in Figure 37, 38640 element out of 44054 has an averaged element quality of 0.93. On the basis of the element quality, created FE Model could be considered as appropriate.

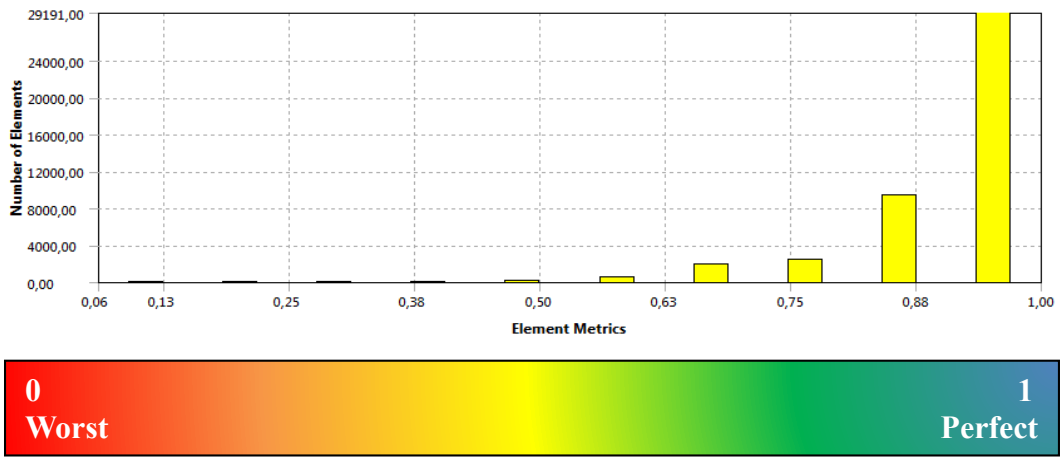

Figure 37: Element Quality Mesh Metric Spectrum

- **Aspect Ratio:** Aspect ratio for an element is calculated using only the corner nodes. Aspect ratio is an indicative of the amount of stretching of an element. Similar to element quality metric, a perfect element has an aspect ratio of one [56]. The average aspect ratio of the FE Model corresponds to 1.26.

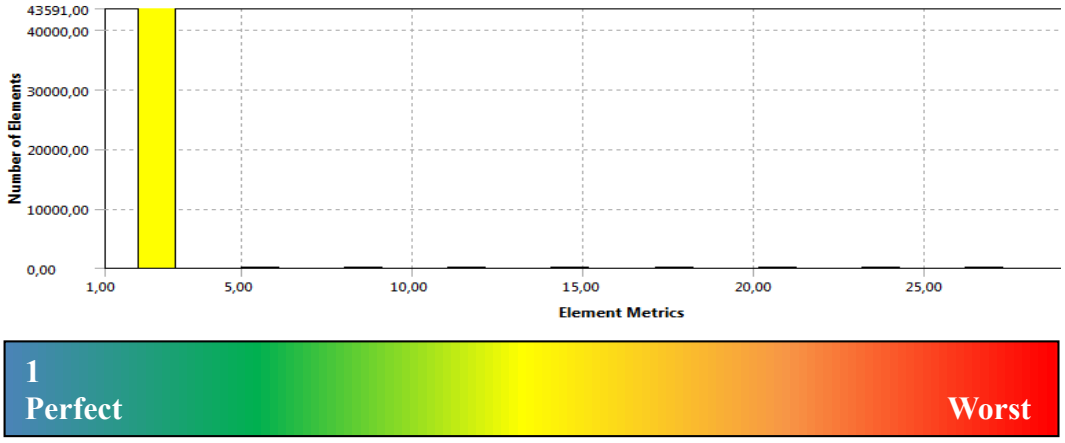

Figure 38: Aspect Ratio Mesh Metric Spectrum

- **Jacobian Ratio:** Jacobian Ratio is a mesh metric indicating the amount of distortion of the nodes on an element when they are compared to the ones on a perfect element [56]. The jacobian ratio of a perfect element is one and for instance, it increases as the node located at the corner moves towards the center. The average jacobian ratio of the FE Model corresponds to 1.15.

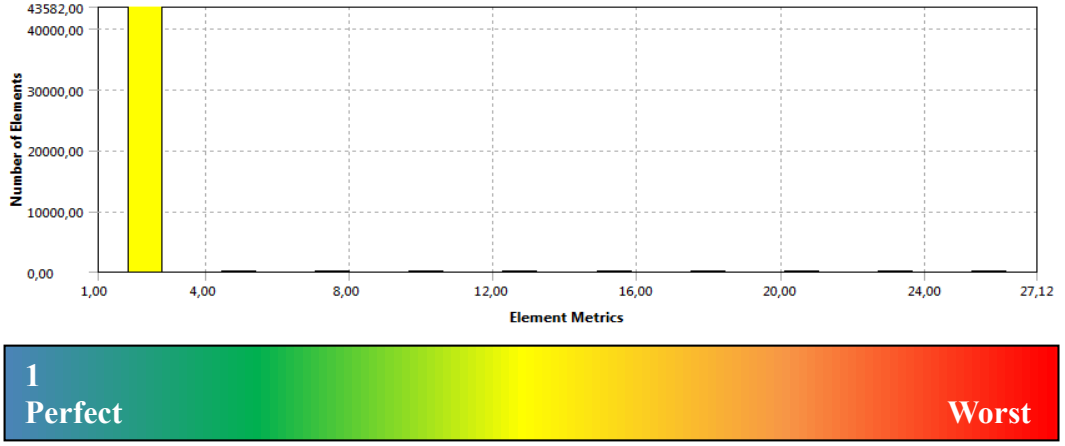

Figure 39: Jacobian Ratio Mesh Metric Spectrum

- **Warping Factor:** As the name of the metric implies, warping factor is a measure for warping on an element. Warping factors reaching about 0.1 become visible, and warping about 1.0 is unacceptable [56]. The average warping factor of the FE Model is around to 0.004.

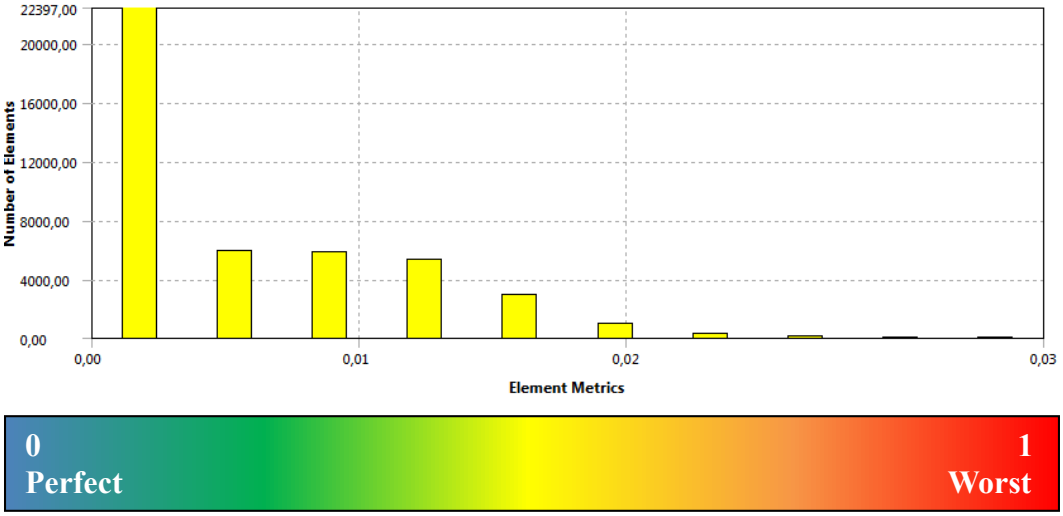

Figure 40: Warping Factor Mesh Metric Spectrum

- **Parallel Deviation:** The best possible deviation is valid for a perfect element with zero degrees [56]. The average parallel deviation of the FE Model is around to 4.9.

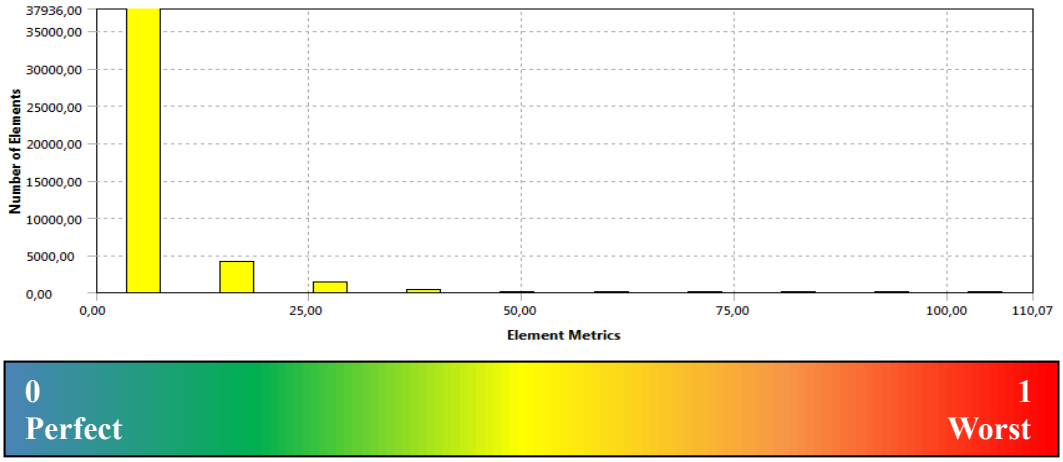

Figure 41: Parallel Deviation Mesh Metric Spectrum

- **Maximum Corner Angle:** The best possible maximum angle is valid for a perfect quadrilateral element with ninety degrees. It is claimed that excessive corner angles would result in poor performance of the FE Model [56]. The average maximum corner angle of the FE Model is around 96.73-degrees.

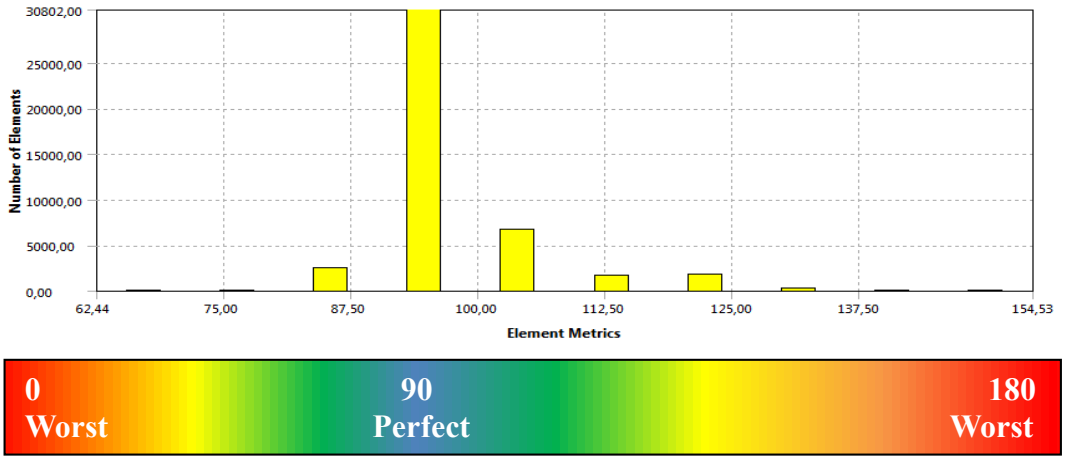

Figure 42: Maximum Corner Angle Mesh Metric Spectrum

- **Skewness:** Skewness is one of the most important mesh metric used to quantify the mesh quality. Skewness is used for checking how the elements are close to the perfect ones. By definition, zero indicates a perfect material, whereas a skewness value of unity corresponds to completely degenerated elements [56]. The skewness of the FE Model is around to 0.083.

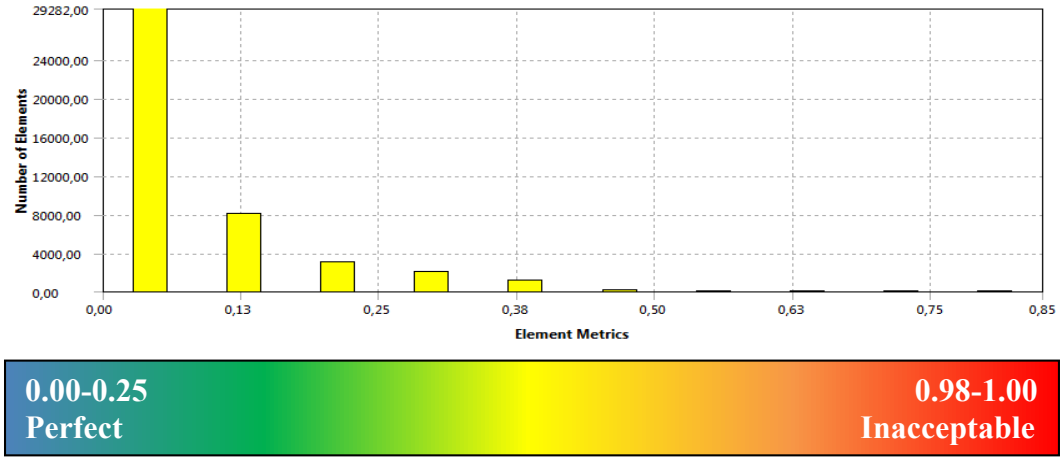

Figure 43: Skewness Mesh Metric Spectrum

- **Orthogonal Quality:** Orthogonal quality metric determines the alignment of face normal vector. This mesh metric has a range of zero to one where zero being the worst and one defines the best possible quality of orthogonality [56]. The orthogonal quality of the FE Model is around to 0.98.

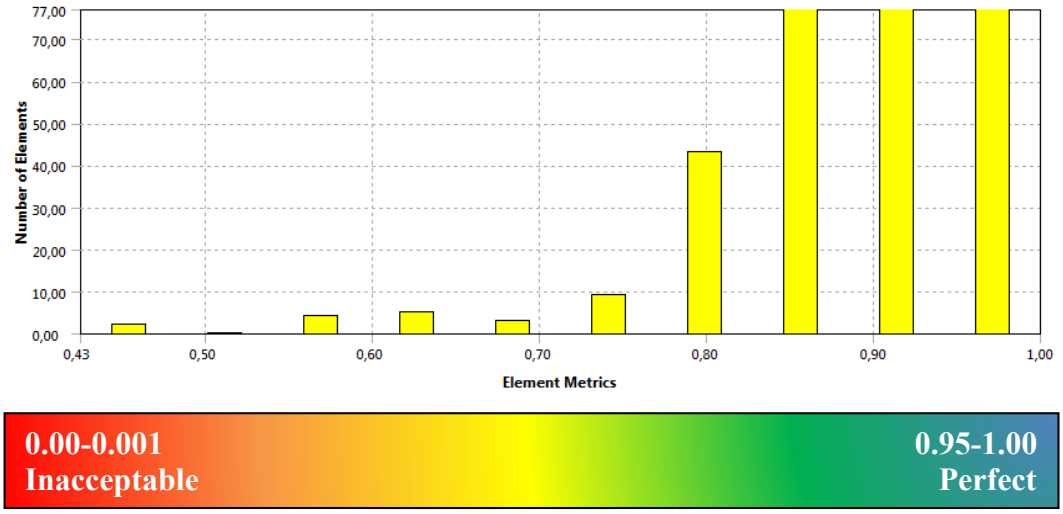

Figure 44: Orthogonal Quality Mesh Metric Spectrum

As mentioned before, checking the mesh quality is vital for a simulation-driven verification process. In the light of all the results, generated FE Model succeeds to capture proper density and mesh quality with respect to the available mesh metrics. Figure 45 gives some details of the high quality quad-dominant global mesh details of the outer shell of the EFT.

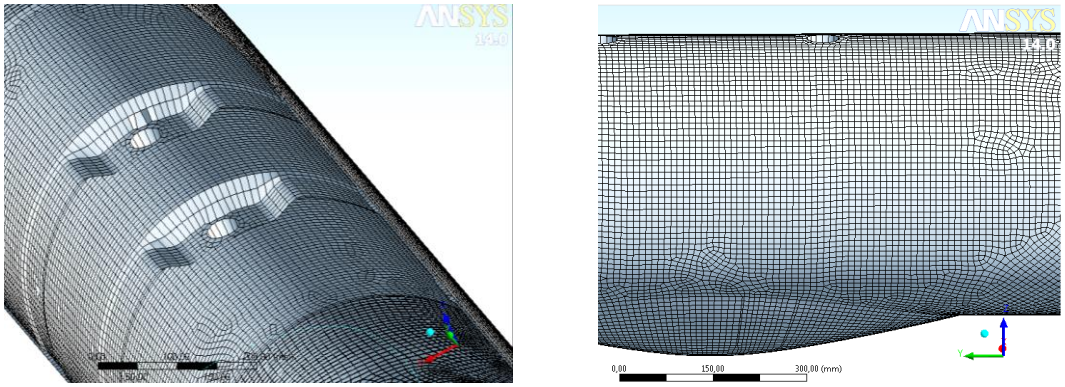

Figure 45: Global Mesh Details of the EFT

3.3. DEFINITION OF THE ENVIRONMENT

The primary goal of the verification process is to keep safety at the forefront. The design of the external fuel tanks must ensure integrity in order to maintain a safe flight during the defined operational spectrum. It is obvious that the structural requirements and reliability of the external fuel tanks are directly related to the operational capabilities of the platform. Therefore, recognition of the most critical loading conditions becomes significant. As in the definition of design characteristics of the external fuel tank, the loads that are encountered should identified by the manufacturer of the air platform.

The maneuver and flight loads that an attack helicopter like Boeing's AH64 Apache experiences, are given in the following tables respectively.

Table 11: Maneuver Loads

Load Components			**Status**
X Component	Y Component	Z Component	
-1.50 g	1.00 g	4.75 g	Ground
0.80 g	0.75 g	-5.50 g	Flight

Table 12: Flight Loads

Side	± 2.00 g
Down	3.75 g
Up	0.75 g

Table 12 (continued)

Forward	2.00 g
Backward	2.00 g

Fuel induced forces, which must be accommodated within the structure increases rapidly during an emergency situation called hard landing. Hard landing refers to the case of landing where the approaching speed and the forces are much greater when compared to a common and normal landing case. During a hard landing, the loads could reach up to one and a half times of flight loads especially when the fuel tanks are full.

Table 13: Hard Landing Loads

Side	± 3.00 g
Down	5.63 g
Up	1.13 g
Forward	3.00 g
Backward	3.00 g

During verification process, the most critical conditions must be examined using maximum loads with the maximum fuel load defined in each of the three axes [26,42].

It is assumed that the specified in-flight loads and the response of the structure vary slowly with respect to time. Therefore, static structural analysis is performed in order to find structural response, displacements and stress resultants.

Other than the static loadings, the behavior of the structure under the vibration loads is a significant structural issue. Determining the natural frequencies and associated mode shapes for dynamic loading conditions provides a detailed understanding of the response of the structure. Together with modal analysis, vibration loads that are random in nature should also be taken into consideration. Random vibration loads are generally non-periodic and they contain multiple frequencies. Random vibrations are identified statistically in time history, which is called Power Spectral Density (PSD). PSD is an informative table, which gives spectral values against frequency [56].

External fuel tanks undergo various combinations of vibrations excited by main and tail rotors whose characteristics are defined in Test Method Standard for Environmental Engineering Considerations and Laboratory Test, MIL-STD-810F Method 514.5 [59]. The vibration exposure profile could be derived from the graph depicted in Figure 46.

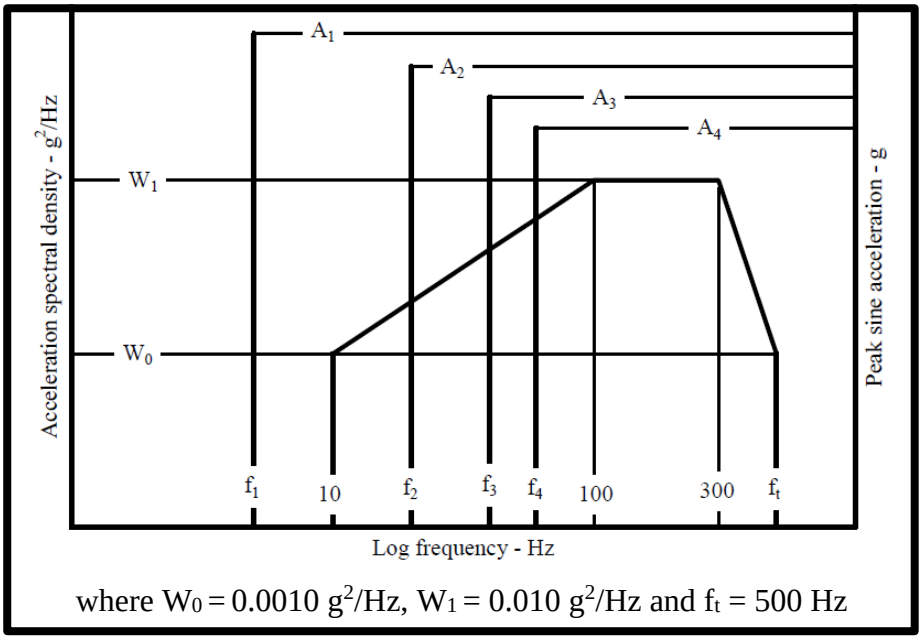

Figure 46: Helicopter Vibration Exposure [44]

Random vibration analysis could be performed by providing the vibration profiles as input to ANSYS Mechanical.

According to MIL-T-18847, the EFT should have the ability to survive from the ground impact when the tanks is inadvertently ejected from the store rack unit onto a concrete surface minimum 48-inches (1219.2 mm) below the tank centerline [51]. As a result of inadvertent ejection test, any structural damage or leakage is not allowed. It is expected that the fuel tank maintain its structural condition to be remounted to the store rack units.

Another requirement mentioned in MIL-T-18847 states that an EFT should withstand the explosive pressure generated by the rapid ignition of the fuel vapor. Upon the ignition that reaches at least 6.5-atmospheres within 60-milliseconds, no structural damage is allowed [51].

Moreover, in a rotary-wing air platform, in case of an engine failure, the engine and the rotor system is disengaged automatically by a unit called freewheeling. Disengaging the main rotor system from the engine initiates the rotors to rotate freely. As the collective pitch control lowered by the pilot, both angle of attack and drag decreases while rotor rpm increases which enables pilot to control the rapid descent of the platform [8]. Due to the possibility of the post-crash fire, external fuel tanks could not be jettisoned during an autorotation landing. Since landing with autorotation imposes very large loads on platform [26], the external tanks should have the ability to resist the forces occurring when the platform crashes to the ground surface with a vertical velocity of 50 fps (15.24 m/s) and a longitudinal velocity of 23 fps (7 m/s). Immediately after the crash, landing gear absorbs the great majority of the energy and resets the impact velocities within 0.3-seconds. Therefore, the EFT should not leak when subjected to impact velocities, which are dissipated within 0.3-seconds.

To simulate such situations, consideration of the loads, which vary with time, is required. The dynamic behavior of the structure under a time dependent load could be performed using transient structural analysis.

3.4. DEFINITION OF THE MATERIAL PROPERTIES AND PLY DEFINITIONS

In this section, the choice of the materials, which would be used in the FEA and the reasons underlying this selection, are described. Firstly, the considerations to be taken are discussed and the method for deriving material properties for the widest range of operation conditions is examined. After identifying the properties required for FEA, detail definition of the individual plies are included.

3.4.1 Material Properties

In a filament-winding process, a band of continuous resin-impregnated reinforcing roving is wrapped around a mandrel [28]. Almost all of the continuous fiber reinforcing materials and resin systems available in market could be used in this particular manufacturing process. Among the infinitely many number of material combinations, the process of materials selection plays a critical role in the development process. The task of defining the unique combination of reinforcing fiber and resin system requires the consideration of the performance requirement and operational environment [28].

To be precise, the positive and negative aspects of the candidate reinforcing fibers and matrix materials to be used in manufacturing the tank structure are given in the Table 14 and Table 15 respectively.

Table 14: Properties of Reinforcing Fibers

Fiber	Advantages	Disadvantages
Carbon	- High strength to weight ratio - Structural stiffness - High fatigue strength	- Low impact resistance - Low strain to failure
Aramid	- Low density - High tensile strength - Ballistic and impact resistance	- Machining problems - Low compressive strength
Glass	- High tensile strength - High chemical resistance	- Low tensile modulus - Low fatigue resistance

Table 15: Properties of Selected Matrix Materials

Matrix	Advantages	Disadvantages
Epoxy	- Fuel resistance - Good mechanical properties - Good bonding characteristics	- Relatively long curing cycles
Others (Polyesters, vinyl esters)	- Low Cost - Fast Curing	- No fuel resistance - Relatively low mechanical properties

In order to ensure the survivability of the structure from hostile fires, impacts and severe in-flight loads, a hybrid material solution is required. It is worth to highlight that aramid could provide ballistic resistance and low density, while carbon could add superior mechanical properties and structural stiffness needed for the EFT. By combining carbon and aramid 50% by volume suits the operational requirements. To make use of the ability to resist the exposure of aviation fuel for long periods of time, epoxy is the only option as the resin system.

Determining strains, stresses and failure of the filament-wound composite shell requires modeling the composite shell in the form of individual layers. This method is called meso-scale approach, which requires mechanical properties, thicknesses and arrangements of fiber with varying angles [60]. Numerical approaches including micro-, meso- and macro-scale approaches are illustrated in Figure 47.

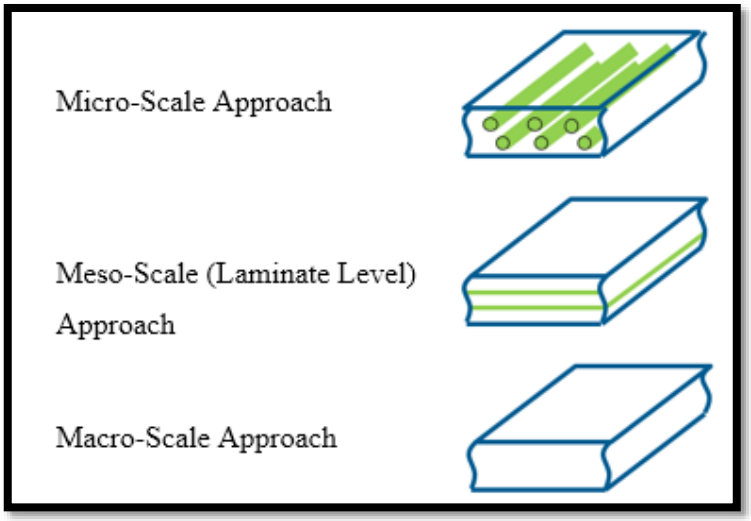

Figure 47: Numerical Approaches of Composite Design [60]

The mechanical properties directly depend on the technique and the quality of the manufacturing process. The orthotropic nature of the composite materials introduces both advantage and complexity for the designer. Tailoring the material properties to meet operational requirements is essential [61]. Therefore, proper definition of the mechanical properties requires special attention.

Orthotropic materials have three planes of material symmetry whose relations can be derived by using 180º rotations about each of the coordinate axes as shown in Figure 48.

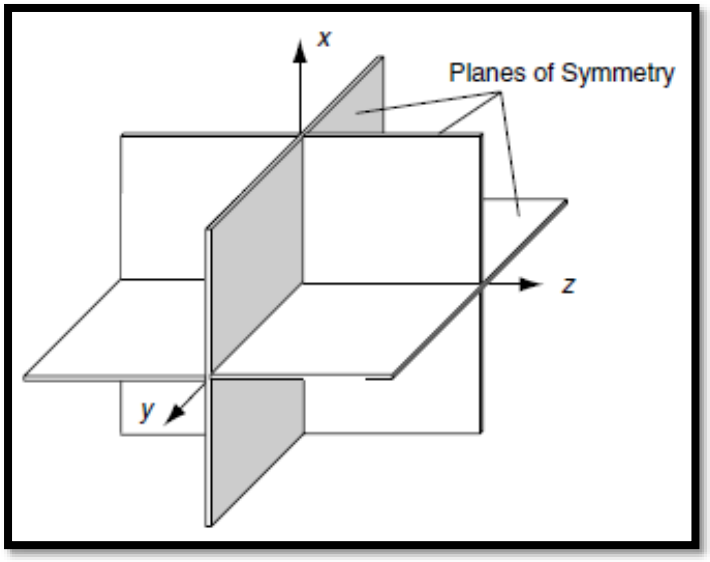

Figure 48: Planes of Symmetry of an Orthotropic Material [62]

The Stress-Stain relation for orthotropic materials can be expressed in the matrix form as follows [62]:

$$\begin{bmatrix} \varepsilon_{xx} \\ \varepsilon_{yy} \\ \varepsilon_{zz} \\ \varepsilon_{xy} \\ \varepsilon_{yz} \\ \varepsilon_{xz} \end{bmatrix} = \begin{bmatrix} \frac{1}{E_{xx}} & -\frac{v_{yx}}{E_{yy}} & -\frac{v_{zx}}{E_{zz}} & 0 & 0 & 0 \\ -\frac{v_{xy}}{E_{xx}} & \frac{1}{E_{yy}} & -\frac{v_{zy}}{E_{zz}} & 0 & 0 & 0 \\ -\frac{v_{xz}}{E_{xx}} & -\frac{v_{yz}}{E_{yy}} & \frac{1}{E_{zz}} & 0 & 0 & 0 \\ . & . & . & \frac{1}{G_{xy}} & 0 & 0 \\ . & . & . & . & \frac{1}{G_{yz}} & 0 \\ . & . & . & . & . & \frac{1}{G_{xz}} \end{bmatrix} \begin{bmatrix} \sigma_{xx} \\ \sigma_{yy} \\ \sigma_{zz} \\ \sigma_{xy} \\ \sigma_{yz} \\ \sigma_{xz} \end{bmatrix} \quad (1)$$

where E_{ij} are Young's Modulus in the three directions of material symmetry, v_{ij} are the Poisson's ratio and G_{ij} are the shear modulus in i-j planes.

For orthotropic materials, there are nine independent elastic constants that need to be determined; $E_{xx}, E_{yy}, E_{zz}, G_{xy}, G_{yz}, G_{xz}, v_{xy}, v_{xz}, v_{yz}$.

Composites composed of fibers, which are arranged in a unidirectional manner, are regarded as transversely isotropic material [45]. Transversely isotropic materials are a special configuration of orthotropic materials having an isotropic material behavior in one symmetry plane. A unidirectional layer illustrated in Figure 49 poses a transversely isotropic material behavior.

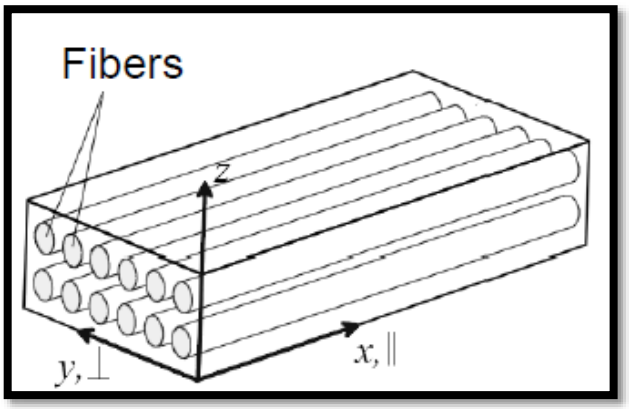

Figure 49: Unidirectional Layer [60]

Taking the fiber direction as the axis of symmetry, mechanical properties in y and z directions are assumed to be equal [28].

$$E_{yy} = E_{zz} \tag{2}$$

$$v_{xy} = v_{xz} \tag{3}$$

$$G_{xy} = G_{xz} \tag{4}$$

$$G_{yz} = \frac{E_{yy}}{2(1 + v_{yz})} \tag{5}$$

Rearranging the stress-strain relationship given in (1) according to (2) through (5), the number of independent material properties would be reduced to five; $E_{xx}, E_{yy}, G_{xy}, v_{xy}, v_{yz}$. These five elastic constants are required to identify the mechanical behavior of the structure.

For unique combinations of fiber and matrix, mechanical properties should be derived from theoretical calculations or physical mechanical testing [61]. The best implementation to proceed is to combine physical testing and theoretical calculations. Since the mechanical properties strongly dependent on the quality of the manufacturing process, the material database of the manufacturer is regarded as a reliable source. Owing to the wide manufacturing experience gained over the years, BARIS Electrical Ind. has been able to attain the quality in her manufacturing. BARIS has a broad material database including different manufacturer's products. BARIS has the ability to manufacture the test samples using various types of fabrics, fibers and matrix. These samples are put through a rigorous mechanical testing, and the material database is created according to the characterization result.

Table 16 lists the mechanical properties of Carbon-Epoxy and Aramid-Epoxy respectively.

Table 16: Mechanical Properties and Orthotropic Stress Limits of the Selected Materials [63]

Orthotropic Elasticity Volume Content of Fibers≈60%	**Carbon-Epoxy**	**Aramid-Epoxy**
E_{xx} [MPa]	147000	83000
E_{yy} [MPa]	8000	7000
E_{zz} [MPa]	8000	7000
G_{xy} [MPa]	5500	2600
G_{yz} [MPa]	2900	1900
G_{xz} [MPa]	5500	2600
v_{xy}	0.27	0.34
v_{yz}	0.41	0.44
v_{xz}	0.27	0.34
Orthotropic Stress Limits		
Tensile X direction [MPa]	1700	1400
Tensile Y direction [MPa]	150	120
Tensile Z direction [MPa]	150	120
Compressive X direction [MPa]	1500	231
Compressive Y direction [MPa]	250	150
Compressive Z direction [MPa]	250	150
Shear XY [MPa]	70	60
Shear YZ [MPa]	70	60
Shear XZ [MPa]	70	60

To create the ply properties for FEA, the individual mechanical properties of Carbon-Epoxy and Aramid-Epoxy are combined using the Micromechanics theory [28].

$$E_{xx} = E_{xx}^{c} \,.\, \varphi^{c} + E_{xx}^{a} \,.\, \varphi^{a} \tag{6}$$

$$E_{yy} = \frac{E_{yy}^{c} \,.\, E_{yy}^{a}}{E_{yy}^{c}.\, \varphi^{c} + E_{yy}^{a}.\, \varphi^{a}} \tag{7}$$

$$G_{xy} = \frac{G_{xy}^{c} \,.\, G_{xy}^{a}}{G_{xy}^{c}.\, \varphi^{c} + G_{xy}^{a}.\, \varphi^{a}} \tag{8}$$

$$v_{xy} = \varphi^{c}.\, v_{xy}^{c} + \varphi^{a}.\, v_{xy}^{a} \tag{9}$$

$$v_{yx} = v_{xy} \,.\, \frac{E_{yy}}{E_{xx}} \tag{10}$$

$$v_{yz} = v_{zy} = v_{xy} \,.\, \frac{1 - v_{yx}}{1 - v_{xy}} \tag{11}$$

where φ is the volume fraction of aramid- and carbon-fibers in hybrid combination relative to each other. Among the 60% of the volume content of the fibers, carbon constitutes the half of the volume content (≈30%), while the other half consists of aramid, which makes $\varphi \cong 0.5$.

The mechanical properties of the selected combination could be calculated using the rules of mixtures whose relations are given in Equations (6) through (11). In order to derive the constants, it is necessary to make certain assumptions [28].

1. Fibers and matrix are linearly elastic.
2. Fibers are uniformly distributed in the matrix.
3. Fibers are continuous and perfectly aligned in the 1-direction.
4. There is perfect and void free bonding at fiber-matrix interface.

Table 17 lists the calculated mechanical properties of hybrid combination in accordance with the aforementioned assumptions.

Table 17: Mechanical Properties and Orthotropic Stress Limits of the Unique Hybrid Combination

Orthotropic Elasticity Volume Content of Carbon Fiber≈30% Volume Content of Aramid Fiber≈30%	**Carbon&Aramid-Epoxy**
E_{xx} [MPa]	115000
E_{yy} [MPa]	7467
E_{zz} [MPa]	7467
G_{xy} [MPa]	3531
G_{yz} [MPa]	2592
G_{xz} [MPa]	3531
ν_{xy}	0.31
ν_{yz}	0.44
ν_{xz}	0.31
Orthotropic Stress Limits *	
Tensile X direction [MPa]	1400
Tensile Y direction [MPa]	120
Tensile Z direction [MPa]	120
Compressive X direction [MPa]	231
Compressive Y direction [MPa]	150
Compressive Z direction [MPa]	150
Shear XY [MPa]	60
Shear YZ [MPa]	60
Shear XZ [MPa]	60

*The smaller of the two orthotropic stress limits is taken for the hybrid combination in order to stay on the safe side.

It should be emphasized that the filament winding process is a method of manufacturing composite structures having high fiber volume content. The mechanical properties of the structure are a function of fiber volume content. Theoretically, load carrying capacity of the composites increase directly with increasing fiber volume since the fibers carry almost 70% of the composite load [28]. A quality manufacturing process of a composite structure that requires high performance would bring a fiber volume fraction of ≈60%-70%. Above this practical limit, the matrix could not wet the fibers, and the mechanical properties tend to decrease since there would not be enough bonding to hold the fibers together. Therefore, the elastic constants gathered by means of micromechanical approach must be verified according to the contained fiber volume content. For this purpose, test specimens reflecting the actual winding configuration and material combination were manufactured. Thermo Gravimetric Analysis (TGA) provides quantitative characterization of the specimen. The insight provided by TGA allows examining the change in the mass of specimen by temperature. The results revealed that the fiber volume content of the manufactured specimens matched the theoretical volume fraction used in the calculations. Therefore, the resulting material properties for the hybrid material model could be used in the verification process with confidence.

3.4.2 Ply Definitions and Element Orientations

Besides defining the mechanical properties, ANSYS Composite Preprocessor provides a user-friendly interface to define plies and stacking sequence. Arranging the plies in a stacking sequence would require the consideration of orientation of the plies. A ply is generally defined by careful selection of the material, the layup region and the vectors for layup, fiber direction and normal direction. Firstly, a total of five particular groups of elements on the outer surface of the structure where

the layup is applied are identified. To be more precise, together with the surfaces where plies are combined to form inner frame, hoop and helical winding surfaces illustrated in Figure 50 are introduced to the ACP preprocessor prior the stacking sequence.

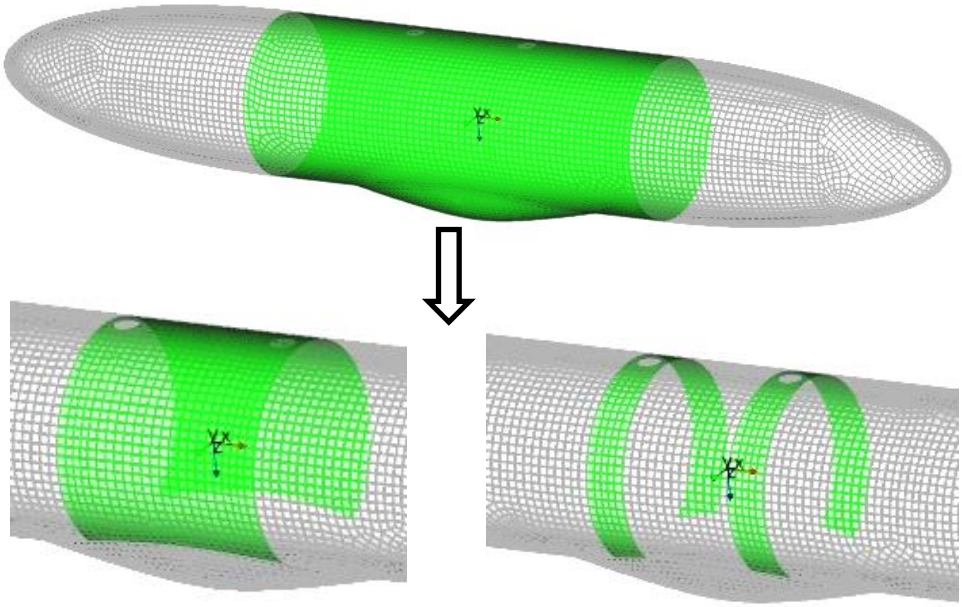

Figure 50: Defined Element Sets

Fiber directions and normal direction vectors are defined by a Rosette, which is a tool, based on the global coordinate system. In order to represent the through-thickness of the structure correctly, the definition of the vectors is important. Figure 51 illustrates how the rosettes are used to define the reference and normal vectors.

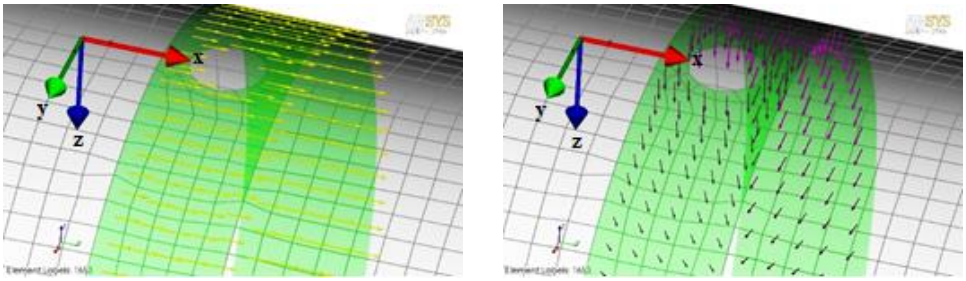

Figure 51: Reference and Normal Direction Vectors

The x-axis of the rosette indicates the reference direction. Since the stacking is selected to be applied inward, the direction of the normal vector is downward.

After defining the element sets and orientations, ply groups are modeled. The sequence of lamination is initiated with the inner frame, which is constructed by a hoop winding. A customary lamination sequence for such a high performance structural product includes two hoop winding applied to the cylindrical mid-sections of the structure and a helically wound layer in between. The overall performance of the EFT is a function of the winding angle, as shown in Figure 52.

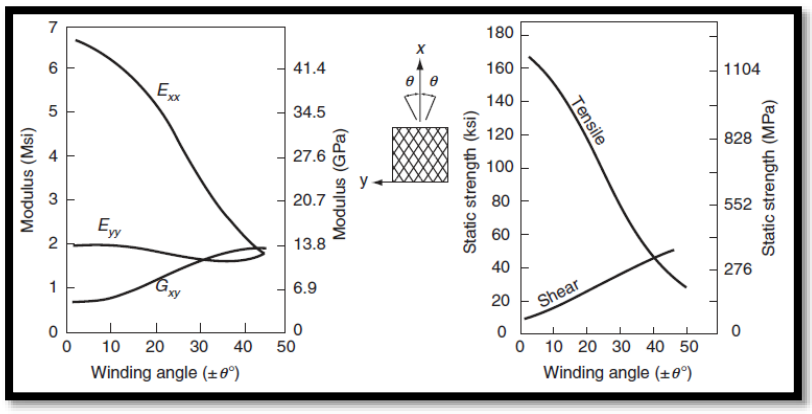

Figure 52: Variation of the Elastic Constants with the Winding Angle [28]

It is a well-known fact that the composite design requires an iterative approach where the candidate plies are created with different element orientations, their performance is examined and if necessary, stacking sequence is modified accordingly [64].

Assigning the helical winding angle and ply thicknesses as variables, the details of the stacking sequence is listed below.

Table 18: Stacking Sequence

Element Set	Material	Thickness	Orientation
Outer Shell	Carbon & Aramid-Epoxy	2 mm	$\pm\alpha$
Cylindrical Mid-Section	Carbon & Aramid-Epoxy	2.5 mm	90º
Inner Frame	Carbon - Epoxy	2.5 mm	90º
Suspension Lug Interface	Carbon - Epoxy	30 mm	90º

The selection of the ply thicknesses presented in Table 18 is based on the engineering judgment, prior design experience with advanced composite structures and detailed comprehension of structural behavior with preliminary FEA.

3.5. PERFORMING THE ANALYSIS

Structural analyses are performed by means of ANSYS Mechanical application. Integrated with preprocessor capabilities, ACP allows importing ply properties directly to ANSYS Workbench platform [52]. Figure 53 illustrates how the mechanical applications are introduces to the FEA workflow.

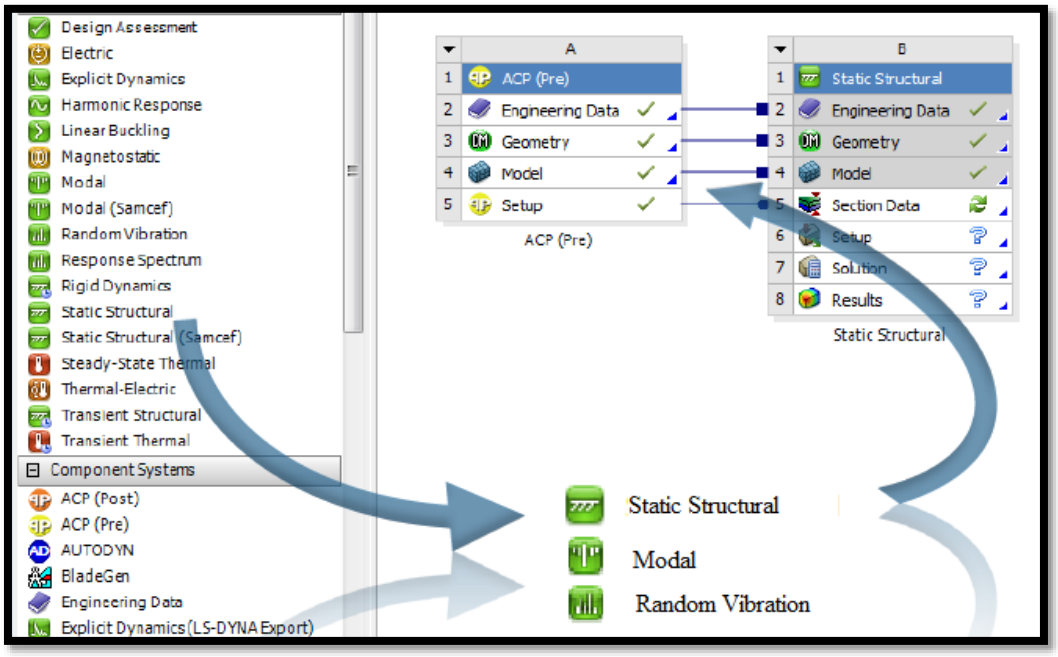

Figure 53: Adding Mechanical Applications to the Project [60]

Pre-defined environmental loading conditions including loads and supports are identified in Mechanical Application. Both supports and loads must be defined correctly in order to capture the accurate behavior. Considering the fact that the EFT are integrated to the platform by means of two hard points, the faces

corresponding the suspension lug interface is fixed so that the associated faces are constrained from deformation (see Figure 54).

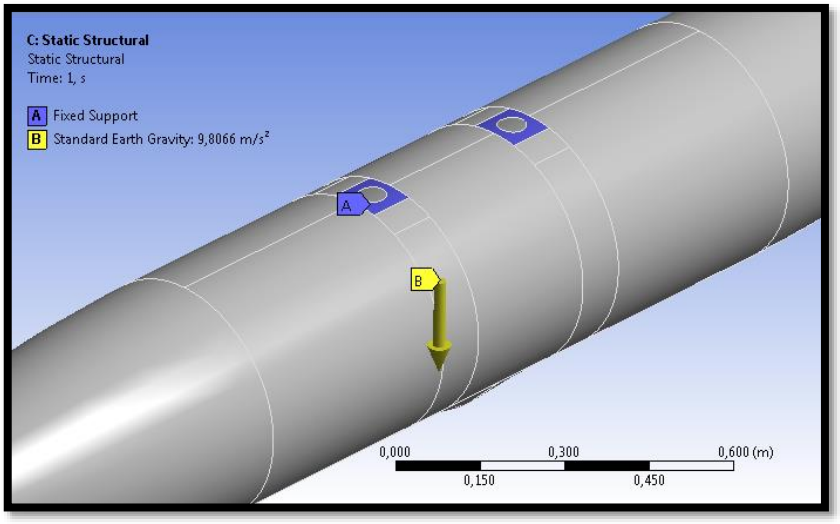

Figure 54: Fixed Supports

In order to simulate the fuel inside the EFT, the pressure induced by the weight of the fuel is used. For this purpose, the faces enclosing the fuel are introduced to the ANSYS Mechanical. Next step is the definition of the fluid density, hydrostatic acceleration components and free surface location.

- The density of JP8 is specified as 0.81 kg/L (810 kg/m^3) according to MIL-DTL-83133H [45].
- The hydrostatic acceleration could be either standard earth gravity or the magnitude and the direction of a unique acceleration of the critical load cases being analyzed in Section 3.3 could be defined as input.

- Finally, free fluid location, which the location of the free fluid surface is defined.

Proper definition of these parameters enables to visualize the pressure contours [56]. Figure 55 shows the pressure contours resulting from the maximum g-force encountered, which is the downward acceleration, occurs during maneuvers of the platform.

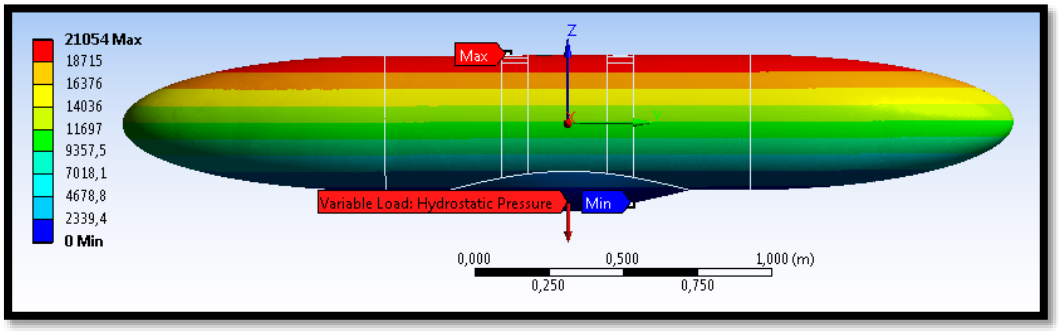

Figure 55: Pressure Contours for Downward Acceleration

3.6. INTERPRETTING THE RESULTS

The post processor capabilities of the ACP enable the designer to examine the structural integrity and the behavior of the structure reflecting the real-world outcomes [65].

Post processing tools reveals the stress resultants, strains and deformations. The results, which are presented as contours or vector plots, could be viewed globally

or they could be inspected layer by layer. Figure 56 illustrates how the post processor is integrated to the mechanical applications.

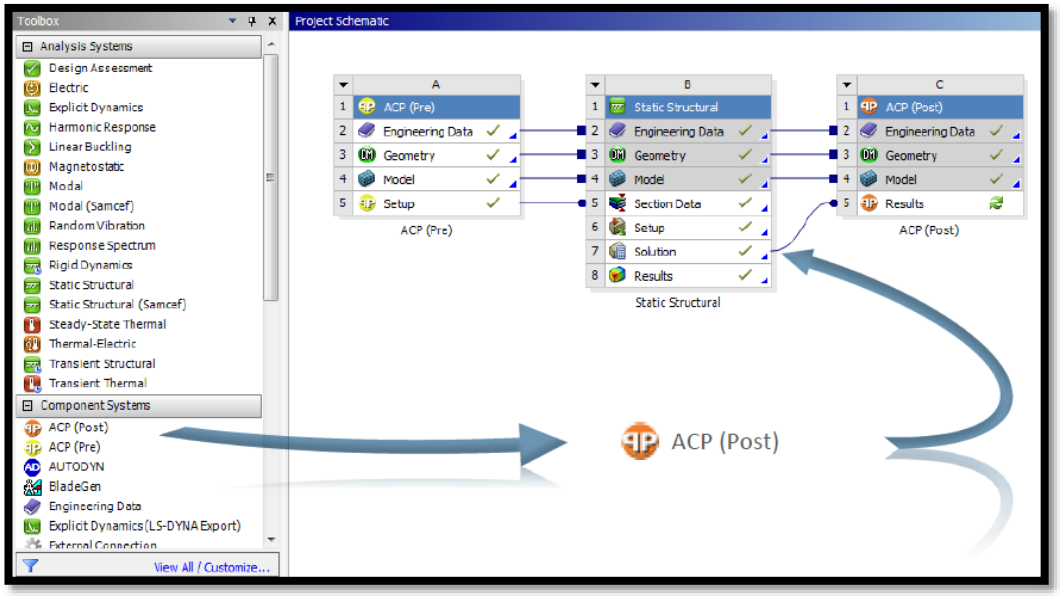

Figure 56: Integration of the ACP Post Processor [46]

For a given design load, an accurate comparison of the allowable stress level with the calculated stress resultant is vital. This comparison is generally based on the failure prediction criteria. ACP supports all state-of-art failure criteria including Tsai-Wu, Tsai-Hill, Hashin and Puck, LaRC (Langley Research Center) [52,60]. Although, the selection among the available failure theories requires intensive experience about FEA of the advanced composite structures, Tsai-Wu failure criterion has gained acceptance and is valued due to its use for the analysis of the composite materials [61]. Tsai-Wu criterion has an interactive approach considering both tensile and compressive stresses in failure prediction [61].

The failure theories indicates the failure by means of the concept of failure index (I_F) or reserve factor (RF). Unlike most of the FEA software, ANSYS uses reserve factor, which could be defined as

$$RF = \frac{1}{Failure\ Index} = \frac{Ultimate\ Strength}{Ultimate\ Stress}$$

Failure is predicted when RF is equal or less than one.

The RF for Tsai-Wu criterion could be defined as [66]:

$$RF = \left(-\frac{B}{2A} + \sqrt{\left(\frac{B}{2A}\right)^2 + \frac{1}{A}} \right) \tag{12}$$

$$A = -\frac{\sigma_x^2}{\sigma_{xt}^f.\sigma_{xc}^f} - \frac{\sigma_y^2}{\sigma_{yt}^f.\sigma_{yc}^f} - \frac{\sigma_z^2}{\sigma_{zt}^f.\sigma_{zc}^f} + \frac{\sigma_{xy}^2}{\left(\sigma_{xy}^f\right)^2} + \frac{\sigma_{yz}^2}{\left(\sigma_{yz}^f\right)^2} + \frac{\sigma_{xz}^2}{\left(\sigma_{xz}^f\right)^2} \tag{13}$$

$$+\frac{C_{xy}.\sigma_x.\sigma_y}{\sqrt{\sigma_{xt}^f.\sigma_{xc}^f.\sigma_{yt}^f.\sigma_{tc}^f}} + \frac{C_{yz}.\sigma_y.\sigma_z}{\sqrt{\sigma_{yt}^f.\sigma_{yc}^f.\sigma_{zt}^f.\sigma_{zc}^f}} + \frac{C_{xz}.\sigma_x.\sigma_z}{\sqrt{\sigma_{xt}^f.\sigma_{xc}^f.\sigma_{zt}^f.\sigma_{zc}^f}}$$

$$B = \left(\frac{1}{\sigma_{xt}^f} + \frac{1}{\sigma_{xc}^f}\right).\sigma_x + \left(\frac{1}{\sigma_{yt}^f} + \frac{1}{\sigma_{yc}^f}\right).\sigma_y + \left(\frac{1}{\sigma_{zt}^f} + \frac{1}{\sigma_{zc}^f}\right).\sigma_z \tag{14}$$

where σij is the stress in layers, σ_{it}^f is the failure stress i-direction in tension, σ_{ic}^f is the failure stress i-direction in compression and C_{ij} are the Tsai-Wu coupling coefficients and they are set to be -1 by default. *(i=x, y, z)*

CHAPTER 4

RESULTS

This chapter provides the results of the FEA whose methodology is described in considerable detail within the scope of Chapter 3. Firstly, in order to be able to determine an accurate winding angle, static loadings are taken into account, and stress, deformation and reserve factor variation is observed with respect to a variable angle ranging from 0º to 90º. After determining the winding angle, vibration and transient structural analysis are carried out. To avoid information pollution, the deformed contour plots corresponding to each winding angle and each load case would not be presented. But rather, graphical illustrations are used to indicate the results in a compact form.

4.1. RESULTS OF THE STATIC ANALYSES

In static structural analysis, the maximum g-forces, which would be exposed by the platform, are considered in all three orthogonal axes. Instead of solving for each load case individually, the ultimate loads occurring on each axis is defined and solved respectively.

Table 19: Maximum g-Forces in Three Orthogonal Plane

Side	± 3.00 g	Hard Landing
Down	5.63 g	Hard Landing
Up	4.75 g	Maneuver Load
Back & Forward	± 3.00 g	Hard Landing

The stacking sequence, which is presented in Table 18, is employed to validate the winding angle. After the preliminary results, the sequence might be refined or revised.

Following figures gives the variation of the RF, maximum stress resultants and total deformation with respect to winding angle respectively.

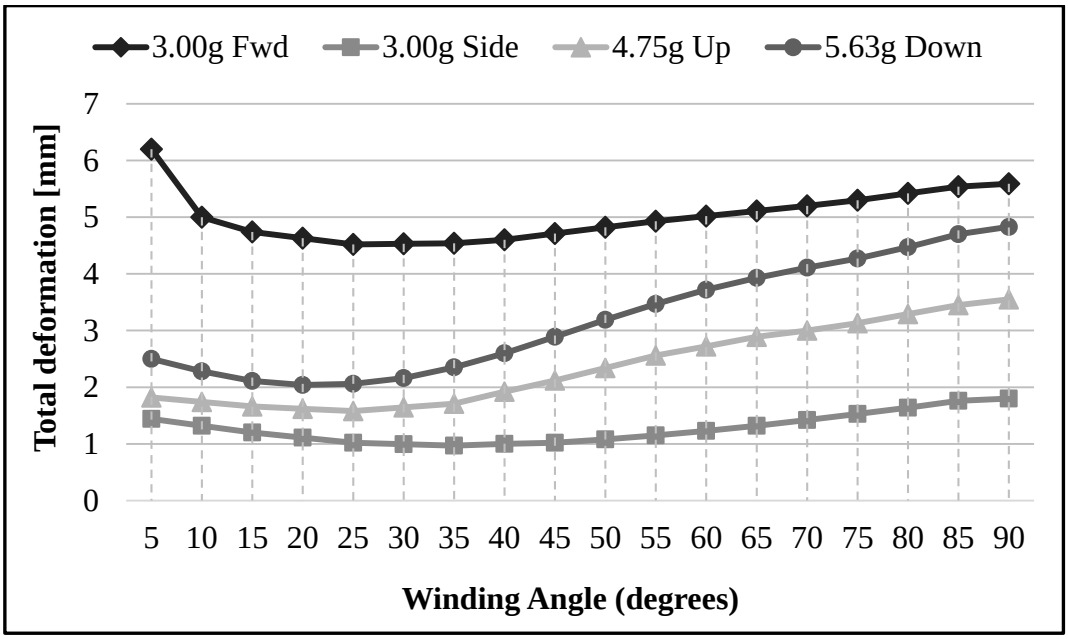

Figure 57: Variation of the Total Deformation by Winding Angle

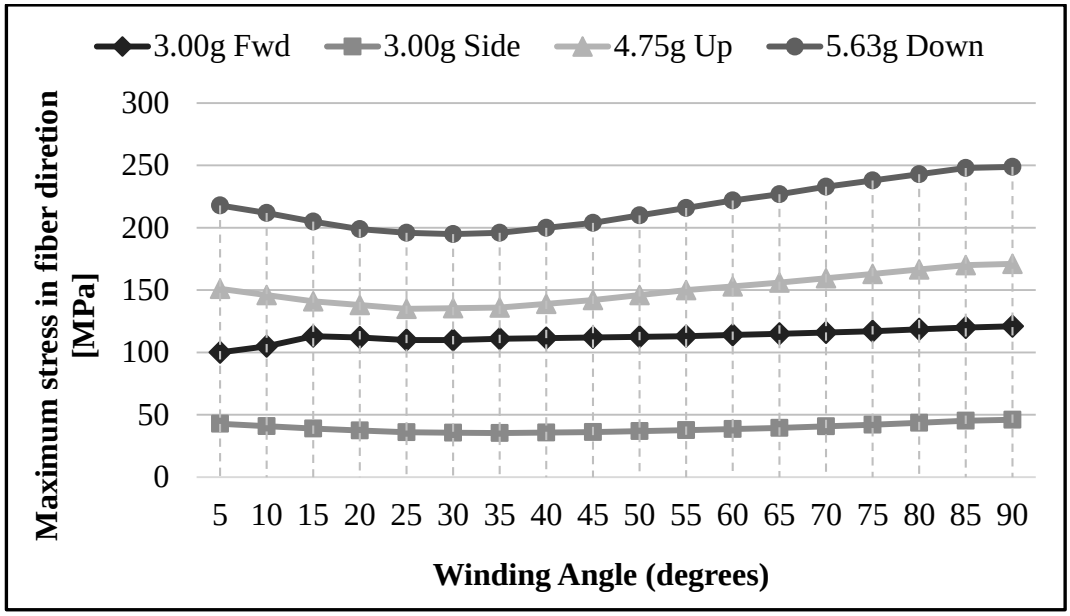

Figure 58: Variation of the Maximum Stress in Fiber Direction by Winding Angle

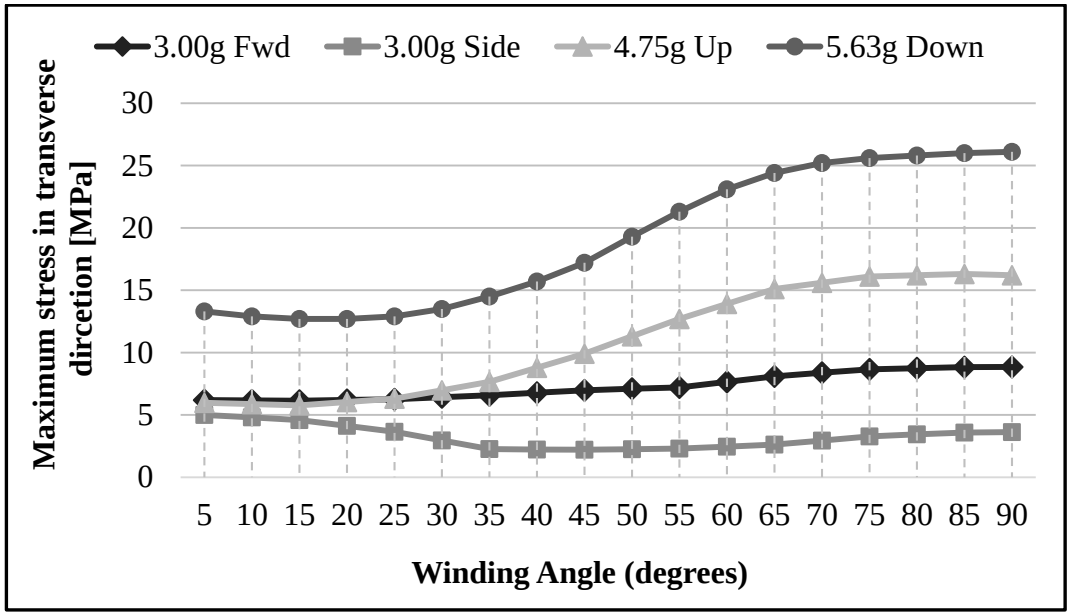

Figure 59: Variation of the Maximum Stress in Transverse Direction by Winding Angle

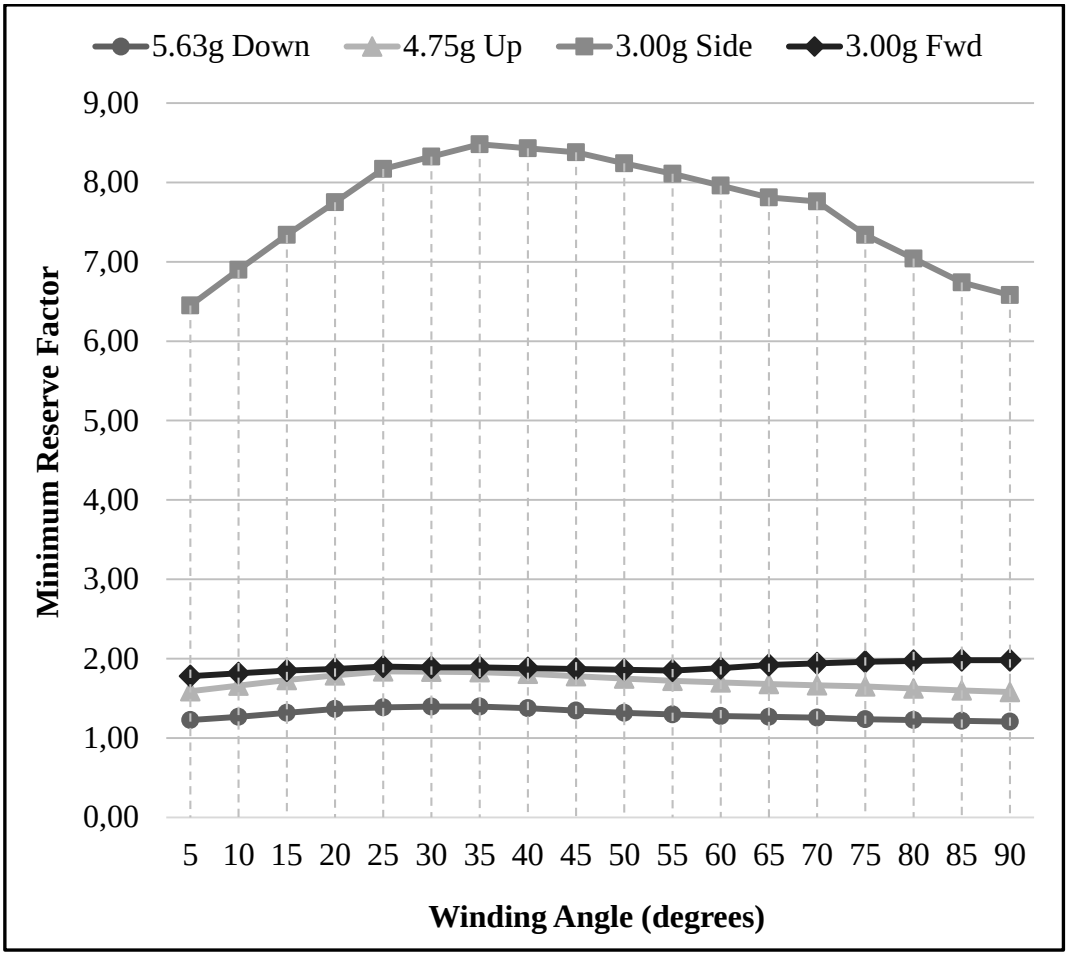

Figure 60: Variation of the Minimum RF by Winding Angle

Figure 57 through 60 provides in-depth information about the performance of the structure for a given design loads and a winding angle. Examining the data presented in the tables shows that a winding angles less than or equal to 30º could be regarded as appropriate for static loadings. Together with the deformation, stresses in both fiber and transverse directions could be observed to be increasing for winding angles larger than 30º. Therefore, the optimum angle for the filament winding process could be selected as 30º.

Detailed FEA results, which belong to the most critical loading condition with a winding angle of 30 °, are given in Figures 61, 62 and 63.

The total deformation arising from the upward acceleration effect is 2.16 mm. As could be seen from the figures, the maximum deformation is observed at both ends of the External Fuel Tank.

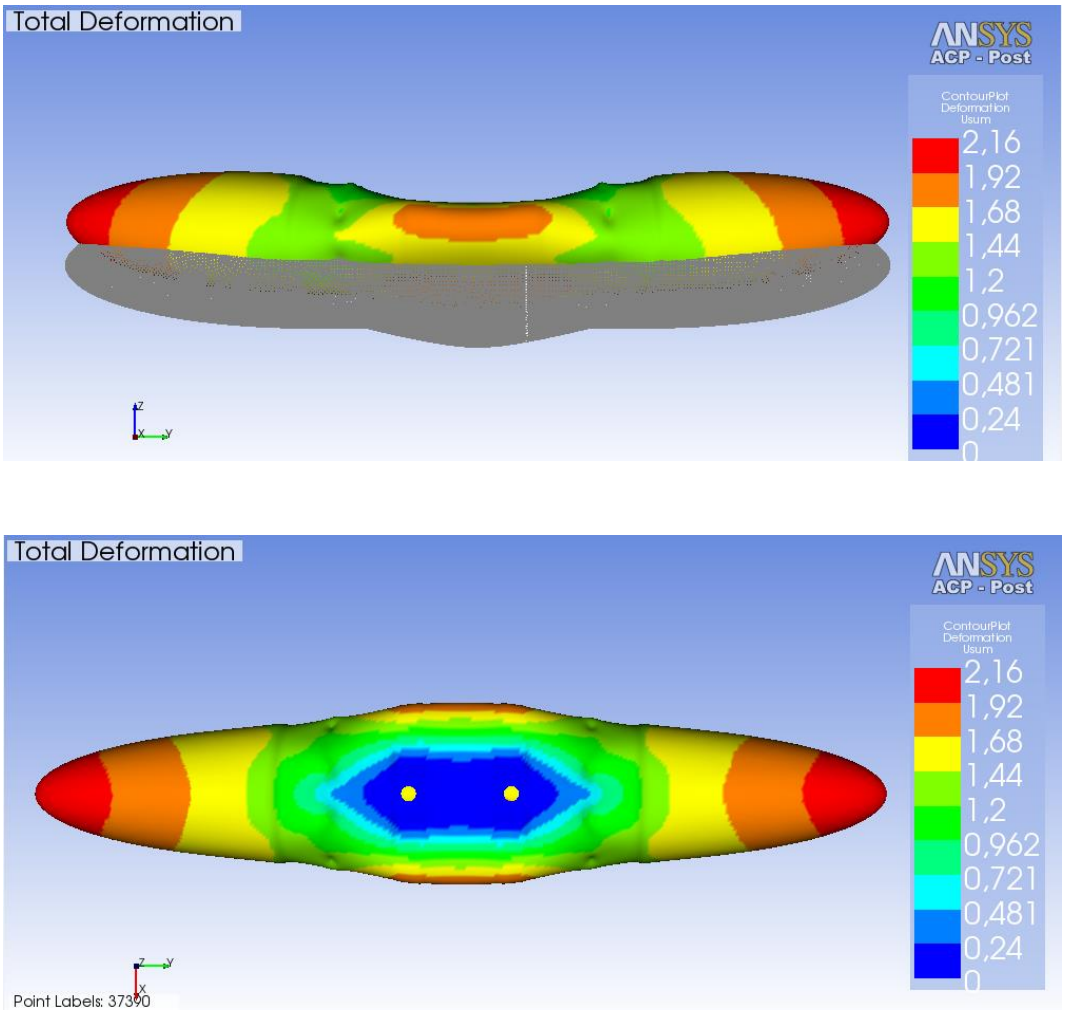

Figure 61: Total Deformation

The maximum stress calculated for the maximum g-force remains below the allowable stress limits. The load case occurring on the upper surface of the shell is compression, and the maximum stress in the fiber direction observed around edges of the suspension lug interface is 195 MPa.

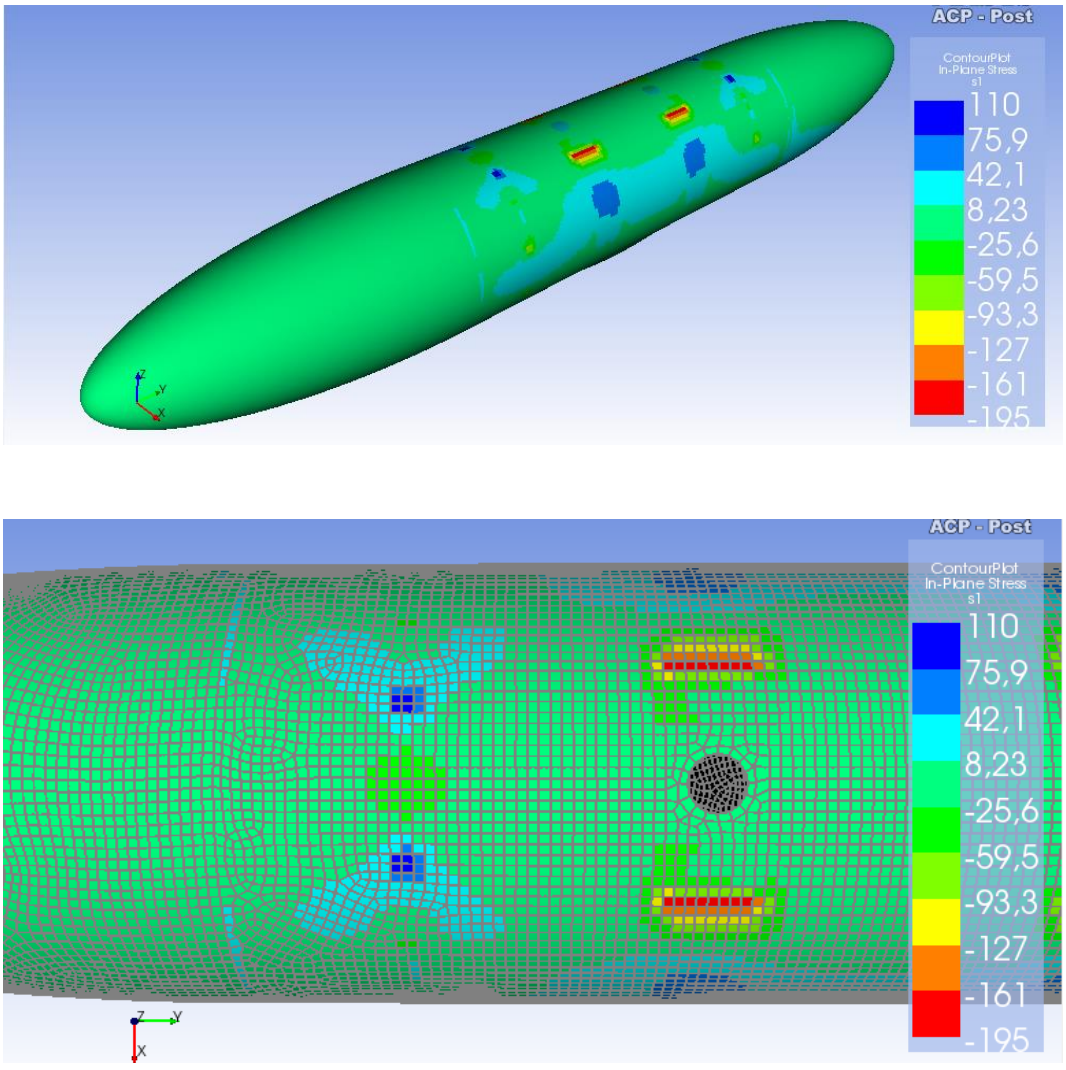

Figure 62: Stress Variation in Fiber Direction

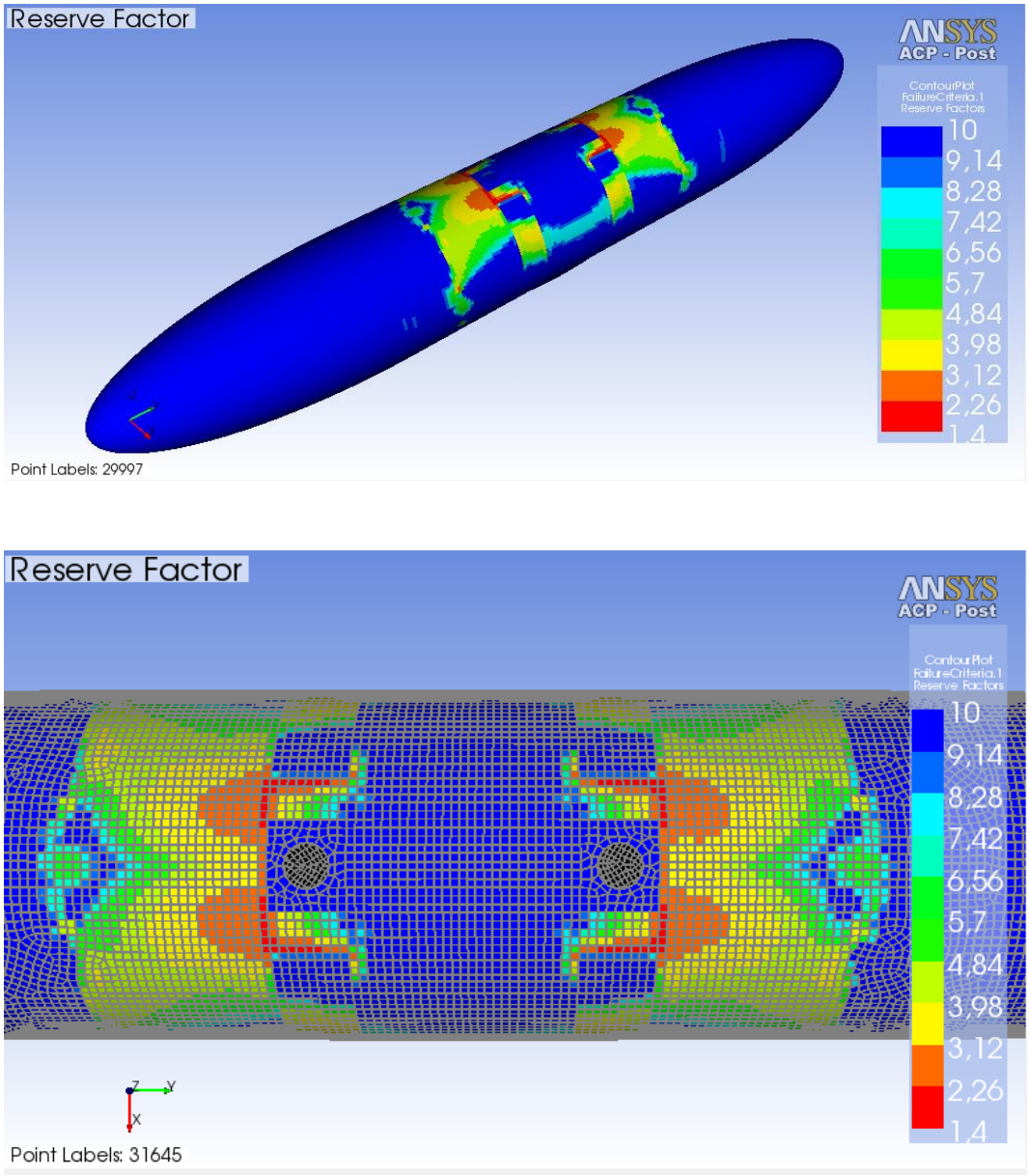

Figure 63: Overall Reserve Factor Distribution

According to the Reserve Factor index calculated for Tsai-Wu Failure Theory, no failure is predicted. The performance of the structure does not constitute a risk for the platform. As a result, along with the predicted stacking sequence, the integrity of the structure against the static loadings is found to be sufficient.

Despite the successful performance of the structure under static loadings, before making any modifications on the stacking sequence, it is required to run all of the analyses including vibration and transient structural analysis.

4.2. RESULTS OF THE VIBRATION ANALYSES

In order to determine the natural frequency and the mode shapes, a modal analysis is conducted. Although pre-stress effect is not a prerequisite for modal analysis, it is better to include pre-stress effects to get more realistic natural frequencies and mode shapes [56]. For the initial conditions (loads and supports) to be included in the analysis, the modal analysis application should be linked to the static structural analysis as shown in Figure 64.

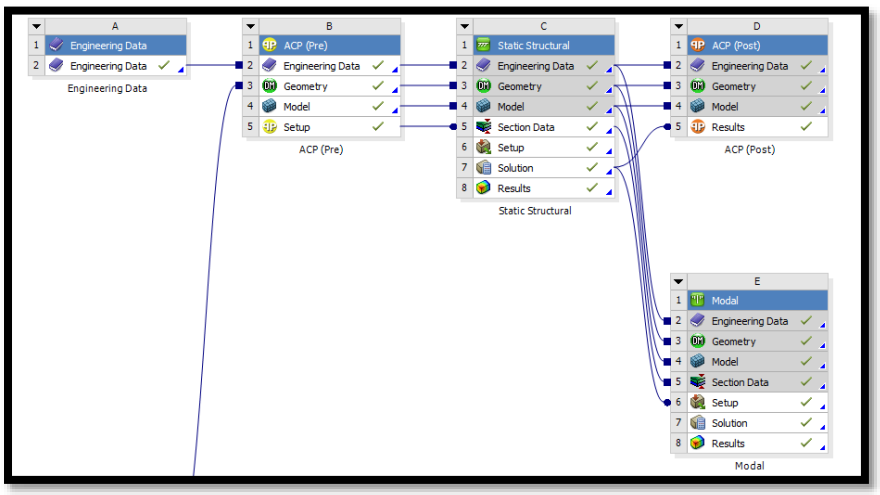

Figure 64: Project Schematic for the Pre-Stressed Modal Analysis

The conducted modal analysis whose results are given in Table 20 obtains the first six modes. The mode shapes associated with the natural frequencies could also be evaluated for visual representation.

Table 20: Natural Frequencies Obtained By Modal Analysis

Mode	Frequency [Hz]
1	42.4
2	86.3
3	117.9
4	172.2
5	178.8
6	217.1

These obtained modes reflect the dynamic characteristics of the structure and they need to be compared with the main and tail rotor forcing frequencies identified in MIL-STD-810F [59]. Main and tail rotor frequencies can be calculated by using the equations (15) though (18) [59].

Fundamental $$f = i \quad (15)$$

Blade passage $$f = n.i \quad (16)$$

1st harmonic $$f = 2\,.n\,.i \quad (17)$$

2nd harmonic $$f = 3\,.n\,.i \quad (18)$$

where the term i stands for rotation speeds for the main (1P) and tail rotors (1T) and *n* is the number of blades which should be determined from Table 21.

Table 21: Main and Tail Rotor Frequencies [59]

Helicopters	MAIN ROTOR		TAIL ROTOR	
	Rotation Speed [Hz]	Number of Blades n	Rotation Speed 1T [Hz]	Number of Blades n
AH-1	5.40	2	27.7	2
AH-6J	7.80	5	47.5	2
AH-64(early)	4.82	4	23.4	4
AH-64(late)	4.86	4	23.6	4
CH-47D	3.75	3	No tail rotor	
MH-6H	7.80	5	47.5	2
OH-6A	810	4	51.8	2
OH-58A/C	5.90	2	43.8	2
OH-58D	6.60	4	39.7	2
UH-1	5.40	2	27.7	2
UH-60	4.30	4	19.8	4

The rotation speeds for the main and tail rotors are listed for various rotary-wing air platforms. 1P and 1T are selected from the data provided for the attack helicopter Boeing's AH-64 Apache. After determining the rotation speed, the primary frequency sources calculated by using Equations (15)-(18) could be tabulated as in Table 22.

Table 22: Frequency Sources for AH-64(late)

	Main Rotor		Tail Rotor	
	Hz	rpm	Hz	rpm
Fundamental	4.9	291.6	23.6	1416
Blade passage	19.4	1166.4	94.4	566.4
1st harmonic	38.9	2332.8	188.8	11328
2nd harmonic	58.3	3449.2	283.2	16992

The vibration environment for an EFT installed on an air platform is induced commonly by the major rotating components. The peaks are generated at the rotating speeds of main and tail rotors [59]. The effect of vibration exposure on an EFT as an external store susceptible to such excitations should be evaluated carefully. Coupling of the natural frequencies of the EFT and the entire frequencies generated by the major sources might lead to failure of the structure. Therefore, a direct match between these resonant frequencies should be avoided. The common practice suggests that the clearance between the rotor speeds and the natural frequencies should be at least five percent [59]. The range from the lowest to highest frequencies is presented in Figure 65.

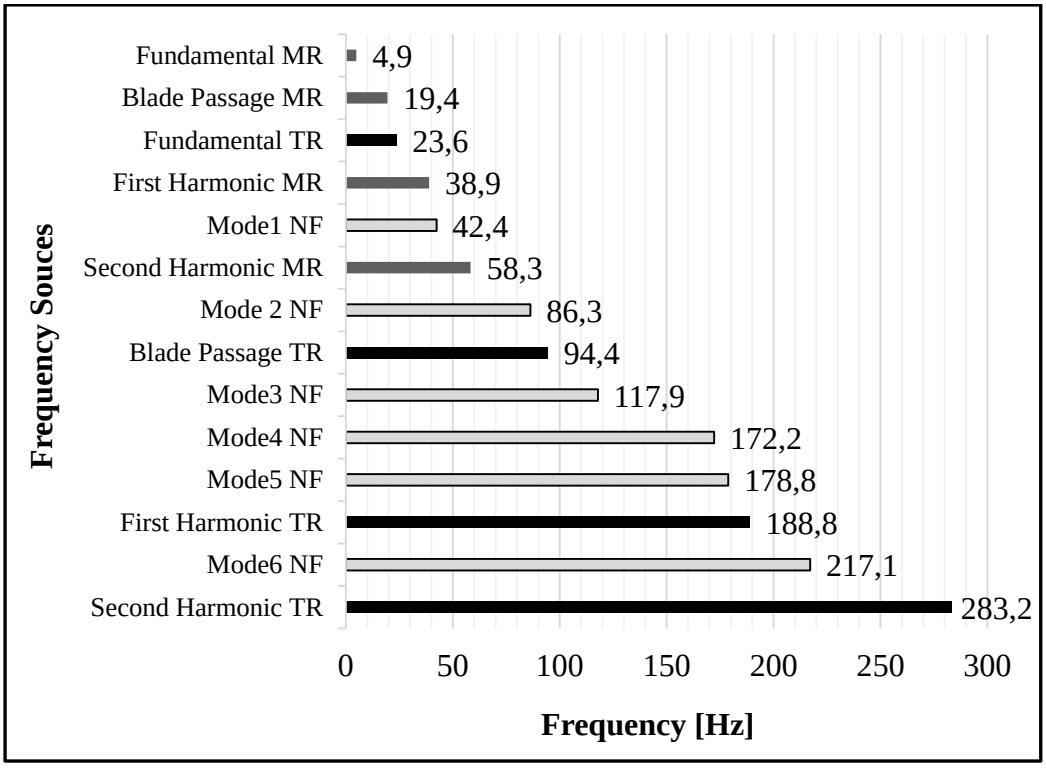

Figure 65: Frequency Range

When the results of the modal analysis and the frequency sources of the platform are compared, it could be seen that the natural frequencies of the tank structure do not match with rotating spends of the main and tail rotors. The clearance is approximately 5.6% between the two closest frequencies, which are the fifth mode of the natural frequency (178.8 Hz), and the first harmonic frequency of the tail rotor (188.8 Hz). In addition, the difference between the first mode of natural frequency with the first harmonic of the main rotor is on the order of %8.9.

Using the conducted modal analysis as a prerequisite, random vibration profiles could be introduced to the current analysis session. The vibration profile suggested by MIL-STD-810F (see Figure 66), could easily be imported in the form of a tabulated data created specifically for PSD g-Acceleration.

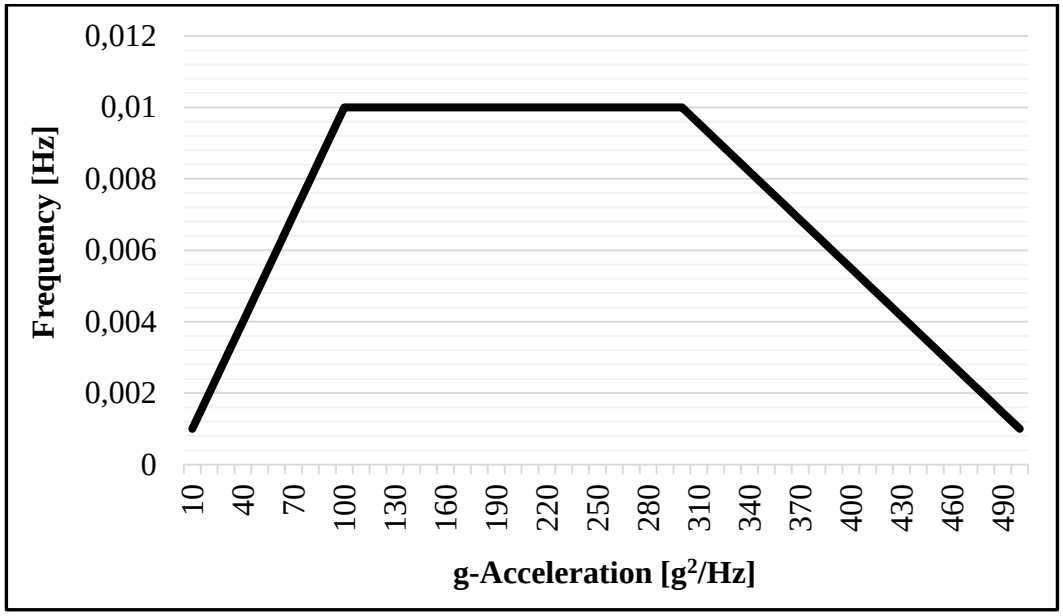

Figure 66: Random Vibration Profile

The results of the random vibration analysis are one standard deviation values assuming a mean value of zero. Statistically, it is assumed that about 68.3% of the results coincide with one standard deviation [56]. Since the results are directly depend on the statistical interpretations, the individual outputs belonging to the three orthogonal axes are examined.

The EFT survives and functions as intended without any damages in an environment including a random vibration. The resulting deformation basing on one sigma probability factor is about 0.69 mm when the random vibration analysis is performed in x-axis. The deformation observed in y-direction is 0.38 mm, and in z-direction is 0.0022 mm.

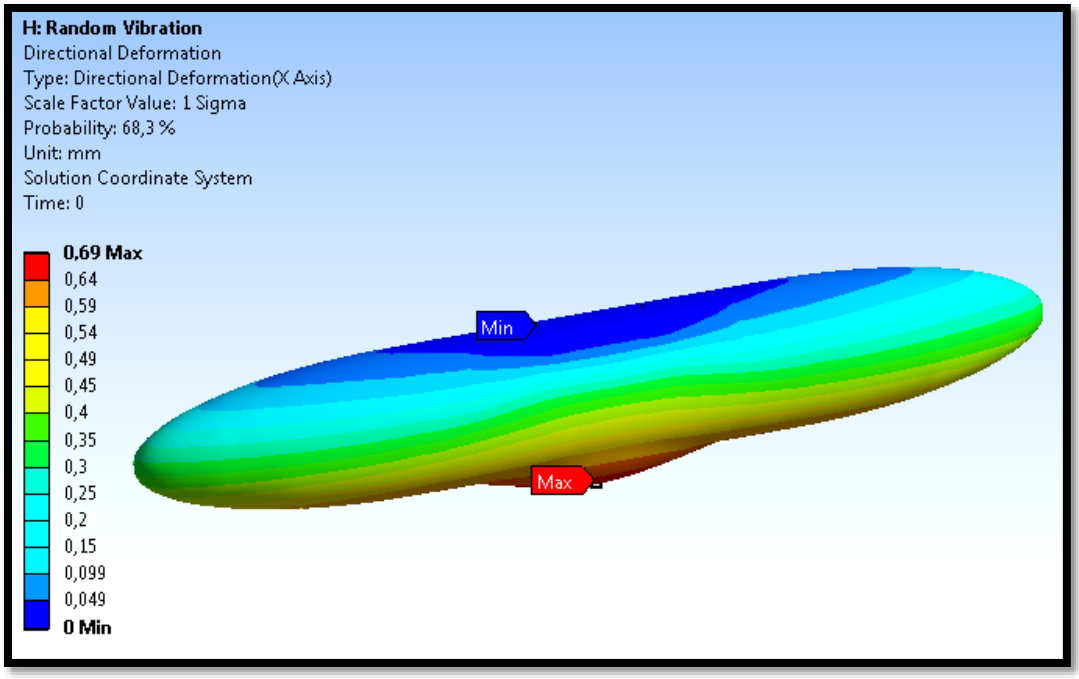

Figure 67: Random Vibration Output – Deformation in X-axis

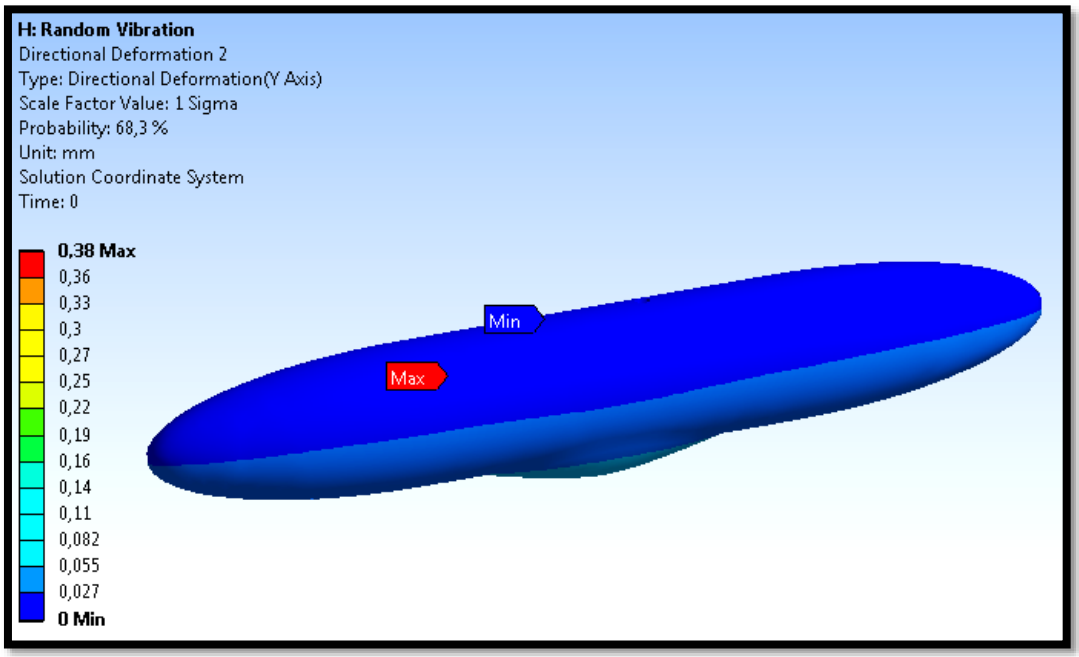

Figure 68: Random Vibration Output – Deformation in Y-axis

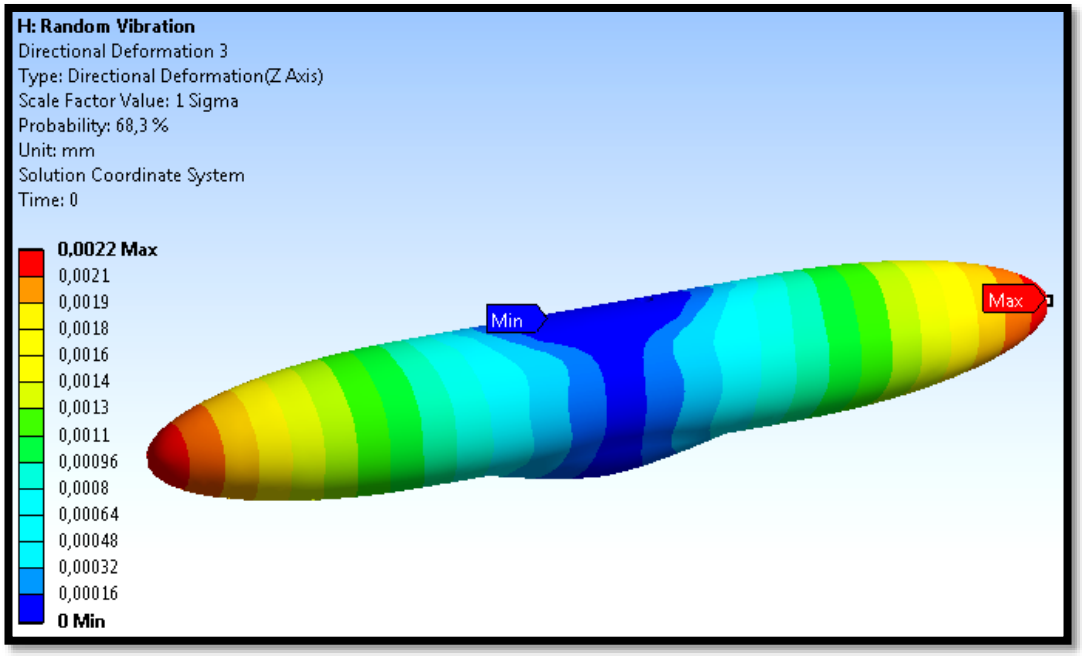

Figure 69: Random Vibration Output – Deformation in Z-axis

4.3. RESULTS OF THE TRANSIENT STRUCTURAL ANALYSES

In order to examine the dynamic response of the EFT against a time dependent load such as ground impact and fuel vapor ignition, transient structural analysis is performed. The main feature that distinguishes the transient analysis from static is the time dependency. Therefore, the preparing the transient analysis requires special attention.

4.3.1. Inadvertent Ejection Analysis

Considering the height defined by MIL-T-18847, integration of an EFT having an outer diameter of 430 mm and a sump depth of 80 mm to the store rack unit would results in a ground clearance of 924.2-millimeters as illustrated in Figure 70.

This distance is taken into account to calculate the velocity of the EFT prior to ground impact, which would be used as an initial condition for the transient analysis. The formula given below could be used to determine the free fall velocity.

$$V = \sqrt{2 \, . \, g \, . \, h} \tag{19}$$

$$V = \sqrt{2 \, . \, 9.806 \, . \, 0.924} = 4.257 \, m/s$$

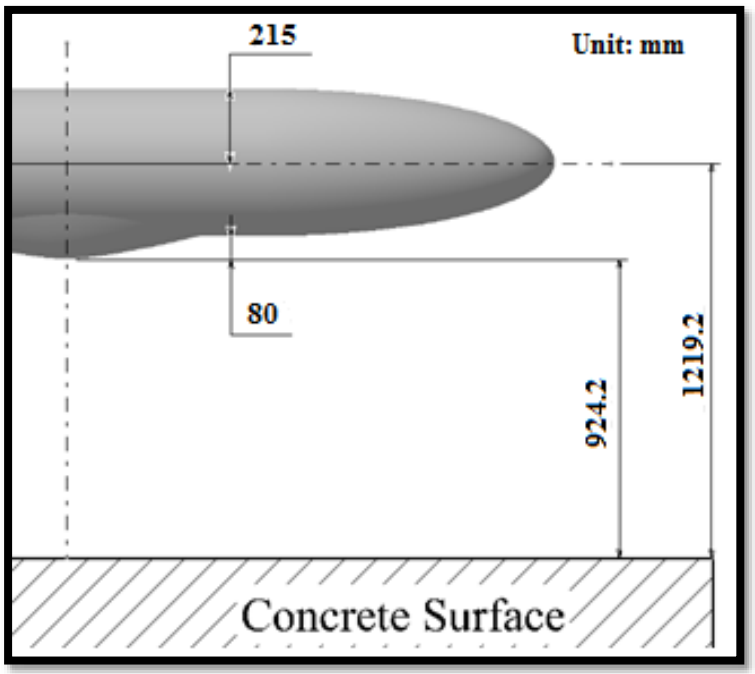

Figure 70: Heights for the Forced Ejection Test

Calculated velocity is introduced to the FEM used in static structural analysis. In addition to the available FEM, a body forming the impact surface is added. The material assigned for the body is concrete which is readily available in ANSYS Mechanical Library (see Figure 71).

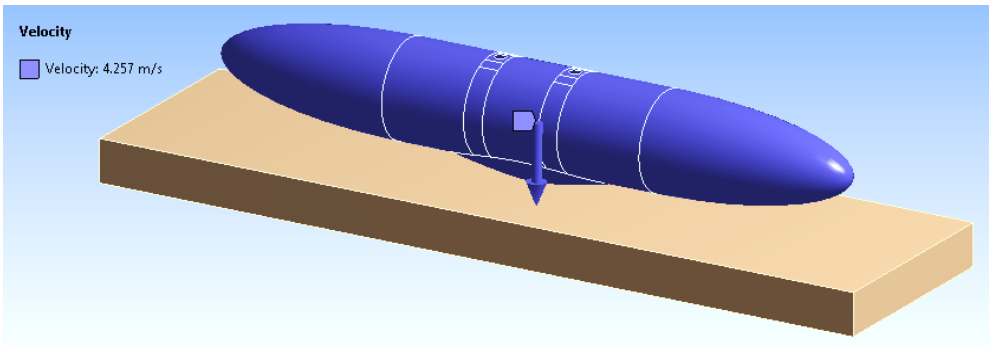

Figure 71: Definition the Initial Velocity

The solutions of the transient analyses require very long periods of time. In order to shorten the run time, a mesh density varying throughout the geometry is employed. At the contact point between the concrete surface and the sump is refined to be able to capture the stress gradients that occur due to the ground impact. The resulting FEM shown in Figure 72 comprises 15206 nodes and 10730 elements.

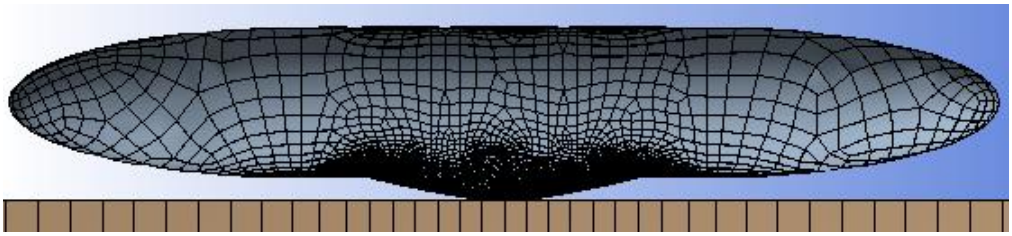

Figure 72: FEM for Forced Ejection Analysis

Together with the impact velocity, the standard earth gravity acting on the structure and the hydrostatic pressure of the fuel under the effect of standard gravity is defined as the load case, whereas the fixed supports are defined at the sidewalls of the concrete surface. A contact is identified for the FEM so that the EFT could not penetrate through the concrete surface (see Figure 73).

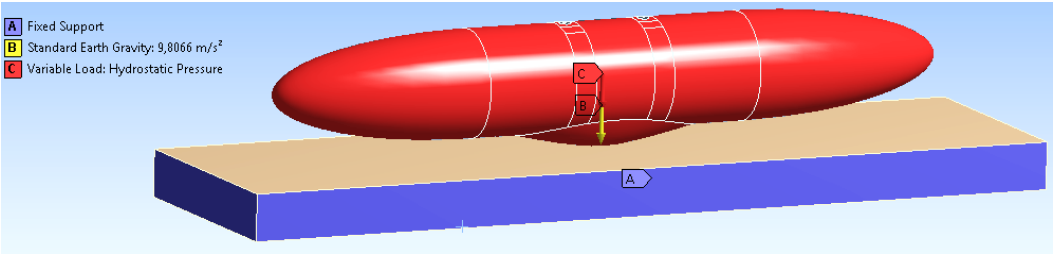

Figure 73: Boundary Conditions of the Forced Ejection Analysis

The characteristics of the analysis whose preparation is provided above are listed in Table 23.

Table 23: Characteristics of the Inadvertent Ejection Analysis

Physics	Transient Structural
Solver	Mechanical APDL*
Step End Time [s]	0.25
Initial Time Step [s]	0.001
Minimum Time Step [s]	0.0001
Maximum Time Step [s]	0.001

* APDL: ANSYS Parametric Design Language

The solution is converged by a total of 3862 iterations. The performance of the structure is evaluated by means of the deformation and RF variation by time. By examining the directional motion oriented in Z-axis as shown in Figure 74, the behavior of the EFT might be well understood upon the ground impact.

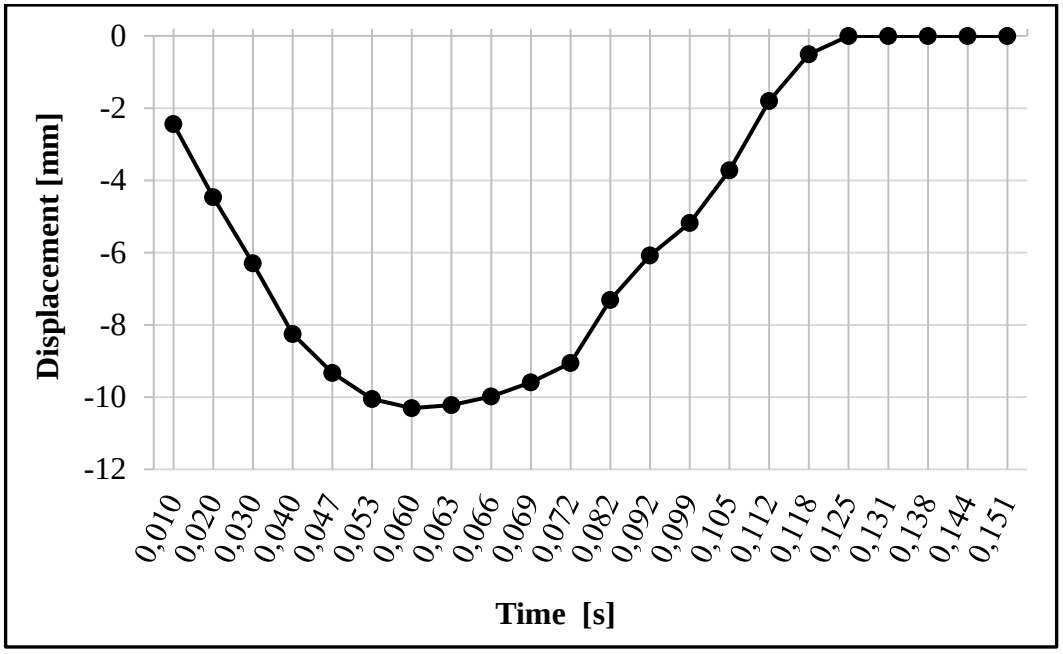

Figure 74: Displacement of the EFT in Z-axis during Forced Ejection

With the help of the graph provided in Figure 74, it could be interpreted that investigating the first 0.125-seconds of the motion is required. After that time, EFT rebounds and loses its contact with the concrete surface.

Damage assessment as in static structural analysis is performed according to Tsai-Wu failure theory. ACP postprocessor capabilities allow designer to capture RF corresponding to each time step. Figure 75 gives the determined minimum RF plotted against the defined time interval.

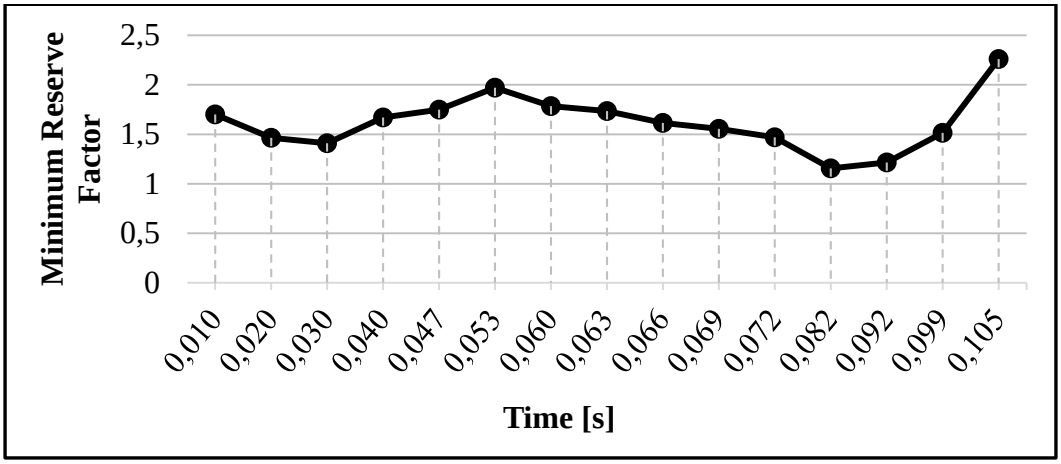

Figure 75: Variation of the Minimum RF by time

In order to present the RF range more accurately, the values between 0.112s and 0.125s are excluded, since the corresponding RF are far from being considered as critical. By examining the variation of the RF for the given time interval, it could be seen that the most critical case occurs at 0.0082-seconds. The RF variations on the tank structure at t=0.0082s are shown in Figure 76 and 77.

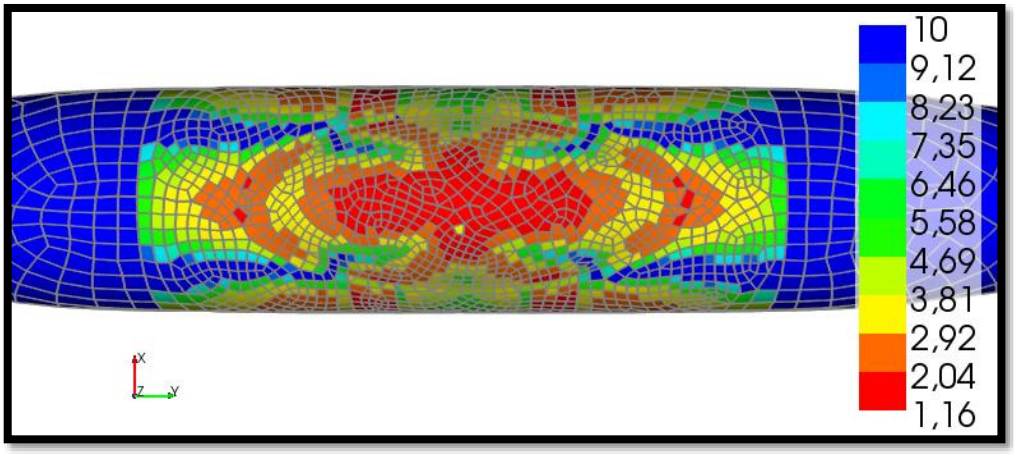

Figure 76: Bottom View of the RF Distribution at t=0.082 s

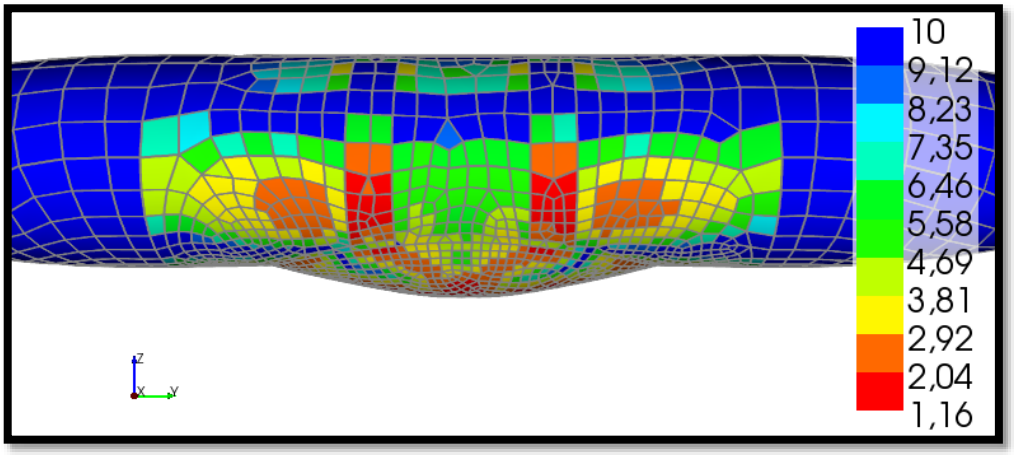

Figure 77: Front View of the RF Distribution at t=0.082 s

A sump located at the bottom of a cylindrical body distorts the geometric axial symmetry. Although, a failure is not observed according to the results of the FEA, it should be highlighted that as a protrusion, sump poses vulnerability against impacts. Being close to the theoretical failure limit, consecutive impacts might

result in a rupture leading to fuel leakage, which precludes the employment of the external tanks.

4.3.2. Fuel Vapor Ignition Analysis

Ventilation is one of the major design requirement for a fuel system. The management of the space above the free fuel surface is one of the most important operational issue especially for the operations including high altitudes. The rate of evolution of the fuel vapor increases rapidly as the altitude of the operation is increased. Evolution of the fuel vapor is a serious threat for the flight safety, since the vapor has the risk of being ignited. Flammability arises from the vapor, since it is the vapor that burns rather than the liquid form of the fuel [26]. Therefore, it must be ensured that the EFT withstands the explosive pressure caused by the ignition of the fuel vapor.

According to MIL-T-18847, the explosion produces a pressure peak at least 6.5 atmospheres (0.6586 MPa) within 60-milliseconds [51]. However, the standard does not identify the pressure profile after the peak rise. Therefore, a custom pressure profile plotted against the time is created as shown in Figure 78.

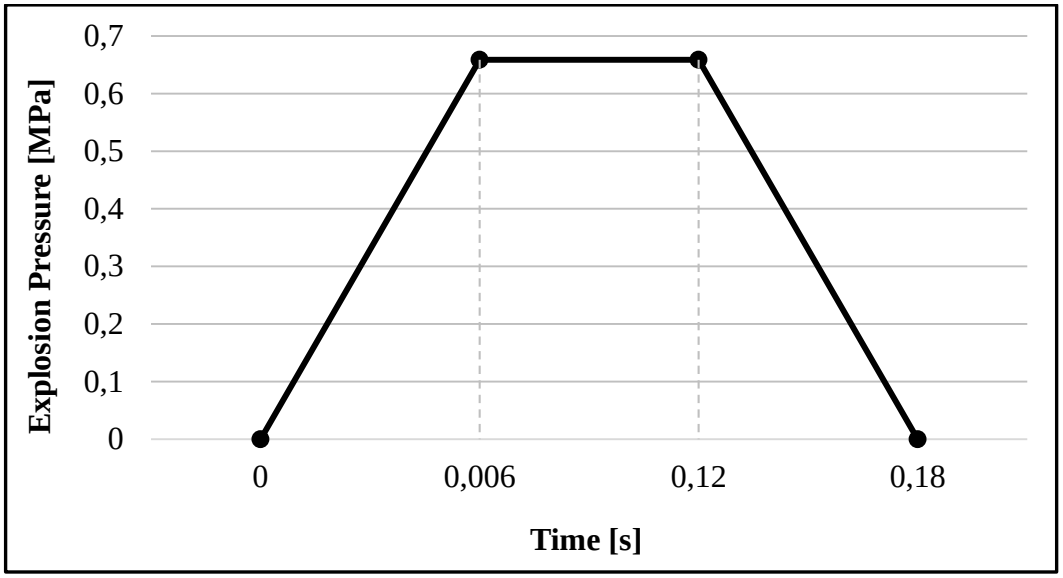

Figure 78: Explosion Pressure Profile

The profile created suggests that the pressure reaches its peak, for the next 0.06 seconds it remains constant at 6.5-atmospheres, and the pressure is revealed within 0.06 seconds. It should be noted that depressurizing the tank with a rate equal to explosion poses a challenging condition.

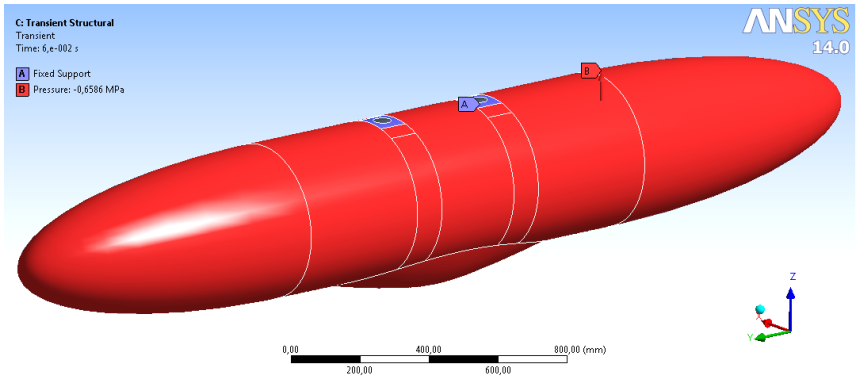

Figure 79: Boundary Conditions of the Explosion Pressure Analysis

The supports are identical to those defined for the static structural analysis (see Figure 79). Three steps are identified as the analysis settings in accordance with the defined pressure profile. The characteristics of the analysis are listed in the following table.

Table 24: Characteristics of the Fuel Vapor Ignition Analysis

Physics	Transient Structural
Solver	Mechanical APDL
Number of Steps	3
End Time [s]	0.18
Initial Time Step [s]	0.001
Minimum Time Step [s]	0.0001
Maximum Time Step [s]	0.001

The solution is obtained after 4173 iterations. The time-dependent change of the deformation occurring in the structure under the effects of explosion is presented in Figure 80.

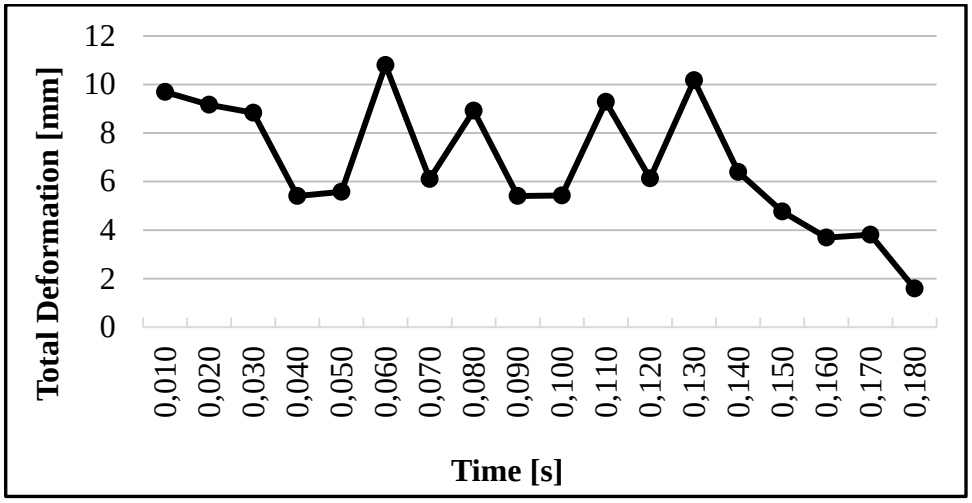

Figure 80: Total Deformation of the EFT during the Explosion

The maximum deformation observed within the specified time period is about 10.8-millimeters. RF corresponding to the deformations could be examined in Figure 81.

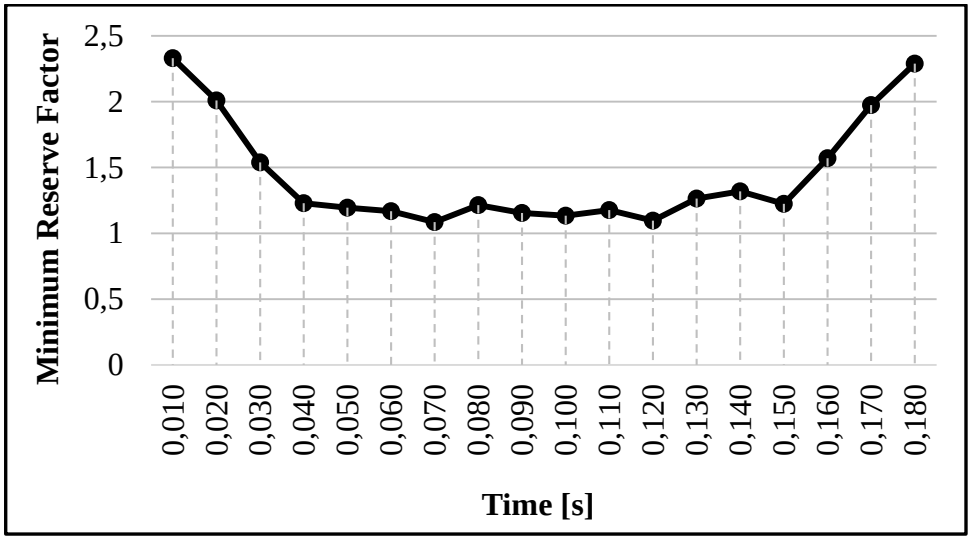

Figure 81: Variation of the minimum RF by Time During the Explosion

The plot of the minimum RF variation is similar to the mirror image of the pressure profile. At two points, the reserve factors are estimated just above the failure limit. The RF distribution given in Figure 82 and 83 reveals that the explosion pressure generated by the fuel vapor ignition is the most challenging conditions for the structural integrity.

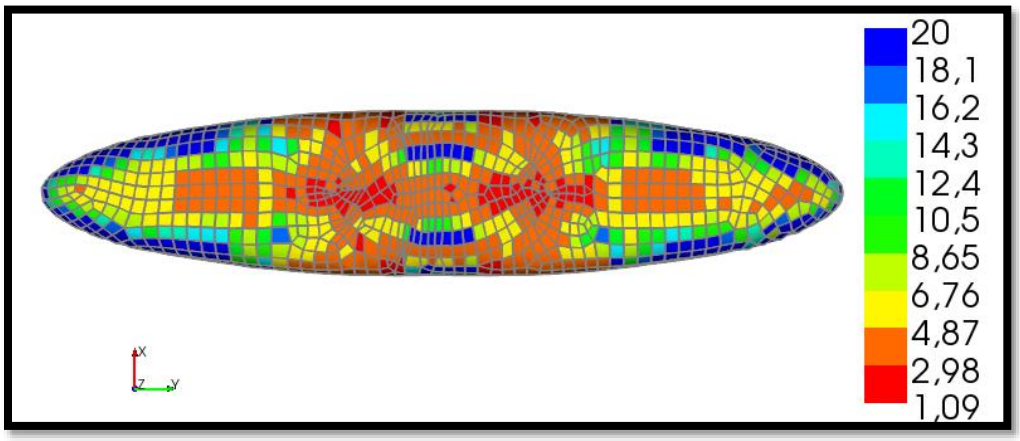

Figure 82: Bottom View of the RF Distribution at t=0.120 s

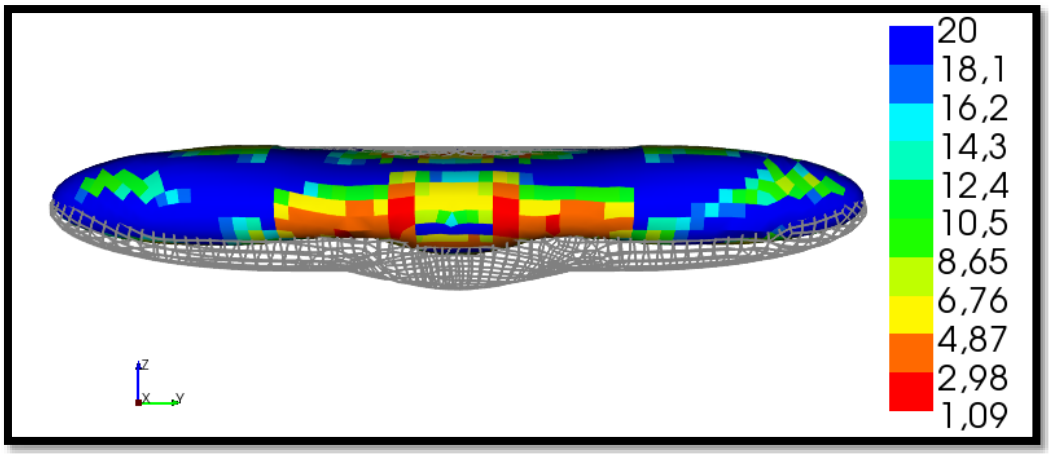

Figure 83: Front View of the RF Distribution at t=0.120 s

Reserve factor could be defined as a measure of comparing the material limits with the ultimate stress resultant that the EFT experiences in its service life. By definition, RF of unity means that the structure would not be able to withstand the loads more than the ultimate design loads. Additional loads with unpredictable magnitudes beyond the ultimate limit would lead to the failure of the structure. Determining a proper RF requires an accurate identification of the design requirement and the nature of the loads. Therefore, in order to compensate such uncertainties involved for known reasons, considering larger RF might be desirable in design process. However, restrictions for meeting the design requirements and weight considerations prevent larger RF from being employed in the verification process. Since the weight of the prototype in this study has reached up to its target limit specified in the design requirements, any further improvements could not be made. However, the minimum RF, which was obtained by means of the FEA of the fuel vapor ignition, is close to the theoretical failure limit. In this case, in order to make a feasible judgment, ballistic test should be performed to examine the ballistic resistance of the EFT. Structural capabilities of the tanks could be regarded as acceptable if the tank structure maintains the integrity after the projectile penetrates through the filament wound shell.

4.4. CRASH IMPACT TEST

Determining the structural behavior and the loads acting on the personnel during a crash provides valuable information for studying or validating the crashworthiness of air platforms. With a right tool capable of performing explicit transient dynamic simulations, various crash scenarios could be evaluated quickly. New generation simulation tools such as LS-DYNA and MSC Dytran allow designer to evaluate sophisticated models including large deformations and progressive failure. However, the level of consistency of the analytical analysis in obtaining predictions

should be demonstrated. Therefore, full-scale crash tests are conducted. In this particular, Impact Dynamics Research Facility (IDRF) located at NASA Langley Research Center in Virginia was recognized as a central base. The IDRF was built as a lunar landing simulator in 1965. Apollo astronauts were trained to gain landing experience under various conditions. The IDRF was converted into a full-scale crash test facility in 1970's. Until the facility was decided to be closed by NASA Langley in 2003, the IDRF had been used to conduct 41 full-scale crash tests of aircrafts and 11 full-scale crash test of rotorcraft. In order to perform full-scaled tests and support the full weight of the platforms, a steel gantry structure being 240 ft. (73.15 m) high, 400 ft. (121.92 m) long and 265 ft. (80.77 m) wide was constructed at the base [67] (see Figure 84).

Figure 84: IDRF Gantry [67]

A pendulum swing technique was used to achieve various forward and vertical velocities depending on the requirement. There was a winch used to adjust the

height of the platform, and when the platform was lifted to the desired height, it was released to swing towards the impact surface. Prior to the ground impact, all of the cables controlling the swing were cut which left the platform completely unconstrained [67]. Figure 85 provides the schematic illustration of the full-scale crash test setup of IDRF.

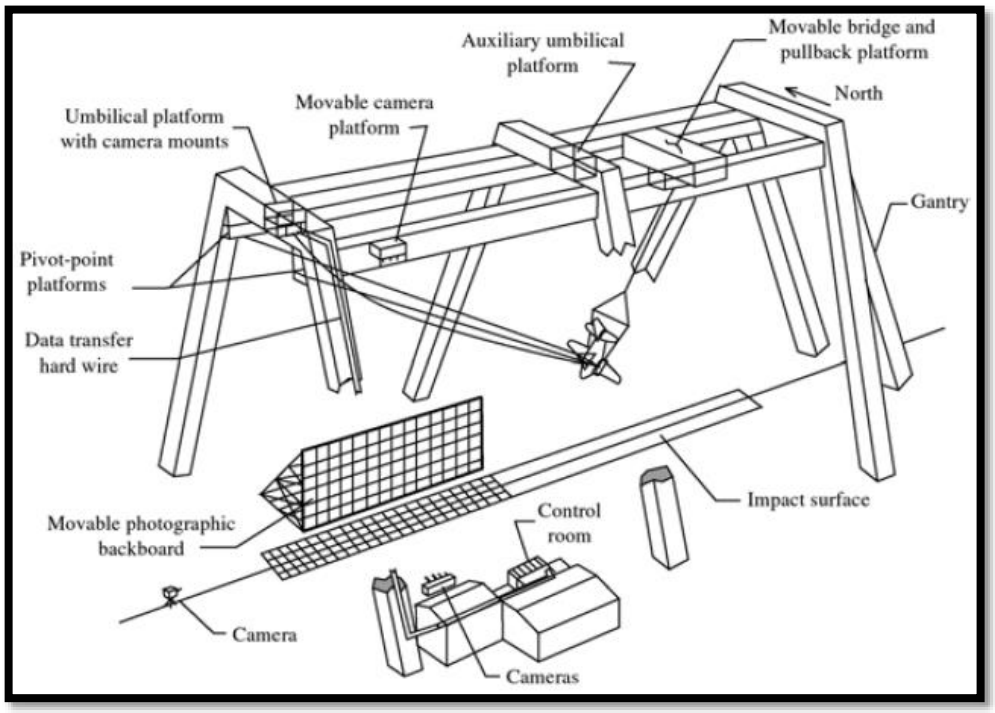

Figure 85: Full Scale Crash Test Setup [67]

The impact responses of the external fuel tanks are evaluated together with a full-scale platform employing External Stores Support System (ESSS). To eliminate the potential risks, water was used instead of fuel. Accelerometers and transducers were placed on each EFT to capture the response during impact. Photographs of the helicopter and EFT taken during crash test are shown in Figure 86.

(a) Side View of the Platform During Impact

(b) Pre-test Release Position

Figure 86: Photographs of the Full Scale UH-60 Crash Test [67]

It should be recognized that, conducting full-scale crash test is not feasible within the scope of a sub-system development project. Therefore, the search for a domestic test center capable of simulation the crash test was initiated. Unfortunately, there is no such test center or institution that provides comprehensive services like IDRF. However, as a result of the research, it was found out that the crash test could be performed within the capabilities of the METU-BILTIR Vehicle Safety Unit. In 2009, the first non-destructive sled test facility of Turkey was established in order to be able to conduct test according to international regulations and standards. The events of frontal and rear crashes could be simulated by employing a linear actuator. The test system shown in Figure 87, which was accredited in 2011, consists of a catapult unit and a sled system [68].

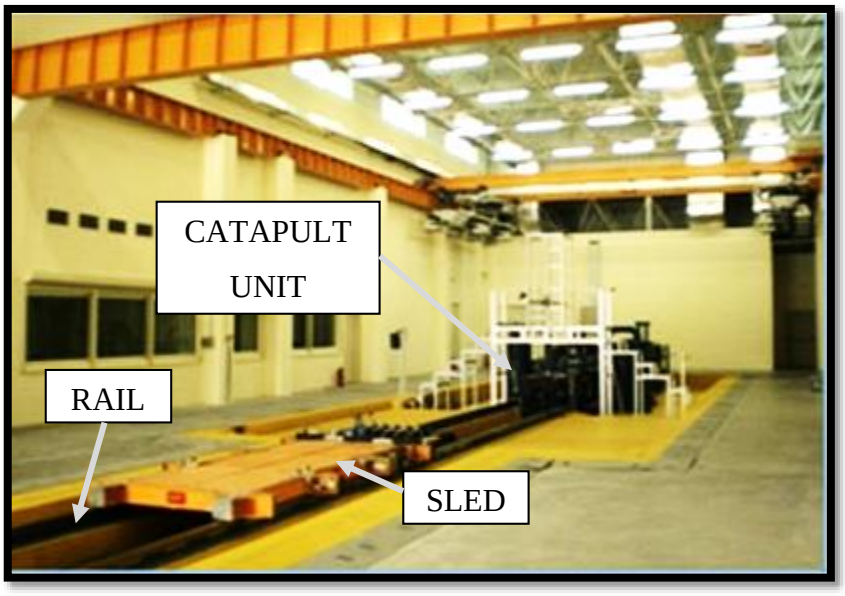

Figure 87: Crash Simulation Test System in METU-BILTIR [68]

Technical details and the properties of the components are as follows [68].

Catapult Unit:

- 2500 kN Nominal Force
- 1700 mm Working Stroke
- 140.000 l/min 4-Stage Servovalve
- Hydraulic Power Supply: 250 l/minimum flow rate
- Hydraulic Power Supply: 280 bar Pressure

Sled and Rail System:

- 2500 kg payload
- 1800 x 4100 mm sled dimensions
- 90 g maximum acceleration
- 90 km/h maximum velocity
- 32 m long precise rails

Unlike ground vehicles, the crash of an air platform includes a vertical velocity condition. Thus, simulating the crash and evaluating the structural performance of the EFT requires a unique test fixture.

Based on the vertical and forward velocity components, resultant velocity is calculated. The resultant g-force can easily be derived from the defined velocity component by taking into account the total period of time of the acceleration that the structure undergoes during crash. An inclination of 24-degrees from vertical ensures that the axis of the resultant force coincides with the axis of the motion. However, in this position, the effect of the gravitational acceleration acting on the structure is against the nature of the crash event. To eliminate the aforementioned effect illustrated in Figure 88, the inclination angle should be increased by 10-degrees.

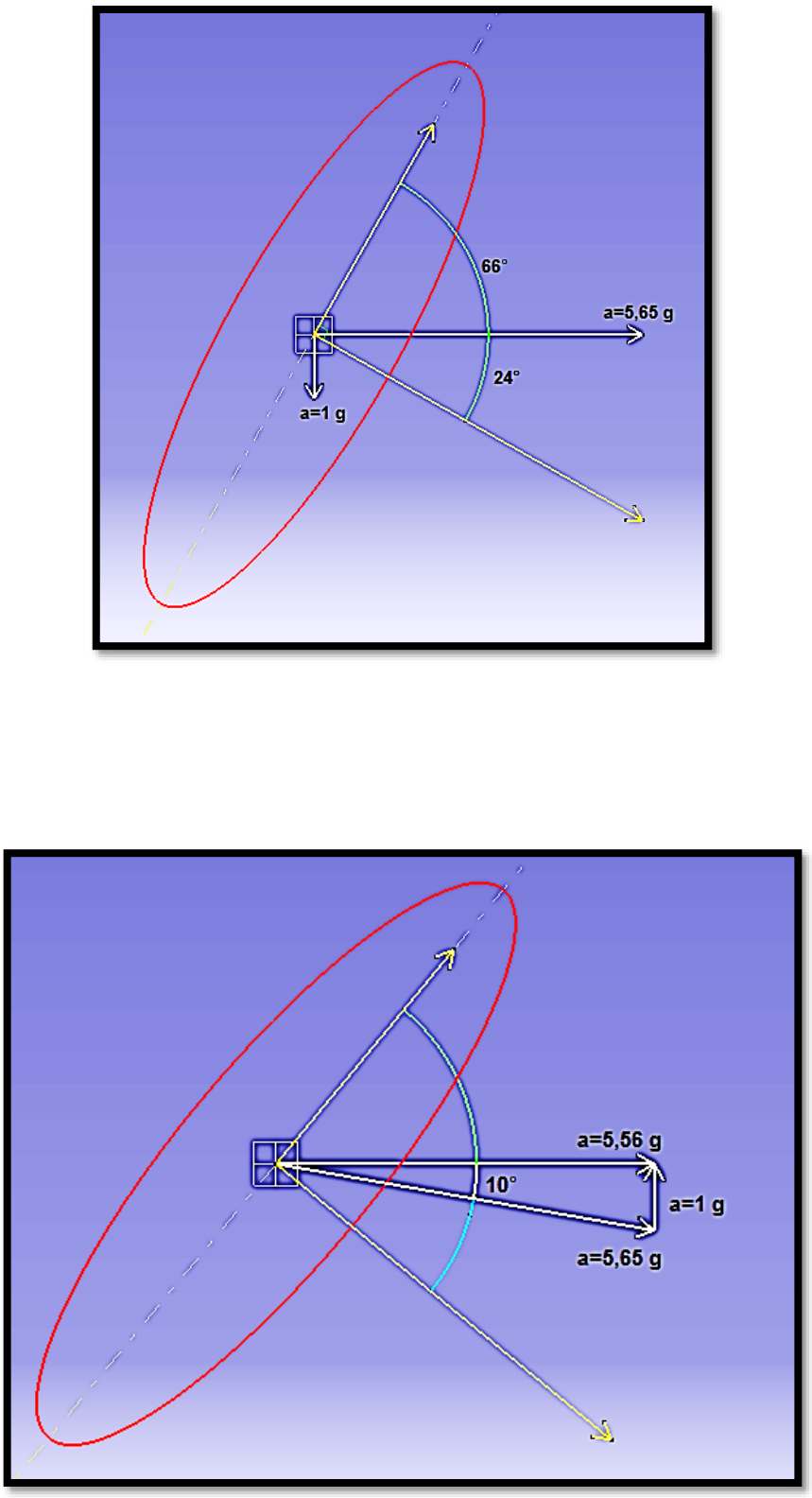

Figure 88: Determining the Test Parameters

After determining the orientation, a fixture, which is capable of supporting the EFT when it is filled with grains to simulate the weight of the full tank, was designed. In this embodiment wide flange H beams were used, and the EFT was fixed from two hard points simulating the actual integration to the BRU. The designed test fixture is shown schematically in Figure 89.

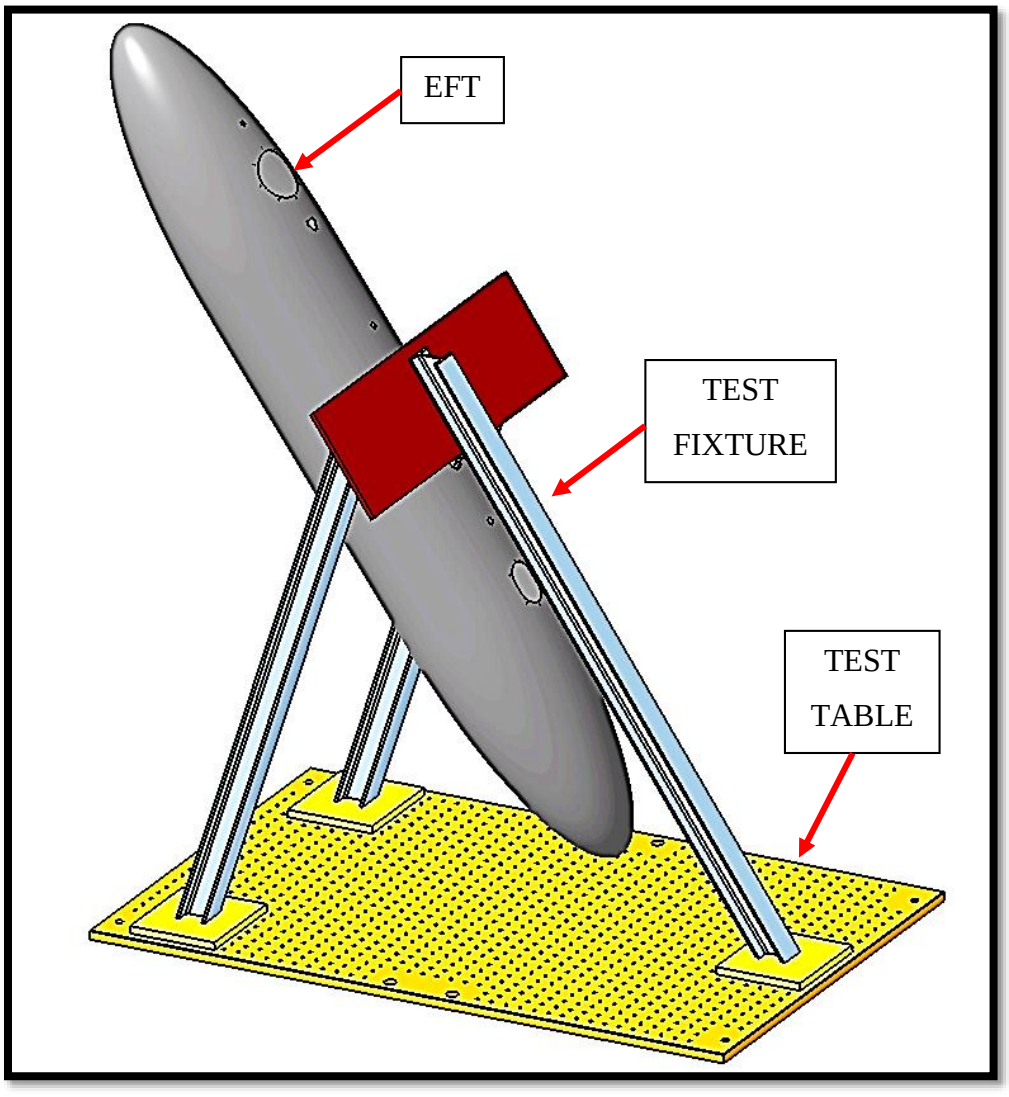

Figure 89: Crash Test Fixture

(a) Overview of the EFT

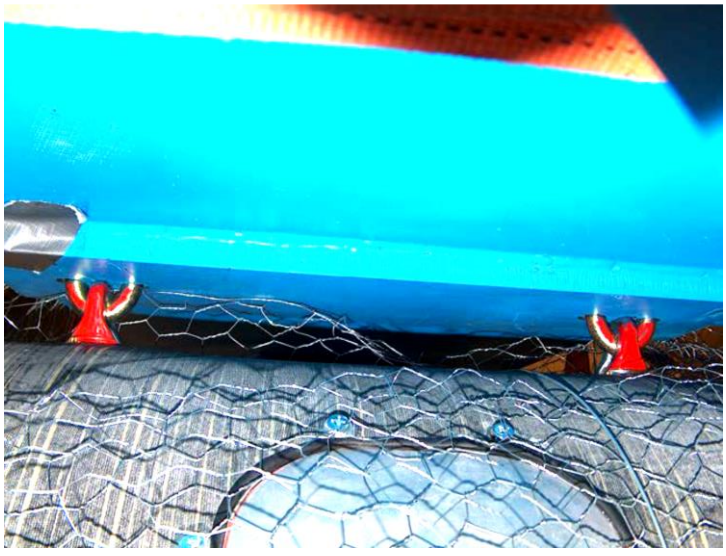

(b) Close-up View of the Suspension Lugs

Figure 90: Pre-test Photographs

Figure 89 gives the photographs of the EFT prior to the crash simulation. The target impulse profile was provided to the system prior to the test. This suggested impulse should be established by taking the capabilities of the test facility into account. Due to the nature of the crash impact, the real-world physics is based on a deceleration through 0.3-seconds. However, the crash test was performed in the form of an acceleration within 0.28-seconds in a control manner by means of the catapult unit. The target impulse plotted against time is given in Figure 91.

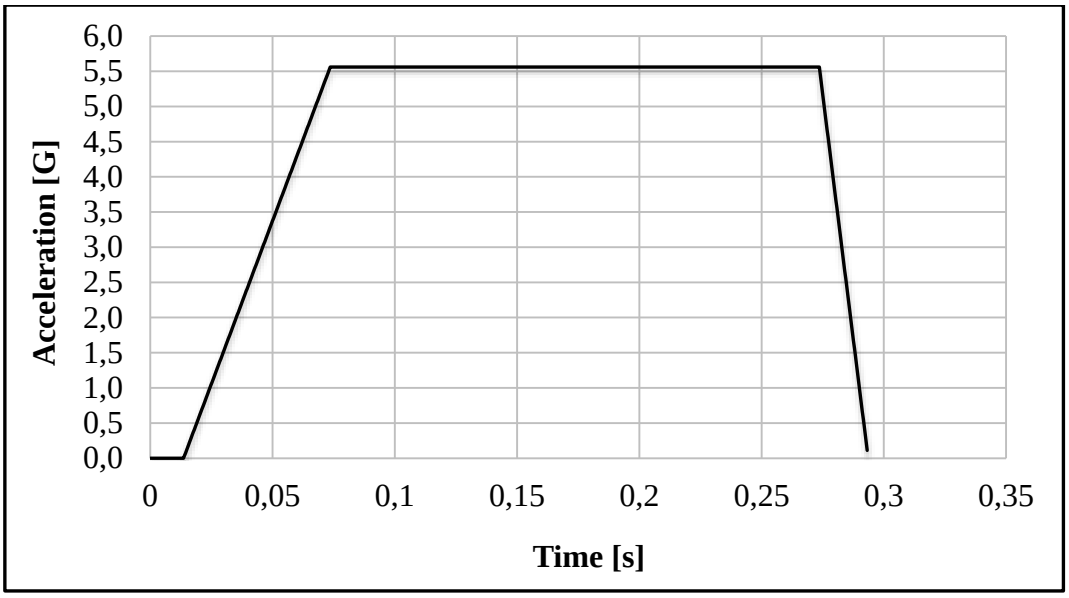

Figure 91: Target Impulse of the Crash Simulation

After the authorized test operators introduced the required settings such as brake pressure and peak acceleration into the system, the test was performed without any problem. The results obtained in the test are presented below.

Table 25: Crash Test Characteristics

Piston Load	High
Maximum G	7.45
Acceleration Time [s]	$281x10^{-3}$
Brake Pressure [bar]	50
Brake Time [s]	0.2
Total Distance [m]	9.2

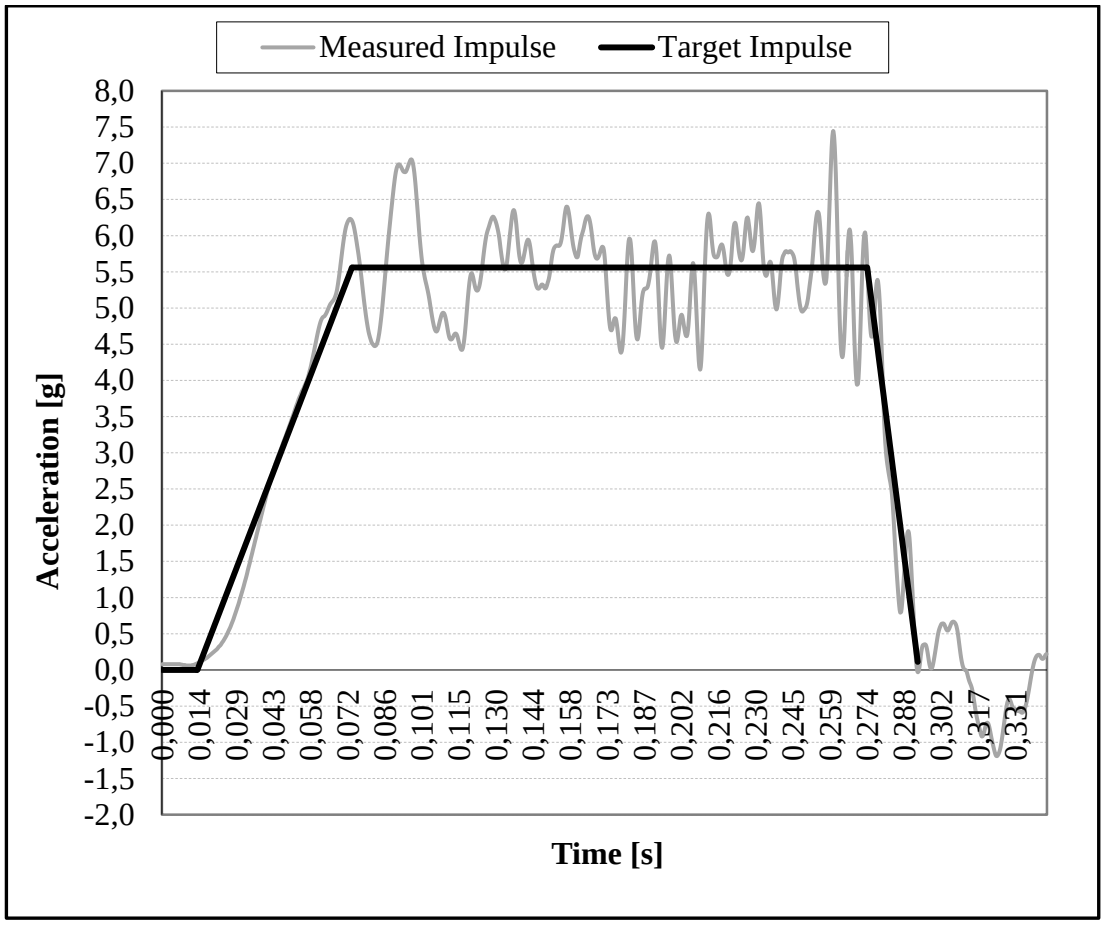

Figure 92: Result of the Crash Impact Simulation

When the profile obtained from the crash impact simulation is compared to the target impulse noticeable oscillations attract the attention. The main reason underlying is that the contained load is the significant portion of the total weight of the full-tank. In addition, the fact that there is interaction between the tank and the test fixture gives rise to these oscillations.

The results of the test indicate that the EFT could survive from a crash impact condition. Although the tank structure experienced more severe g-loads than expected, it remained attached to the text fixture. The tank appeared to have no visible structural deformation or fracture. In order to examine the entire structure to detect any damage visually, the exterior surface of the tank was coated with powder and the tank was filled with water to its full capacity. No rupture cracks that would allow leakage were observed. A post-test photograph showing the overall view of the EFT is shown in Figure 93. From the close-up views of the critical locations, it could be concluded that the tank structure met the design criteria.

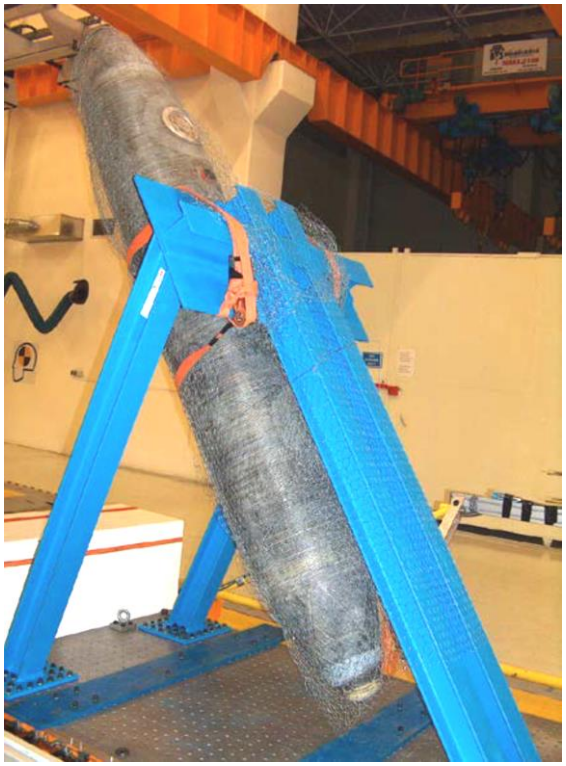

(a) Overview of the EFT

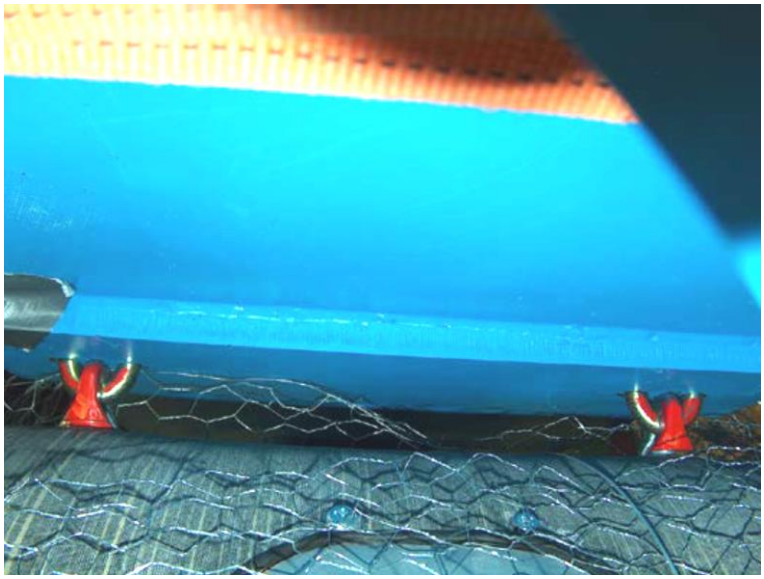

(b) Close-up View of the Suspension Lugs

Figure 93: Post-test Photographs

CHAPTER 5

CONCLUSION AND FUTURE WORK

The study reported in this thesis provides all stages of a simulation-driven development of an External Fuel Tank (EFT). Within the development cycle, initial task is the design process. During this process, considerable research needs to be conducted in order to recognize of the particular need. The design synthesis should capture all relevant functional considerations of the EFT being developed including the product definition, interchangeability with existing tanks that are in use, standardized subsystems, reliability, operational objectives and safety. From the system definition, fuel system components and interface requirements were derived accordingly. After the preliminary design reviews, the design process was completed by forming the general assembly which was confirmed at both system and equipment level. 3D Model of the EFT was created by using one of the core element of the CAE tools which was a CAD software called CATIA™ V5.

Each design should be tested and verified in some way. Regardless of the product being developed, it must be examined in every aspect against the specifications. Therefore, the performance of the proposed design solution should be checked to confirm that the requirements have been met. In the real-world environment, EFT experiences wide range of forces including aerodynamic and maneuver loads. However, conducting physical testing for each load case is not feasible due to the cost-effectiveness. The required approach has become available in the form of powerful simulation tools. Commercially available simulation tools enable the designer to reflect the real-world into a virtual environment. In order to model the

multi-layered nature of the composite structure Composite PrepPost which is an add-on module of ANSYS was used. The Finite Element Model was created in an automated manner with the help of the capabilities of the ANSYS. The operational environment, defined in Section 3.3, was introduced to the Workbench based workflow. Since the in-flight loads vary slowly in time, static structural analyses were performed to determine the structural behavior with respect to a given winding angle. Since the mechanical properties of a helically wound structure depends heavily on the winding angle, it would be rational to make an inference of the winding angle based on the output of the static analyses. The variation in stress, deformation and Tsai-Wu failure criteria was examined against a variable winding angle ranging 0- to 90-degrees. A winding angle of 30-degrees was found to be resulted in an instant increase in performance. Therefore, the proper winding angle was determined to be 30-degrees. The performed FEA after determining the winding angle shows that no failure is predicted for static loading consisting of potential worst-case loading environments. In addition, external fuel tanks experience various combinations of vibrations excited by main and tail rotors. The modal and random vibration analyses were carried out in order to identify the dynamic response of the structure, natural frequencies and the mode shapes. No coincidence was observed when the natural frequencies were compared to the main and tail rotor frequencies. According to the random vibration outputs, the tanks structure remains undamaged and fully functional in an environment including random vibration.

The time-dependent loading conditions that the EFT undergoes throughout the operational envelope are defined in the Military Specification of the design, test and installations of EFT, MIL-T-18847. EFT should have the ability to withstand the ground impact when it is released from the BRU inadvertently. Moreover, the EFT being developed should withstand the pressures generated by the fuel vapor ignition. The dynamic behavior of the EFT against such time dependent load could only be examined by performing a transient structural analysis. Although no failure

was observed according to the Tsai-Wu failure criteria, inadvertent release and the explosive pressure of the fuel vapor were found to be the most challenging conditions for the EFT. The RF values obtained both for inadvertent release and the fuel vapor ignition analyses are just above the theoretical failure limit. . Since the weight of the prototype in this study has reached up to its target limit specified in the design requirements, any further improvements could not be made.

The impact response of the EFT during a crash was evaluated by conducting crash test at METU-BILTIR Vehicle Safety Unit. In order to capture the vertical and horizontal velocity components, a unique test fixture was designed and constructed. Although, more severe g-loads were obtained during the test, EFT maintained its structural integrity and remained attached to the test fixture. Therefore, it could be said that the EFT would survive and perform as desired during a crash condition.

To sum up, an all composite external fuel tank meeting the design requirements was developed within the scope of the thesis. The tank structure was verified against the ultimate loads that the EFT would experience during its life cycle. The design with the unique material combination satisfies the target weight limit and provides a minimum RF value above unity for all loading conditions.

To propose a safe and sufficiently strong EFT structure, several FEA were conducted, and the results were presented in this thesis. In order to go beyond these results, further simulations and experiments could be proposed. External fuel tanks are likely to be employed in the operational environments including hostile fire. Therefore, the ballistic performance of the structure should be examined. Solid-fluid interaction is one of the major issues, which has been attracting attention in recent years. The issues related to the effect of a solid motion traveling at a high speed in fuel, the response of the structure upon the impact of the projectile, and the hydraulic ram effect generated by the projectile damage at entrance and exit remains to be studied as the future work.

In addition, most of the scientific efforts have been addressed to develop rubberized bladders, which have the ability to seal the tank structure against fuel leakage after being penetrated. Such self-sealing bladders feature a mixture of the rubber derivatives, which prevents fuel loss through the entrance of the projectile. Since there were no attempts to develop a new bladder within the scope of the thesis, the determination of the proper material solutions could be considered as a future study [69].

The possibility of post-crash fire poses a major obstacle for the EFT to be jettisoned especially at the low altitude flight regimes. During a crash sequence, a rupture crack could be formed, which might lead to fuel spillage. Needless to mention that fuel spillage causes a post-fire crash, which vanishes the chance of survivability [25]. Structural aspects of the crash survival design have been studied extensively in order to improve the survival of the EFT. Establishing the design criteria together with the implementation of crashworthiness principals in the development process of the tank structures being developed requires an intense study. In the construction of the tank structure, materials capable of resisting and absorbing the impact forces upon crash could be studied in the future [70]. Since the crashworthy design approach brings inevitable increase in weight, a refinement or a revision of the target weight is required.

REFERENCES

[1] Aircraft (n.d.). In Cambridge Dictionaries Online. Retrieved September 4, 2013, from http://dictionary.cambridge.org/dictionary/british/aircraft?q=aircraft

[2] Aircraft (2013). In Citizendium Online Encyclopedia. Retrieved September 4, 2013,from http://en.citizendium.org/wiki/Aircraft

[3] Kumar, B. (2005). *An Illustrated Dictionary of Aviation.* New York, NY: McGraw-Hill.

[4] *Airplane*, (2013). In Encyclopedia Britannica. Retrieved September 4, 2013, from http://www.britannica.com/EBchecked/topic/11014/airplane

[5] Kundu, A. (2010). *Aircraft Design*. New York, NY: Cambridge University Press.

[6] Federal Aviation Administration (2003). *Glider Flying Handbook (FAA-H-8083-1).*

[7] Kramer, D. C. (2001). *U.S. Patent Application 09/761,575*.

[8] Federal Aviation Administration (2012). *Helicopter Flying Handbook (FAA-H-8083-21).*

[9] *Helicopter* (2013). In Encyclopedia Britannica. Retrieved September 6, 2013, from http://www.britannica.com/EBchecked/topic/259992/helicopter

[10] *Military aircraft* (2013). In Encyclopedia Britannica. Retrieved September 6, 2013, from http://www.britannica.com/EBchecked/topic/382295/military-aircraft

[11] Boyne, W. (2011). *How The Helicopter Changed Modern Warfare.* New York, NY: Pelican Publishing.

[12] Marzocca, P., *AE 429 Aircraft Performance and Flight Mechanics 2003*. (Clarkson University, Lecture Notes) http://people.clarkson.edu/~pmarzocc/AE429/AE429index.html (Accessed September 10, 2013).

[13] *Aircraft Range* (2008). In NASA Glenn Research Center - The Beginner's Guide to Aeronautics. Retrieved from http://www.grc.nasa.gov/WWW/k-12/airplane/range.html

[14] Stern, D. (2008). *UH-60 External Tanks.* Retrieved September 10, 2013, from http://www.aeroscale.co.uk/modules.php?op=modload&name=SquawkBox&file=index&req=viewtopic&topic_id=118930&page=1

[15] U.S. Department of Defense (1994). Military Standard: *General Design Criteria for Bomb Rack Unit, (MIL-STD-2088A*).

[16] Rahman, T., & Miles, D. (2009). *WIPO Patent No. 2009137942*. Geneva, Switzerland: World Intellectual Property Organization.

[17] International Defense Magazine - Defense Update (2004). *Extending the F-16 Range.* Retrieved September 4, 2013, from http://defense-update.com/products/f/f-16-fuel.htm

[18] Robertson Fuel Systems (n.d.). *Crashworthy External Fuel Tank*. Retrieved September 10, 2013, from http://www.robbietanks.com/products?type=aircraft

[19] Federal Aviation Administration (2007). *Aircraft Weight and Balance Handbook (FAA-H-8083-1A*).

[20] U.S. Army Aviation Systems Command (1983). *Preliminary Airworthiness Evaluation of the UH-60A Configured with the External Stores Support System*. U.S. Army Aviation Engineering Flight Activity, Edwards Air Force Base, California.

[21] LeGault M. (2011). *Carrier-Capable, All-Composite External Fuel Tank,* High-Performance Composites Magazine May 2011 Issue.

[22] Kurrle, C. (1944). *U.S. Patent No. 2,355,084*. Washington, DC: U.S. Patent and Trademark Office.

[23] Morrisey, E. J. (1984). U.S. Patent No. 4,453,995. Washington, DC: U.S. Patent and Trademark Office.

[24] Lyman, R. R. (1990). U.S. Patent No. 4,948,070. Washington, DC: U.S. Patent and Trademark Office.

[25] Bracken, J., Crane, R., & York, B. (2002). U.S. Patent No. 6,491,255. Washington, DC: U.S. Patent and Trademark Office.

[26] Langton, R. et al. (2009). *Aircraft Fuel System*. West Sussex: John Wiley&Sons.

[27] Campbell, F.C. (2010). *Structural Composite Materials.* Materials Park, OH: ASM International.

[28] Mallick, P.K. (2008). *Fiber-Reinforced Composites*. Boca Raton, FL: CRC Press.

[29] Federal Aviation Administration (2008). *Aviation Maintenance Technician Handbook (FAA-H-8083-30) – Advanced Composite Materials.*

[30] Peters, S.T. (2011). *Composite Filament Winding.* Materials Park, OH: ASM International.

[31] Cohen, D. (1997). Influence of filament winding parameters on composite vessel quality and strength. *Composites Part A: Applied Science and Manufacturing*, *28*(12), 1035-1047.

[32] Xia, M., Takayanagi, H., & Kemmochi, K. (2001). Analysis of multi-layered filament-wound composite pipes under internal pressure. Composite Structures, 53(4), 483-491.

[33] Mertiny, P., Ellyin, F., & Hothan, A. (2004). An experimental investigation on the effect of multi-angle filament winding on the strength of tubular composite structures. Composites science and technology, 64(1), 1-9.

[34] Rousseau, J., Perreux, D., & Verdiere, N. (1999). The influence of winding patterns on the damage behaviour of filament-wound pipes. Composites Science and Technology, 59(9), 1439-1449.

[35] Buragohain, M., & Velmurugan, R. (2011). Study of filament wound grid-stiffened composite cylindrical structures. Composite Structures, 93(2), 1031-1038.

[36] Mertiny, P., Ellyin, F., & Hothan, A. (2004). Stacking Sequence Effect of Multi–angle Filament Wound Tubular Composite Structures. *Journal of composite Materials*, *38*(13), 1095-1113.

[37] Hernández-Moreno, H., Douchin, B., Collombet, F., Choqueuse, D., & Davies, P. (2008). Influence of winding pattern on the mechanical behavior of filament wound composite cylinders under external pressure. *Composites Science and Technology*, *68*(3), 1015-1024.

[38] Tarakçioğlu, N., Gemi, L., & Yapici, A. (2005). Fatigue failure behavior of glass/epoxy ±55 filament wound pipes under internal pressure. *Composites science and technology*, *65*(3), 703-708.

[39] Will, M. A., Franz, T., & Nurick, G. N. (2002). The effect of laminate stacking sequence of CFRP filament wound tubes subjected to projectile impact. Composite structures, 58(2), 259-270.

[40] Martin, A. R., Fernando, G. F., & Hale, K. F. (1997). Impact damage detection in filament wound tubes using embedded optical fibre sensors. Smart materials and structures, 6(4), 470.

[41] *Auxiliary Fuel Management System* (2010). Army Aviation Study guides. Retrieved September 13, 2013, from http://www.usarmyaviation.com/studyguides/

[42] Federal Aviation Administration (2008). *Aviation Maintenance Technician Handbook (FAA-H-8083-30) – Aircraft Fuel Systems.*

[43] Abildskov, D. et al. (1970). *Filament Wound Fiber Glass Wing Tank*, Technical Report of Air Force Materials Laboratory Wvright-Patterson Air Force Base, Ohio.

[44] Shipp, M., (1993). *Aviation Boatswain's Mate*, Non-resident Training Course, Naval Education and Training Professional Development & Technology Center.

[45] U.S. Department of Defense (2012). Detailed Specification: *Turbine Fuel, Aviation, Kerosene Type JP-8 (MIL-DTL-83133H).*

[46] U.S. Department of Defense (2005). Design Criteria: *Airborne Stores, Suspension Equipment and Aircraft-Store Interface (MIL-STD-8591).*

[47] U.S. Department of Defense (1975). Military Specification: *Cap, Fluid Tank Filler (MIL-C-38373B).*

[48] Moir, I. & Seabridge, A. (2008). *Aircraft Systems*. West Sussex: John Wiley&Sons.

[49] National Aeronautics and Space Administration (1969). Space Vehicle Design Criteria: *Slosh Suppression.*

[50] U.S. Department of Defense (1953). Military Specifications: *Fuel System Components (MIL-F-8615).*

[51] U.S. Department of Defense (1986). Military Specifications: *Design and Installation of Auxiliary External Aircraft Fuel Tanks (MIL-T-18847C).*

[52] Ansys Inc. (2012). White Paper, *Simulating Composite Structures.*

[53] Mohan, M., (2008). The Advantages of Composite Materials in Marine Renewable Energy Structures, RINA Marine Renewable Energy Conference, UK.

[54] Siemens PLM Software (n.d.). *FEA Finite Element Analysis*. Retrieved November 13, 2013, from http://www.plm.automation.siemens.com/en_gb/plm/fea.shtml

[55] Bathe, Klaus-Jürgen. *2.092 Finite Element Analysis of Solids and Fluids I, Fall 2009*. (MIT OpenCourseWare: Massachusetts Institute of Technology),http://ocw.mit.edu/courses/mechanical-engineering/2-092-finite-element-analysis-of-solids-and-fluids-i-fall-2009 (Accessed 23 Nov, 2013).

[56] ANSYS, Inc. (2011). Workbench User's Guide. Southpointe, PA.

[57] Agarwai, R. *Computer Aided Design in Mechanical Engineering, Spring 2013*. (San Jose State University, FEA Lecture Notes). http://www.engr.sjsu.edu/ragarwal/ME165/ME165_Lecture_Notes_files/FEA_Lectures (Accessed 25 Nov, 2013).

[58] Madenci, E. and Güven İ. (2006). *The Finite Element Method and Applications in Engineering Using ANSYS*. New York, NY: Springer Science&Business Media.

[59] U.S. Department of Defense (2000). Test Method, Standard: .*Environmental Engineering Considerations and Laboratory Tests (MIL-STD-810F*).

[60] ANSYS, Inc. (2011). *Composite Introduction*. ANSYS Composite and ACP Training Lecture Notes.

[61] Fornaro, D. (2011). *Advancement in the Application of Finite Element Analysis to the Optimization of Composite Yacht Structures*. The 20th Chesapeake Sailing Yacht Symposium, Maryland 2011.

[62] Sadd, M. (2005). *Elasticity*. Burlington: Elsevier Inc.

[63] Barış Elektrik Endüstrisi A.Ş. (1996). TUBİTAK MİSAG-39, Filaman Sargı Tekniği ile Kompozit Malzeme Kullanarak Basınca Dayanıklı Optimum Boru Tasarımı Projesi Sonuç Raporu.

[64] Meunier, M. & Knibbs, S. (n.d). *Design Tool for Fibre Reinforced Polymer Structures*. National Composites Network Best Practice Guide.

[65] ANSYS, Inc. (2011). ACP Product Brochure*: Composites*. Retrieved 10 Jan, 2014, from http://www.ansys.com/staticassets/ANSYS/staticassets/resourcelibrary/brochure/ansys-composites-14.0.pdf

[66] Barbero, E. J. (2008). *Finite Element Analysis of Composite Materials.* Boca Raton, FL: CRC Press.

[67] Jackson K. et al. (2004). *A History of Full-Scale Aircraft and Rotorcraft Crash Testing and Simulation at NASA Langley Research Center*. Fourth Triennial International Aircraft and Cabin Safety Research Conference; Lisbon; Portugal. Retrieved 02 Jan., 2014, from http://naca.larc.nasa.gov/search.jsp?R=20040191337&qs=Ns%3DPublication-Date%7C1%26N%3D4294708474

[68] METU-BILTIR Center (2011). *Vehicle Safety Unit*. Retrieved 11 Jan., 2014, from http://www.biltir.metu.edu.tr/tasitguvenligi.html

[69] Merrill, J. A. (1947). U.S. Patent No. 2,424,701. Washington, DC: U.S. Patent and Trademark Office.

[70] Carper et al. (1989). *Evolving Crashworthiness Design Criteria.* Aviation Applied Technology Directorate, U.S. Army Research and Technology Activity (ASCOM). Fort Eustis, Virginia.